Comprehensive investigation on synthetic cannabinoids: metabolic behaviour, detectability and potency testing, using 5F-APP-PICA and AMB-FUBINACA as model compounds

Short title: Comprehensive investigation on synthetic cannabinoids

David Fabregat-Safont[1], Marie Mardal[2], Carolina Noble[2], Annelies Cannaert[3], Christophe P. Stove[3], Juan V. Sancho[1], Kristian Linnet[2], Félix Hernández[1] and María Ibáñez[1*]

[1] Research Institute for Pesticides and Water, University Jaume I, Avda. Sos Baynat s/n, 12071, Castellón, Spain.

[2] Department of Forensic Medicine, Section of Forensic Chemistry, Faculty of Health and Medicinal Sciences, University of Copenhagen, Frederik V's vej 11, 2100 København Ø, Denmark

[3] Laboratory of Toxicology, Department of Bioanalysis, Faculty of Pharmaceutical Sciences, Ghent University, Ottergemsesteenweg 460, 9000 Ghent, Belgium

[*]Corresponding autor

María Ibáñez,

Research Institute for Pesticides and Water, University Jaume I, Avda. Sos Baynat s/n, 12071, Castellón, Spain

E-mail: ibanezm@uji.es

Tel.: +34964387339

Fax: +34964387368

Abstract

Synthetic cannabinoids (SCs) represented 45% of the new psychoactive substances seizures in Europe (data from 2016). The consumption of SCs is an issue of concern due to the still unknown toxicity and effects on human health, the great variety of compounds synthetized and continuous modifications in their chemical structure to avoid regulatory issues. These compounds are extensively metabolised in the organism and therefore often cannot be detected as the intact molecule in human urine. For this reason, the monitoring of SCs in forensic samples must be performed by the analysis of its metabolites. In this work, a workflow for the comprehensive study of SC consumption is proposed and applied to 5F-APP-PICA (also known as PX 1 or SRF-30) and AMB-FUBINACA (also known as FUB-AMB or MMB-FUBINACA), based not only on the elucidation of their metabolites but also including functional data. Both cannabinoids were completely metabolised by human hepatocytes (12 and 8 metabolites were elucidated by high resolution mass spectrometry for 5F-APP-PICA and AMB-FUBINACA, respectively) and therefore suitable consumption markers have been proposed. The bioassays revealed that 5F-APP-PICA presented lower activity than AMB-FUBINACA at CB1 and CB2 receptors. These results are in agreement with the different intoxication cases found in literature for AMB-FUBINACA.

Keywords

Synthetic cannabinoids, 5F-APP-PICA, AMB-FUBINACA, high resolution mass spectrometry, metabolite identification

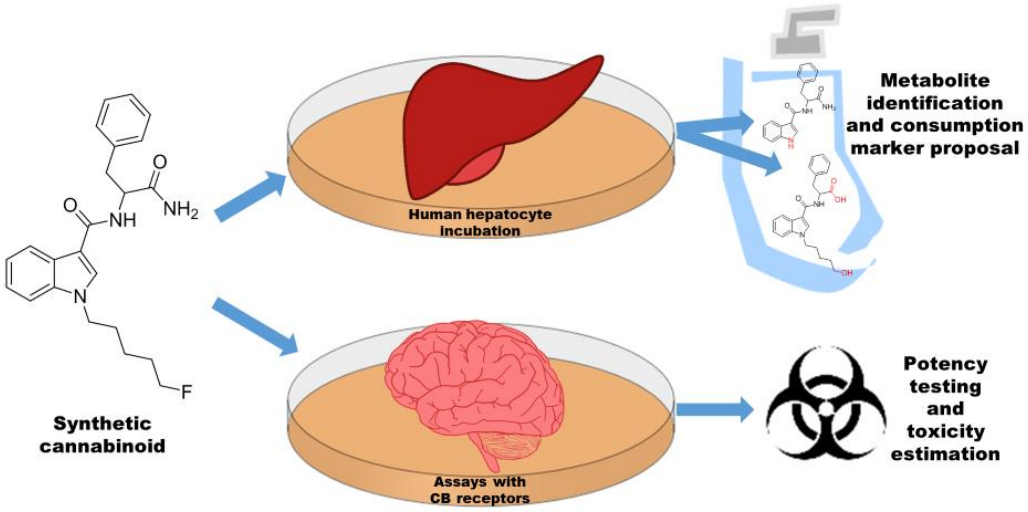
Synthetic cannabinoid
Human hepatocyte incubation
Metabolite identification and consumption marker proposal
Assays with CB receptors
Potency testing and toxicity estimation

1. Introduction

Synthetic cannabinoids (SCs) are among the most frequently seized new psychoactive substances (NPS), according to the 2018 *European Monitoring Centre for Drug and Drug Addiction* (EMCDDA) report [1]. In 2016, SCs represented 45% of the NPS seizures in Europe, being the largest NPS group monitored by the EMCDDA (179 compounds) [1]. Although these compounds can be found as faux hash and e-liquids for vaping [2], they are typically sold on webpages or in smartshops [3–5] as "herbal blends" or "spice", and used as cannabis substitution. In the last years, SCs are also being found as powder [1]. In 2017, 10 new SCs were detected for the first time in Europe [1], illustrating the continuous emergence of this type of substances [1,6]. The constant modifications in the chemical structure of these compounds constitute an analytical challenge for forensic laboratories, which must apply state-of-the-art techniques for compound identification, such as high-resolution mass spectrometry (HRMS) or nuclear magnetic resonance (NMR) [7–9], in most cases without having reference standards available for their rapid confirmation.

It is known that several SCs present more intense psychoactive and side effects than THC, given their full agonism at the cannabinoid receptors CB1 and CB2, while THC only partially activates these [10,11]. The fact that SCs possess higher potency at the CB1 and CB2 could also increase the health risk for drug consumers, as reported in several overdose cases [12–18]. Nevertheless, it has not been confirmed yet that toxicity of SCs is strictly a function of potency and/or efficacy.

As most of the drug tests performed for the treatment of cannabis dependence are based on the detection of THC-COOH (the main urinary metabolite of THC), SCs can be used to by-pass urine controls [19]. Monitoring SC consumption is very important, for example in intoxication cases in hospitals or psychiatric centres. Such control cannot be performed by targeted methodologies directed towards the parent compounds, as these are rapidly

metabolised in the liver, resulting in little or no unaltered compound in urine [20]. This forces analytical laboratories to develop methodologies focused on the major urinary metabolites [21,22], which constitutes an additional challenge for detecting the use of SCs. Ideally, in order to stablish the best consumption biomarkers, urine samples from SC consumers [23–26] should be collected to study their metabolism. However, the availability of this type of samples is mostly limited to medical emergency cases. To circumvent this problem, different strategies can be used. In the *in vivo* approach, healthy animals (typically mice[27] or rats[28–30]) are exposed to the compound of interest, and blood and urine samples are usually collected in order to elucidate the metabolites. Nevertheless, it is possible that some metabolites obtained with an animal model are not found in humans, or the major metabolites identified in humans are not the major ones in other species. As an alternative, *in vitro* approaches using human liver microsomes [31], S9 fractions or hepatocytes [31], have produced reliable human excretory metabolites when studying pharmaceuticals. Human liver microsomes [26,32] or hepatocytes [24,33,34] have already been used for the metabolism study of new synthetic drugs such as SCs. Confirmation of these *in vitro* metabolites via the analysis of authentic samples (especially urine) has proven the suitability of the different *in vitro* strategies to predict human metabolic products [24,32].

As important as the determination of the most suitable consumption biomarkers of SCs is the evaluation of their potency and/or affinity at CB1 and CB2 receptors [35–37], which reveals another important aspect of these drugs and brings new insights on their pharmacology. To this aim, different bioassays have been used for both SCs as well as their metabolites and degradation products.

In order to obtain a complete overview on the problem of SC consumption, a three-step strategy has been used in this work: i) Metabolism study for establishing the metabolic pathway and the most suitable consumption biomarkers. ii) Detectability and/or stability of the parent

compound and its metabolites during incubation, which could be extrapolated to the excretion through urine in intoxication cases. iii) Estimation of their potency using activity-based CB1 and CB2 receptor bioassays. The proposed strategy has been applied to the 1-pentyl-1*H*-indazole-3-carboxamide derivative 5F-APP-PICA (also known as PX 1 or SRF-30), and the (4-fluorophenyl)methyl-1*H*-indazole-3-carboxamide derivative AMB-FUBINACA (also known as FUB-AMB or MMB-FUBINACA), which are amongst the most common SCs seized in powder and smoking mixtures in Spain and Europe [38], respectively. Several phase I and phase II metabolites have been identified thanks to the use of accurate-mass data provided by HRMS, which has allowed the proposal of useful biomarkers of consumption.

2. Experimental

2.1. Reagents and chemicals

5F-APP-PICA and AMB-FUBINACA were kindly provided by Energy Control (Asociación Bienestar y Desarrollo, Barcelona, Spain). Compound purity was tested by nuclear magnetic resonance. 5F-Py-PICA (internal standard, IS) was kindly provided by the Slovenian National Forensic Laboratory.

For hepatocyte incubation, diclofenac was purchased from Sigma-Aldrich (St. Louis, MO, USA). Trypan blue solution (0.4%), fetal bovine serum (FBS), Leibovitz's L-15 medium, Gibco cryopreserved hepatocyte recovery medium, methanol, acetonitrile, ultrapure water, Pierce® LTQ Velos ESI positive Ion calibration solution, Pierce™ ESI negative ion calibration solution, and formic acid (LC–MS grade) were obtained from Fisher Scientific (Leicestershire, UK). The pooled human hepatocytes (pHH) from a pool of 10 were purchased from Lonza (Basel, Switzerland), and stored in liquid nitrogen until use.

For cannabinoid receptor bioassays, JWH-018 was purchased from LGC (Wesel, Germany). Poly-D-lysine and fetal bovine serum (FBS) were from Sigma-Aldrich (Steinheim, Germany). Opti-MEM I Reduced Serum, Dulbecco's modified eagle medium (DMEM), trypsin, penicillin, amphotericin B, streptomycin, and glutamine were supplied by Thermo Fisher Scientific (Pittsburg, PA, USA). Nano-Glo® Live Cell substrate furimazine and Nano-Glo® dilution buffer were purchased from Promega (Madison, WI, USA). Methanol and DMSO were purchased from Fisher Scientific.

2.2. Pooled human hepatocyte incubation

Incubation with pooled human hepatocytes was performed at 10 μM of each SC during 180 min, with collection of aliquots at 0, 60 and 180 min. Briefly, cryopreserved pooled human hepatocytes were rapidly thawed in a water bath at 37 °C, mixed with 50 mL preheated recovery medium, and centrifuged at 168 g for 20 min to remove dead hepatocytes. After

aspiration of the supernatant, the hepatocytes were washed by resuspending the pellet in 20 mL growth medium (L-15 with 10% FBS), and centrifuging for 5 min at 50 g. Then, the supernatant was aspirated and the resulting pellet was re-suspended in growth medium for cell counting by the trypan blue exclusion method. The measured viability was 71%. The hepatocyte suspension was diluted to 10^6 viable hepatocytes/mL incubation medium. 5F-APP-PICA, AMB-FUBINACA, or diclofenac (positive control) were added at a final concentration of 10 μM; the maximum organic content of the incubation was 0.3%. The incubations were performed in duplicate for each condition in 96-well plates, at 350 rpm and 37 °C, on a Thermomixer comfort (Eppendorf, Hamburg, Germany). Controls without the addition of hepatocytes were run simultaneously to identify hydrolysis products and artefacts. Aliquots of 20 μL were collected after 0 (with a latency between 2-3 min), 60, and 180 min of incubation and mixed with 80 μL of an ice-cold acetonitrile solution containing 100 ng/mL of IS. The extracts were frozen until analysis.

2.3. Instrumentation

Extracts were analyzed using a Dionex Ultimate 3000 UHPLC system from Thermo Scientific (Germering, Germany) coupled to a Q Exactive high resolution mass spectrometer from Thermo Scientific (Bremen, Germany) equipped with a hybrid quadrupole-Orbitrap mass analyzer.

Chromatographic separation was performed using an Acquity HSS C18 1.8 μm, 2.1×150 mm column from Waters (Wexford, Ireland), which was maintained at 40 °C. The mobile phase consisted of 5 mM ammonium formiate buffer with 0.1% v/v formic acid (solvent A) and 0.1% v/v formic acid in acetonitrile (solvent B), which was delivered at a flow rate of 0.25 mL/min. A 14 min gradient was used for the identification of metabolites, starting at 5% B (0–0.5 min), increasing to 99% B (0.5–10 min), where it remained isocratic for 2 min and followed by re-equilibration for 2 min. The autosampler temperature was 5 °C. The

injection volume was 3 μL.

UHPLC was coupled to the HRMS using a heated electrospray ionization source (HESI-II) (Thermo Scientific, Bremen, Germany) working in positive (ESI^+) and negative (ESI^-) ionization modes. The capillary temperature was 350 °C, and the spray voltage was 4.0 kV in ESI^+ and -4.0 kV in ESI^-. Data were acquired using data-dependent acquisition (dd-MS^2, DDA) and parallel reaction monitoring (PRM, MS/MS). Full-scan data (FTMS) were collected in a scan-range of *m/z* 200–900 using a resolution of 70,000 FWHM, an automatic gain control (AGC) target of 10^6 ions, a maximum injection time of 50 ms and an isolation window of *m/z* 1. DDA MS/MS was acquired at a resolution of 35,000 FWHM, while PRM were acquired at 17,500 FWHM, using an AGC target of 2e5 ions and a maximum IT of 25 ms. Nitrogen was used as the collision gas at normalized collision energy (NCE) of 10, 30 or 50 eV.

The instrument was externally calibrated to a mass accuracy of ±5 ppm using the recommended calibration solutions for this instrument (Pierce® LTQ Velos ESI positive Ion calibration solution, Pierce™ ESI negative ion calibration solution, Thermo Scientific), purchased from Thermo Scientific. The instrument was controlled by XCalibur 4.0 software (Thermo Scientific, MA, Waltham, USA). Data processing was performed using Compound Discoverer 2.0 software (Thermo Scientific) for a preliminary compound identification, and FreeStyle 1.3 (Thermo Scientific) for working with raw data.

2.4. Cannabinoid receptor bioassays

The potency and efficacy (the latter relative to JWH-018, used here as a reference) were estimated via the calculation of the half maximal effective concentration (EC_{50}) and the maximum response (E_{max}), respectively. Both parameters were determined using live cell-based reporter assays based on the application of the NanoLuc Binary Technology, that evaluates the interaction between the cytosolic protein β-arrestin 2 (βarr2) to CB1 and CB2

expressed in human embryonic kidney (HEK) 293T cells. Details regarding the development of the stable CB1 and CB2 cell lines used here and the experimental conditions have been reported elsewhere [39,40]. In brief, cells were seeded on a poly-D-lysine-coated 96-well plate at 5×10^4 cells/well and incubated overnight at 37°C and 5% CO_2. Following 24 h, the cells were washed twice with 150 µL Opti-MEM I Reduced Serum and finally 100 µL of Opti-MEM I was added to each well. The Nano-Glo® Live Cell Reagent (Promega), a nonlytic detection reagent containing the live cell permeable furimazine substrate, was prepared by diluting the substrate 20× in Nano-Glo® LCS dilution buffer, and 25 µL was added to each well. The plate was placed in a luminometer and after stabilization of the signal (~20 min), 10 µL of 13.5× stock solutions (concentration range: 0.01–10 µM) of the 5F-APP-PICA or AMB-FUBINACA in 50% methanol in Opti-MEM I was added and the luminescence was continuously measured for 2 h (n=5-7). Replicates of solvent (50% methanol in Opti-MEM I) were run in all experiments as negative controls and were used to correct the signal. The final concentration of methanol (3.7%) did not pose a problem given the advantage of the short readout time of the assay.

Curve fitting of concentration-effect curves via nonlinear regression (four parameter logistic fit) was employed to determine EC_{50} (measure of potency) and E_{max} values (measure of efficacy). The E_{max} values are normalized to the E_{max} value of JWH-018 (100%), used as a reference in our study, and hence are a 'relative measure' of efficacy.

3. Results and discussion

3.1. Fragmentation of the synthetic cannabinoids

It is expected that parent compounds and metabolites present very similar fragmentation pathways. So, an accurate study of the MS fragmentation of the parent compound is extremely useful for metabolite elucidation. The presence of common fragments between parent and metabolite indicates that the biotransformation has not occurred in this part of the molecule.

The remaining fragments observed for metabolites usually present a mass shift when compared to the corresponding fragments of the parent compound, commonly corresponding to the biotransformation. So the identification of these mass fragments is crucial to correctly locate the position in which the biotransformation has occurred. This methodology has been successfully used for NPS metabolite identification[41,42]. Nevertheless, it has to be taken into account that some biotransformations can affect the whole fragmentation pathway of the metabolite, which may become very different from the parent.

Figure SI1 (in **Electronic Supplementary Information**) shows the MS/MS spectra of 5F-APP-PICA ($C_{23}H_{27}FN_3O_2^+$, *m/z* 396.2083, 0.18 ppm) at 10 eV (top) and 50 eV (bottom) collision energy. **Table SI1** lists its fragments, including accurate mass, elemental composition and mass error. The terminal amide moiety easily breaks similarly to ADB-PINACA, 5F-AB-PICA and AB-FUBINACA, producing the loss of an ammonia molecule (Fragment 1, $C_{23}H_{24}FN_2O_2^+$, *m/z* 379.1815, -0.38 ppm). The Fragment 2 ($C_{14}H_{15}FNO^+$, *m/z* 232.1132, -0.39 ppm) would correspond to the disconnection of the peptide bond of the amide moiety linked to the indole ring. This fragmentation is also observed for ADB-PINACA, 5F-AB-PICA and AB-FUBINACA (which have an indazole group instead of indole) and, APICA and SDB-006 (indole ring). Fragment 2 could also come from the protonated molecule ($[M+H]^+$) when the protonation is produced in the amide moiety linked to the indole ring. Finally, this fragment ion at *m/z* 232, consisting of the indole ring with the *N*-alkyl moiety and the carbonyl moiety, indicates an *N*-dealkylation and consequent release of the indazole with the carbonyl moiety (Fragment 3, $C_9H_6NO^+$, *m/z* 144.0444, -0.02 ppm). This *N*-dealkylation has also been reported for AB-FUBINACA and ADB-PINACA. Nevertheless, the cyclopentylium ion (Fragment 4, $C_5H_9^+$, *m/z* 69.0706, 11.17 ppm) has not been observed for related compounds when a QTOF instrument is used [6]. This could be consequence of the different geometry of the collision cell

used in both instruments. **Figure SI3** shows the proposed fragmentation pathway for 5F-APP-PICA, once evaluated the observed fragmentation.

Figure SI2 and **Table SI2** show the mass spectrometric behaviour of AMB-FUBINACA ($C_{21}H_{23}FN_3O_3^+$, *m/z* 384.1717, -0.35 ppm) at 10 eV (top) and 30 eV (bottom). The first fragment corresponds to the ester bond disconnection and subsequent loss of methanol (Fragment 1, $C_{20}H_{19}FN_3O_2^+$, *m/z* 352.1455, -0.12 ppm), equivalent to the ammonia loss observed for 5F-APP-PICA. Subsequently, a CO loss is produced (Fragment 2, $C_{19}H_{19}FN_3O^+$, *m/z* 324.1507, 0.09 ppm). After that, the peptide bond is disconnected, releasing the indazole ring bonded to the carbonyl moiety (Fragment 4, $C_{15}H_{10}FN_2O^+$, *m/z* 253.0771, -0.14 ppm). Peptide bond can also be disconnected from the $[M+H]^+$ protonated in the amide moiety, as explained in **Figure SI4**. This behaviour has also been reported for ADB-FUBINACA and AB-FUBINACA [26,43]. Finally, an *N*-dealkylation is produced, resulting in a fluorotropylium ion (Fragment 5, $C_7H_6F^+$, *m/z* 109.0451, 3.45 ppm), also reported for cannabinoids with a fluorobenzyl moiety [26,43]. Similarly to Fragment 4, the fluorotropylium fragment ion could be produced directly from the protonated molecule after an *N*-alkyl disconnection (**Figure SI4**). An additional fragment is observed at *m/z* 271.0877 (Fragment 3, $C_{15}H_{12}FN_2O_2^+$, -0.09 ppm), obtained after the addition of a water molecule to Fragment 4. The generation of adducts between unstable ions and neutral molecules, specially water molecules, has been previously reported for Q-Orbitrap instruments [44]. As stated by those authors, these adducts are less promoted in QTOF instruments, due to the different geometry of the collision cell.

Although there are differences in the fragmentation of both compounds, a generic fragmentation pathway can be proposed based on most of the observed ions (see **Figure 1)**. The information about the fragmentation pathway of both synthetic cannabinoids can be used by forensic laboratories for the identification of these SCs, but also for elucidation of similar cannabinoids, as most present similar fragmentation [6,43–45].

Tables SI1 and **SI2** show the fragmentation observed for all the 5F-APP-PICA and AMB-FUBINACA metabolites, respectively, in ESI^+ and ESI^-, including the chromatographic retention time, and the elemental composition and mass error of the (de)protonated molecule and its fragments.

3.2. Analytical strategy for metabolite identification

Once samples were injected into the UHPLC-HRMS system using data dependent acquisition mode (DDA), Compound Discoverer 2.0 software was used for data processing. A list of expected metabolites was obtained based on presumed biotransformations. The software automatically performed extracted ion chromatograms (EIC) (with a mass window of ±5 ppm) for the (de)protonated molecule of the expected metabolites. Compounds that were present in incubation samples but not in blanks nor stability samples were considered as potential metabolites.

MS/MS spectra of the potential metabolites, acquired during DDA, were studied using FreeStyle 1.3 software. Those potential metabolites that presented a plausible fragmentation (i.e. the MS/MS spectra fit with the expected biotransformation) were considered for a re-analysis by UHPLC-HRMS using parallel reaction monitoring acquisition (PRM) at three different collision energies (10, 30 and 50 eV). If not, they were directly discarded.

Based on the observed PRM MS/MS fragmentation, the position of the biotransformation on the structure was determined. Finally, fragmentation pathways were proposed for all metabolites.

3.3. 5F-APP-PICA metabolites

The above strategy allowed the identification of 7 phase I metabolites of 5F-APP-PICA. Regarding phase II metabolites, 5 compounds were found, all of them corresponding to glucuronides (Gluc) of the main phase I metabolites. An exhaustive description on the

identification of all metabolites based on the observed fragmentation, including fragmentation pathways, can be found in **Electronic Supplementary Information**.

Metabolic behaviour

After elucidating the structures for all metabolites, the metabolic pathway for 5F-APP-PICA using human hepatocyte incubation was proposed (**Figure 2**). As an aliquot of the incubation was taken at 0, 60 and 180 min, the prevalence of 5F-APP-PICA and its metabolites in the incubation was also studied. **Figure 3** shows the relative presence of all the identified metabolites, including the parent compound, normalizing all the responses to the one obtained for 5F-APP-PICA at 0 min. For metabolites detected in ESI^+, 5F-APP-PICA $[M+H]^+$ response was used, while metabolites observed in ESI^- were plotted relative to 5F-APP-PICA $[M–H]^-$ response. Obviously, an important limitation here is that this approach assumes similar ionisation and fragmentation efficiencies for the parent compounds and the metabolites, which is not really the case, as can also be deduced from the fact that the sum of the obtained % (strongly) deviates from 100%. Still, this approach allows to get an idea about the appearance and further conversion of metabolites.

Metabolic biotransformations seem to be focused on the removal of heteroatoms from both sides of the molecule. One of the most abundant biotransformations at 0 min was the oxidative defluorination (M1), together with the oxidation of the hydroxyl group in the alkylic chain after oxidative defluorination (M2). These two biotransformations have been reported for other synthetic cannabinoids with an *N*-fluoropentyl moiety, such as MAM-2201 [45], 5F-AB-PINACA [46] and 5F-AMB [47]. The other most abundant biotransformation at 0 min, the oxidative deamination (M3), has also been widely reported in literature for synthetic cannabinoids with terminal amide moieties, such as AB-FUBINACA [24], AB-PINACA [46] and 5F-AB-PINACA [46]. As expected, combinations of these biotransformations were also found (M4 and M5). The *N*-dealkylation of the fluoropentyl moiety (M6) has also been reported for

MAM-2201 [45]. Similarly to M4 and M5, the metabolite M7 was obtained after oxidative deamination from M6. Additional biotransformations described for these cannabinoids, such as *N*-alkyl hydroxylation/oxidation, were not found for 5F-APP-PICA [45,47].

5F-APP-PICA was rapidly metabolised during incubation. At 60 min, only 20% of the initial response was present, with less than 0.5% remaining at 180 min, as depicted in **Figure 3**. M1 presented an important response at 0 min, but it started to decrease at 60 min. It is possible that the increment in the relative response of M2 after 60 min is related to the decrease of M1 at the same time, as M1 is transformed to M2, and also to M4. M2-M5 presented a continuous increase in response over time, with especially M5 increasing substantially after the 60 min time point. M6 presented a relative concentration of 11% at 0 min, while M7, which is derived from M6, was present at 10% at 180 min, with an increase in M7 being accompanied by a decrease in M6. Finally, glucuronide conjugates were not significantly important, all being below 3% of relative response. The most abundant phase II metabolite was M5-Gluc (2.85%), as expected after evaluation of phase I metabolites.

Based on these results, M3, M4 and M5 were the most abundant metabolites at 180 min, and thus could be selected as potential biomarkers for the determination of 5F-APP-PICA consumption in forensic samples. We are not aware of authentic cases that have been reported in literature via which these biomarkers could be validated.

3.4. AMB-FUBINACA metabolites

Six phase I metabolites and one phase II metabolite, corresponding to the glucuronide conjugate of the main phase I metabolite, were identified for AMB-FUBINACA. All the identified metabolites were detected in ESI^+. The fragmentation study performed for the identification of all metabolites can be found in **Electronic Supplementary Information**.

Metabolic behaviour

Once all the AMB-FUBINACA metabolites were identified, the metabolic pathway for this SC was proposed (**Figure 4**). Similarly to 5F-APP-PICA, the prevalence of AMB-FUBINACA and its metabolites was studied, normalizing all the responses to the response obtained for the parent compound at 0 min (**Figure 5**). Also here, a limitation is that similar ionization and fragmentation efficiencies are assumed for the main compound and its metabolites.

Metabolic biotransformations were focused on the increment of polarity of the compound, by dealkylations and hydroxylations. The most abundant metabolite was M1, produced after *O*-demethylation of AMB-FUBINACA. The slight increase in relative response of M1 after 60 min could be owing to small variations in the response of the instrument. The *O*-dealkylation has already been reported for other SCs with terminal ester moieties, such as MDMB-CHMICA [32]. M1 seems to be the precursor compound for the phase I hydroxylated metabolites M2-4. The hydroxylation after an *O*-demethylation has been described in literature, but only in the alkyl moiety (isopropyl for AMB-FUBINACA, and isobutyl for MDMB-CHMICA[32]) positioned between the amide and ester groups. For AMB-FUBINACA, three different positions for hydroxylation could be deduced, based on the observed fragmentation: hydroxylation in each one of the methyl groups (M3) and in the tertiary carbon (M2) of the isopropyl group; for MDMB-CHMICA, instead, the position of the hydroxyl group could not be established unequivocally by the authors [32]. In the case of M4, the hydroxylation took place on the indazole ring. M5 is the result of an indazole hydroxylation directly from the parent compound. So, M5 could also be metabolized into M2 following an *O*-demethylation process. Regarding M6, this metabolite was produced after *N*-dealkylation of M1. This biotransformation has been observed for SCs with an indazole ring and an *N*-fluorobenzyl moiety, such as ADB-FUBINACA and AB-FUBINACA[26,43]. Finally, an additional potential metabolite was obtained after *N*-methylation of M6 (M6-Methyl), as either an enzymatic reaction or artefact formation. No information about the *N*-methylation of related drugs has

been found. *N*-methylation of amines are common artefacts when working with methanolic solutions [48], particularly at elevated temperatures. In the present study, the compounds were dissolved in methanol and later incubated at a low final methanolic concentration level of 0.3%. The quenching solution and mobile phases were acetonitril-based which should not form *N*-methyl artefacts. In order to determine whether M6-Methyl is an artefact or a metabolite, the experiment should be repeated using CD_3OH as dissolving agent to observe if there is a corresponding accurate mass shift. Additional biotransformations described for other imidazole cannabinoids, such as amide *N*-dealkylation or polyhydroxylation, were not found for AMB-FUBINACA [26,43].

AMB-FUBINACA was metabolised extremely fast. At 0 min, M1 represented near 1900% of parent response, illustrating that the *O*-demethylation is the most important and rapid biotransformation. *O*-demethylated metabolite represented less than 1% in the biological blank (incubation without hepatocytes), indicating that this metabolite is not an impurity from the compound or a degradation product. Two hypothesis could explain the huge relative response observed for M1 at 0 min. One reason could be related to the little delay (2-3 min) between the incubation starting and the aliquot collection times, which could be enough for the *O*-demethylation reaction occurring. The second one could be the much higher efficient ionisation of M1 respect to parent compound. At 60 min, only 0.5% of AMB-FUBINACA remained, as can be observed in **Figure 5**. M1-Gluc increased over time, until 16% at 180 min, as expected, given the fact that M1 is the most important compound present in the incubation mixture. The other metabolites (M2-M5) were below 1% at 180 min, and only M6 (1.6% at 180 min) and M6-Methyl (7.2% at 180 min) yielded a noteworthy response in the incubations. It could be possible that other reactions might be more prominent but the resulting metabolites might not give a good MS response. Therefore, based on MS response, M1 would be the most suitable

metabolite to be considered as a biomarker for the determination of AMB-FUBINACA consumption in real samples.

In a recent report where AMB-FUBINACA was associated with a massive intoxication [49], the parent compound was not detected in blood while the carboxylic metabolite was detected at high concentrations in the urine samples. Also Staeheli and colleagues reported on the detection of the M1 metabolite in urine of a SC user, although these authors did find some remaining AMB-FUBINACA main compound in urine as well [50]. Overall, these data are in agreement with the results obtained in this article, showing the usefulness of our *in vitro* studies.

3.5. Potency and efficacy of synthetic cannabinoids

The EC_{50} and E_{max} values were estimated for 5F-APP-PICA and AMB-FUBINACA. The EC_{50} value of 5F-APP-PICA at CB1 could not be estimated as it did not reach a plateau within the tested concentration range, however a maximal effect of 88.9% (relative to JWH-018) at 10 µM was attained, indicating that even very high concentrations of 5F-APP-PICA only result in a partial recruitment of βarr2 to CB1. This weak activity of 5F-APP-PICA at CB1 might be the reason why this SC has not been associated with overdose cases so far. However, the correlation between the signalling pathway (in our case: βarr2 recruitment to the receptor, induced by the agonist) and the effects observed in humans after intake has not been fully elucidated for any of both receptors [51]. On the other hand, 5F-APP-PICA did show activity at CB2, with an EC_{50} of 83.2 nM and showing an E_{max} similar to that observed for the control JWH-018 (i.e. 96.6% of the JWH-018 E_{max}) (**Table 1**). To the best of the authors' knowledge, there are no reference concentrations of 5F-APP-PICA in blood, so it is not possible to extrapolate our EC_{50} value to an *in vivo* situation.

With EC_{50} values of 9.84 nM and 2.40 nM for CB1 and CB2, respectively, AMB-FUBINACA was much more potent than the control JWH-018 at both receptors, for which

EC_{50} values of 41.0 and 12.3 were obtained [40]. Interestingly, also the E_{max} values for this SC are substantially higher than that observed for JWH-018, especially at CB1 (approximately 2.5 fold). Therefore, AMB-FUBINACA is not only more potent, but it also generates a stronger response at CB1 than the reference compound JWH-018 at high concentrations. Although it is difficult to compare EC_{50} values from different assays (due to different experimental setups), our low nanomolar values are in line with those found in other reports investigating the *in vitro* an *in vivo* activity of AMB-FUBINACA [52,53]. More particularly, Banister *et al.* and Gamage *et al.* estimated the EC_{50} and the E_{max} values for AMB-FUBINACA via the FLIPR® assay [49] and via the [^{35}S]GTP binding assay and via the inhibition of forskolin-stimulated cAMP production [50]. Also *in vivo* data is available for AMB-FUBINACA [54]. All these data indicate that AMB-FUBINACA is a potent SC, as also reflected by the reported "Zombie" outbreak caused by AMB-FUBINACA in New York in July 2016 [49] and supported by the very high potency of the closely related ADB-FUBINACA [54]. Future work should include potency testing of the major metabolites, to reveal whether these may contribute to the (toxic) effects observed in users.

4. Conclusions

In this work, a three-step strategy has been proposed for a comprehensive SC *in vitro* study: i) elucidation of the metabolites obtained by pooled human hepatocytes, ii) proposal of consumption biomarkers based on the obtained metabolites and their stability during incubations, and iii) estimation of the potency and efficacy based on their activation of CB1 and CB2 receptors.

This strategy has been applied to two synthetic cannabinoids, 5F-APP-PICA and AMB-FUBINACA, with a detailed explanation of the experimental procedure, data interpretation and compound elucidation. The results obtained revealed that both SCs were extensively

metabolised during incubations, explaining why these synthetic drugs may hardly be found in urine as unaltered compounds. A total of 7 phase I and 5 phase II metabolites were elucidated for 5F-APP-PICA, and 6 phase I and 1 phase I metabolites for AMB-FUBINACA. Three of these metabolites are proposed as consumption biomarkers for 5F-APP-PICA, and only 1 metabolite for AMB-FUBINACA, based on the responses obtained at the end of our *in vitro* incubation studies. The CB bioassays revealed that 5F-APP-PICA does not present a high activity at CB receptors (certainly not at CB1), while AMB-FUBINACA shows a high CB1 activation potential, both in terms of potency and efficacy. The above can be linked to intoxication cases reported for AMB-FUBINACA and the absence of cases for 5F-APP-PICA.

The proposed methodology can be applied to the study of other cannabinoids. The accurate and detailed explanation of compound elucidation, based on HRMS data, included in this work will be useful for forensic laboratories, as many cannabinoids present similar fragmentation pathways.

Acknowledgements

D. Fabregat-Safont, J.V. Sancho, F. Hernández and M. Ibáñez acknowledge financial support from the Ministerio de Economía y Competitividad in Spain (Project CTQ2015-65603-P). D. Fabregat-Safont acknowledges Ministerio de Educación, Cultura y Deporte in Spain for his predoctoral grant (Grant FPU15/02033), and for the financial support received for his research stay at the University of Copenhagen (Grant EST17/00024). Carolina Noble gratefully appreciates the financial support from the National Research and Innovation Agency of Uruguay (ANII). Carolina Noble was sponsored by the Graduate School of Health and Medical Sciences of the University of Copenhagen. C. Stove acknowledges financial support from the Belgian Science Policy Office (NPSSAY) and from the Ghent University Research Council (grants n° 01N00814 and 01J15517).

Conflict of interest

The authors declare that they have no competing interests.

References

[1] European Monitoring Centre for Drugs and Drug Addiction. European Drug Report 2018. *EMCDDA Publ.*, **2018**, DOI 10.2810/88175.

[2] R. P. K. Lam, M. H. Y. Tang, S. C. Leung, Y. K. Chong, M. S. H. Tsui, T. W. L. Mak. Supraventricular tachycardia and acute confusion following ingestion of e-cigarette fluid containing AB-FUBINACA and ADB-FUBINACA: a case report with quantitative analysis of serum drug concentrations. *Clin. Toxicol.*, **2017**, *55*, 662–667.

[3] L. Fattore, W. Fratta. Beyond THC: The New Generation of Cannabinoid Designer Drugs. *Front. Behav. Neurosci.*, **2011**, *5*, 1–12.

[4] M. Ibáñez, L. Bijlsma, A. L. N. van Nuijs, J. V. Sancho, G. Haro, A. Covaci, F. Hernández. Quadrupole-time-of-flight mass spectrometry screening for synthetic cannabinoids in herbal blends. *J. Mass Spectrom.*, **2013**, *48*, 685–694.

[5] R. Gottardo, A. Chiarini, D. Prà, C. Seri, C. Rimondo, G. Serpelloni, F. Tagliaro. Direct screening of herbal blends for new synthetic cannabinoids by MALDI-TOF MS. *J. Mass Spectrom.*, **2012**, 141–146.

[6] L. Bijlsma, M. Ibáñez, B. Miserez, S. T. F. Ma, T. Shine, J. Ramsey, F. Hernández. Mass spectrometric identification and structural analysis of the third-generation synthetic cannabinoids on the UK market since the 2013 legislative ban. *Forensic Toxicol.*, **2017**, *35*, 376–388.

[7] K. N. Moore, D. Garvin, B. F. Thomas, M. Grabenauer. Identification of Eight Synthetic Cannabinoids, Including 5F-AKB48 in Seized Herbal Products Using DART-TOF-MS and LC-QTOF-MS as Nontargeted Screening Methods. *J. Forensic Sci.*, **2017**, 1–8.

[8] C. Liu, W. Jia, Z. Hua, Z. Qian. Identification and analytical characterization of six synthetic cannabinoids NNL-3, 5F-NPB-22-7 N , 5F-AKB-48-7 N , 5F-EDMB-

PINACA, EMB-FUBINACA, and EG-018. *Drug Test. Anal.*, **2017**, DOI 10.1002/dta.2160.

[9] J. Lobo Vicente, H. Chassaigne, M. V. Holland, F. Reniero, K. Kolář, S. Tirendi, I. Vandecasteele, I. Vinckier, C. Guillou. Systematic analytical characterization of new psychoactive substances: A case study. *Forensic Sci. Int.*, **2016**, *265*, 107–115.

[10] M. E. Liechti. Novel psychoactive substances (designer drugs): Overview and pharmacology of modulators of monoamine signalling. *Swiss Med. Wkly.*, **2015**, *145*, 1–12.

[11] R. G. Pertwee. The diverse CB1 and CB2 receptor pharmacology of three plant cannabinoids: Δ9-tetrahydrocannabinol, cannabidiol and Δ9-tetrahydrocannabivarin. *Br. J. Pharmacol.*, **2008**, 199–215.

[12] J. Tournebize, V. Gibaja, J.-P. Kahn. Acute effects of synthetic cannabinoids: Update 2015. *Subst. Abus.*, **2016**, *7077*, 1–23.

[13] I. Yamagishi, K. Minakata, H. Nozawa, K. Hasegawa, M. Suzuki, T. Kitamoto, O. Suzuki, K. Watanabe. A case of intoxication with a mixture of synthetic cannabinoids EAM-2201, AB-PINACA and AB-FUBINACA, and a synthetic cathinone α-PVP. *Leg. Med.*, **2018**, *35*, 44–49.

[14] C. R. Harris, A. Brown. Synthetic Cannabinoid Intoxication: A Case Series and Review. *J. Emerg. Med.*, **2013**, *44*, 360–366.

[15] M. Kusano, K. Zaitsu, K. Taki, K. Hisatsune, J. Nakajima, T. Moriyasu, T. Asano, Y. Hayashi, H. Tsuchihashi, A. Ishii. Fatal intoxication by 5F–ADB and diphenidine: Detection, quantification, and investigation of their main metabolic pathways in humans by LC/MS/MS and LC/Q-TOFMS. *Drug Test. Anal.*, **2018**, *10*, 284–293.

[16] B. Barceló, S. Pichini, V. López-Corominas, I. Gomila, C. Yates, F. P. Busardò, M. Pellegrini. Acute intoxication caused by synthetic cannabinoids 5F-ADB and MMB-

2201: A case series. *Forensic Sci. Int.*, **2017**, *273*, e10–e14.

[17] B. Lovrecic, M. Lovrecic. Novel psychoactive synthetic cannabinoids and synthetic cathinones: the never-ending story of potential clinical toxicity. *Heroin Addict Relat Clin Probl*, **2018**, *20*, 13–24.

[18] L. Zattera, J. Errasti, A. Supervía. Intoxicación por el cannabinoide sintético 5-fluoro-ABD, adquirido como ketamina. *Med. Clin. (Barc).*, **2018**, *151*, 168.

[19] A. L. Ninnemann, W. V. Lechner, A. Borges, C. W. Lejuez. Synthetic cannabinoids to avoid urine drug screens: Implications for contingency management and other treatments for drug dependence. *Addict. Behav.*, **2016**, *63*, 72–73.

[20] X. Diao, M. Huestis. Approaches, Challenges, and Advances in Metabolism of New Synthetic Cannabinoids and Identification of Optimal Urinary Marker Metabolites. *Clin. Pharmacol. Ther.*, **2017**, *101*, 239–253.

[21] M. Jang, I. Shin, J. Kim, W. Yang. Simultaneous quantification of 37 synthetic cannabinoid metabolites in human urine by liquid chromatography-tandem mass spectrometry. *Forensic Toxicol.*, **2015**, *33*, 221–234.

[22] K. B. Scheidweiler, M. J. Y. Jarvis, M. A. Huestis. Nontargeted SWATH acquisition for identifying 47 synthetic cannabinoid metabolites in human urine by liquid chromatography-high-resolution tandem mass spectrometry. *Anal. Bioanal. Chem.*, **2015**, *407*, 883–897.

[23] M. Jang, I. S. Kim, Y. N. Park, J. Kim, I. Han, S. Baeck, W. Yang, H. H. Yoo. Determination of urinary metabolites of XLR-11 by liquid chromatography–quadrupole time-of-flight mass spectrometry. *Anal. Bioanal. Chem.*, **2016**, *408*, 503–516.

[24] M. S. Castaneto, A. Wohlfarth, S. Pang, M. Zhu, K. B. Scheidweiler, R. Kronstrand, M. A. Huestis. Identification of AB-FUBINACA metabolites in human hepatocytes

and urine using high-resolution mass spectrometry. *Forensic Toxicol.*, **2015**, *33*, 295–310.

[25] X. Diao, J. Carlier, M. Zhu, S. Pang, R. Kronstrand, K. B. Scheidweiler, M. A. Huestis. In vitro and in vivo human metabolism of a new synthetic cannabinoid NM-2201 (CBL-2201). *Forensic Toxicol.*, **2017**, *35*, 20–32.

[26] S. Vikingsson, H. Gréen, L. Brinkhagen, S. Mukhtar, M. Josefsson. Identification of AB-FUBINACA metabolites in authentic urine samples suitable as urinary markers of drug intake using liquid chromatography quadrupole tandem time of flight mass spectrometry. *Drug Test. Anal.*, **2016**, *8*, 950–956.

[27] D. Fabregat-Safont, M. Barneo-Muñoz, F. Martinez-Garcia, J. V. Sancho, F. Hernández, M. Ibáñez. Proposal of 5-methoxy-N-methyl-N-isopropyltryptamine consumption biomarkers through identification of in vivo metabolites from mice. *J. Chromatogr. A*, **2017**, *1508*, DOI 10.1016/j.chroma.2017.06.010.

[28] S. Savchuk, S. Appolonova, A. Pechnikov, L. Rizvanova, K. Shestakova, F. Tagliaro. In vivo metabolism of the new synthetic cannabinoid APINAC in rats by GC–MS and LC–QTOF-MS. *Forensic Toxicol.*, **2017**, *35*, 359–368.

[29] L. H. J. Richter, H. H. Maurer, M. R. Meyer. Metabolic fate of the new synthetic cannabinoid 7'N-5F-ADB in rat, human, and pooled human S9 studied by means of hyphenated high-resolution mass spectrometry. *Drug Test. Anal.*, **2018**, 1–13.

[30] R. C. Kevin, T. W. Lefever, R. W. Snyder, P. R. Patel, T. R. Fennell, J. L. Wiley, I. S. McGregor, B. F. Thomas. In vitro and in vivo pharmacokinetics and metabolism of synthetic cannabinoids CUMYL-PICA and 5F-CUMYL-PICA. *Forensic Toxicol.*, **2017**, *35*, 333–347.

[31] D. Dalvie, R. S. Obach, P. Kang, C. Prakash, C. M. Loi, S. Hurst, A. Nedderman, L. Goulet, E. Smith, H. Z. Bu, D. A. Smith. Assessment of three human in vitro systems

in the generation of major human excretory and circulating metabolites. *Chem. Res. Toxicol.*, **2009**, *22*, 357–368.

[32] F. Franz, V. Angerer, B. Moosmann, V. Auwärter. Phase I metabolism of the highly potent synthetic cannabinoid MDMB-CHMICA and detection in human urine samples. *Drug Test. Anal.*, **2017**, *9*, 744–753.

[33] X. Diao, A. Wohlfarth, S. Pang, K. B. Scheidweiler, M. A. Huestis. High-resolution mass spectrometry for characterizing the metabolism of synthetic cannabinoid THJ-018 and its 5-fluoro analog THJ-2201 after incubation in human hepatocytes. *Clin. Chem.*, **2016**, *62*, 157–169.

[34] A. Wohlfarth, S. Pang, M. Zhu, A. S. Gandhi, K. B. Scheidweiler, H. F. Liu, M. A. Huestis. First metabolic profile of XLR-11, a novel synthetic cannabinoid, obtained by using human hepatocytes and high-resolution mass spectrometry. *Clin. Chem.*, **2013**, *59*, 1638–1648.

[35] A. Cannaert, J. Storme, F. Franz, V. Auwärter, C. P. Stove. Detection and Activity Profiling of Synthetic Cannabinoids and Their Metabolites with a Newly Developed Bioassay. *Anal. Chem.*, **2016**, *88*, 11476–11485.

[36] J. L. Wiley, J. A. Marusich, T. W. Lefever, K. R. Antonazzo, M. T. Wallgren, R. A. Cortes, P. R. Patel, M. Grabenauer, K. N. Moore, B. F. Thomas. AB-CHMINACA, AB-PINACA, and FUBIMINA: Affinity and Potency of Novel Synthetic Cannabinoids in Producing 9-Tetrahydrocannabinol-Like Effects in Mice. *J. Pharmacol. Exp. Ther.*, **2015**, *354*, 328–339.

[37] S. D. Banister, J. Stuart, R. C. Kevin, A. Edington, M. Longworth, S. M. Wilkinson, C. Beinat, A. S. Buchanan, D. E. Hibbs, M. Glass, M. Connor, I. S. Mcgregor, M. Kassiou. Effects of Bioisosteric Fluorine in Synthetic Cannabinoid Designer Drugs JWH-018, AM-2201, UR-144, XLR-11, PB-22, 5F-PB-22, APICA, and STS-135. *ACS*

Chem. Neurosci., **2015**, *6*, 1445–1458.

[38] European Monitoring Centre for Drugs and Drug Addiction. Fentanils and synthetic cannabinoids : driving greater complexity into the drug situation. **2018**, DOI 10.2810/006358.

[39] A. Cannaert, F. Franz, V. Auwärter, C. P. Stove. Activity-Based Detection of Consumption of Synthetic Cannabinoids in Authentic Urine Samples Using a Stable Cannabinoid Reporter System. *Anal. Chem.*, **2017**, *89*, 9527–9536.

[40] C. Noble, A. Cannaert, K. Linnet, C. P. Stove. Application of an activity-based receptor bioassay to investigate the in vitro activity of selected indole- and indazole-3-carboxamide-based synthetic cannabinoids at CB1 and CB2 receptors. *Drug Test. Anal.*, **2018**, 1–11.

[41] O. J. Pozo, M. Ibáñez, J. V. Sancho, J. Lahoz-Beneytez, M. Farre, E. Papaseit, R. de la Torre, F. Hernandez. Mass Spectrometric Evaluation of Mephedrone In Vivo Human Metabolism: Identification of Phase I and Phase II Metabolites, Including a Novel Succinyl Conjugate. *Drug Metab. Dispos.*, **2014**, *43*, 248–257.

[42] M. Ibáñez, Ó. J. Pozo, J. V. Sancho, T. Orengo, G. Haro, F. Hernández. Analytical strategy to investigate 3,4-methylenedioxypyrovalerone (MDPV) metabolites in consumers' urine by high-resolution mass spectrometry. *Anal. Bioanal. Chem.*, **2016**, *408*, 151–164.

[43] J. Carlier, X. Diao, A. Wohlfarth, K. Scheidweiler, M. A. Huestis. In Vitro Metabolite Profiling of ADB-FUBINACA, A New Synthetic Cannabinoid. *Curr. Neuropharmacol.*, **2017**, *15*, 682–691.

[44] É. Alechaga, E. Moyano, M. T. Galceran. Ion-molecule adduct formation in tandem mass spectrometry. *Anal. Bioanal. Chem.*, **2016**, *408*, 1269–1277.

[45] J.-H. Kim, T. Y. Kong, J.-Y. Moon, K. H. Choi, Y.-Y. Cho, H. C. Kang, J. Y. Lee, H.

S. Lee. Targeted and non-targeted metabolite identification of MAM-2201 in human, mouse, and rat hepatocytes. *Drug Test. Anal.*, **2018**, *10*, 1328–1335.

[46] A. Wohlfarth, M. S. Castaneto, M. Zhu, S. Pang, K. B. Scheidweiler, R. Kronstrand, M. A. Huestis. Pentylindole/Pentylindazole Synthetic Cannabinoids and Their 5-Fluoro Analogs Produce Different Primary Metabolites: Metabolite Profiling for AB-PINACA and 5F-AB-PINACA. *AAPS J.*, **2015**, *17*, 660–677.

[47] M. Andersson, X. Diao, A. Wohlfarth, K. B. Scheidweiler, M. A. Huestis. Metabolic profiling of new synthetic cannabinoids AMB and 5F-AMB by human hepatocyte and liver microsome incubations and high-resolution mass spectrometry. *Rapid Commun. Mass Spectrom.*, **2016**, *30*, 1067–1078.

[48] C. Sauerschnig, M. Doppler, C. Bueschl, R. Schuhmacher. Methanol Generates Numerous Artifacts during Sample Extraction and Storage of Extracts in Metabolomics Research. *Metabolites*, **2017**, *8*, 1.

[49] A. J. Adams, S. D. Banister, L. Irizarry, J. Trecki, M. Schwartz, R. Gerona. "Zombie" Outbreak Caused by the Synthetic Cannabinoid AMB-FUBINACA in New York. *N. Engl. J. Med.*, **2017**, *376*, 235–242.

[50] S. N. Staeheli, A. E. Steuer, T. Kraemer. Identification of urinary metabolites of the synthetic cannabinoid 5F-CUMYL-P7AICA in human casework. *Forensic Sci. Int.*, **2019**, *294*, 76–79.

[51] M. S. Ibsen, M. Connor, M. Glass. Cannabinoid CB1 and CB2 Receptor Signaling and Bias. *Cannabis Cannabinoid Res.*, **2017**, *2*, 48–60.

[52] S. D. Banister, M. Longworth, R. Kevin, S. Sachdev, M. Santiago, J. Stuart, J. B. C. Mack, M. Glass, I. S. McGregor, M. Connor, M. Kassiou. Pharmacology of Valinate and tert -Leucinate Synthetic Cannabinoids 5F-AMBICA, 5F-AMB, 5F-ADB, AMB-FUBINACA, MDMB-FUBINACA, MDMB-CHMICA, and Their Analogues. *ACS*

Chem. Neurosci., **2016**, *7*, 1241–1254.

[53] M. B. Gatch, M. J. Forster. Cannabinoid-like effects of five novel carboxamide synthetic cannabinoids. *Neurotoxicology*, **2019**, *70*, 72–79.

[54] E. Wouters, L. Mogler, A. Cannaert, V. Auwärter, C. Stove. Functional evaluation of carboxy metabolites of synthetic cannabinoid receptor agonists featuring scaffolds based on L-valine or L- tert -leucine. *Drug Test. Anal.*, **2019**, dta.2607.

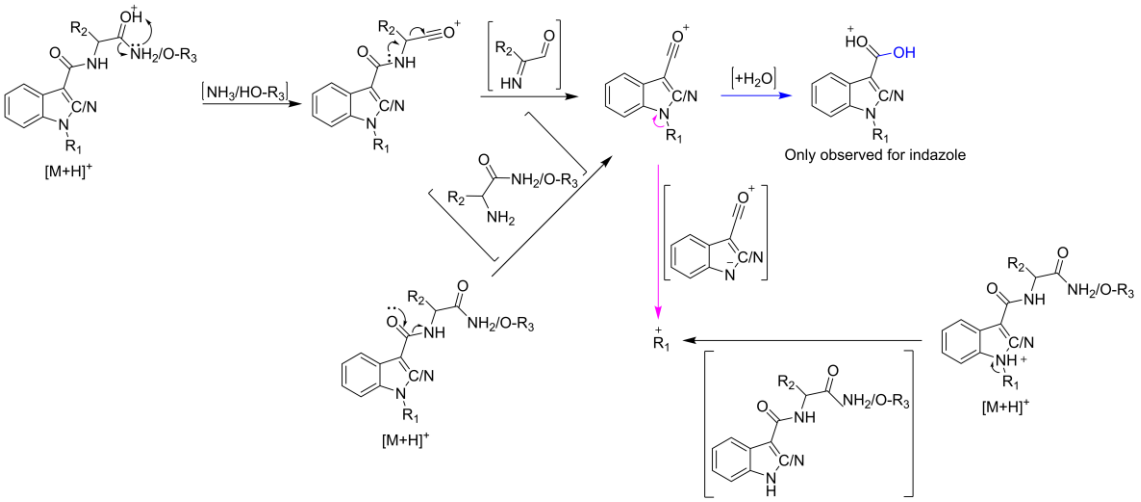

Fig. 1 Common fragmentation pathway for 5F-APP-PICA and AMB-FUBINACA. Moieties that are different between both cannabinoids are indicated with a "/"

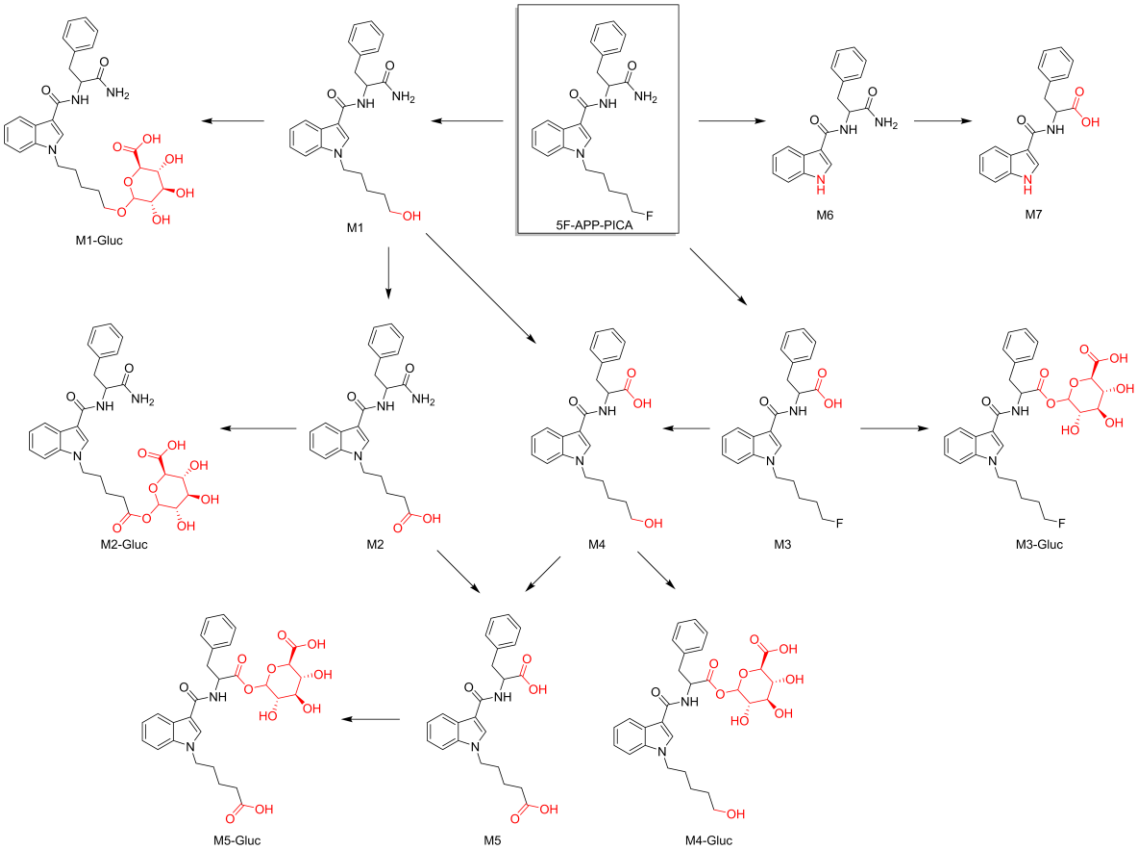

Fig. 2 Proposed metabolic pathway for 5F-APP-PICA, based on the metabolites elucidated by UHPLC-HRMS

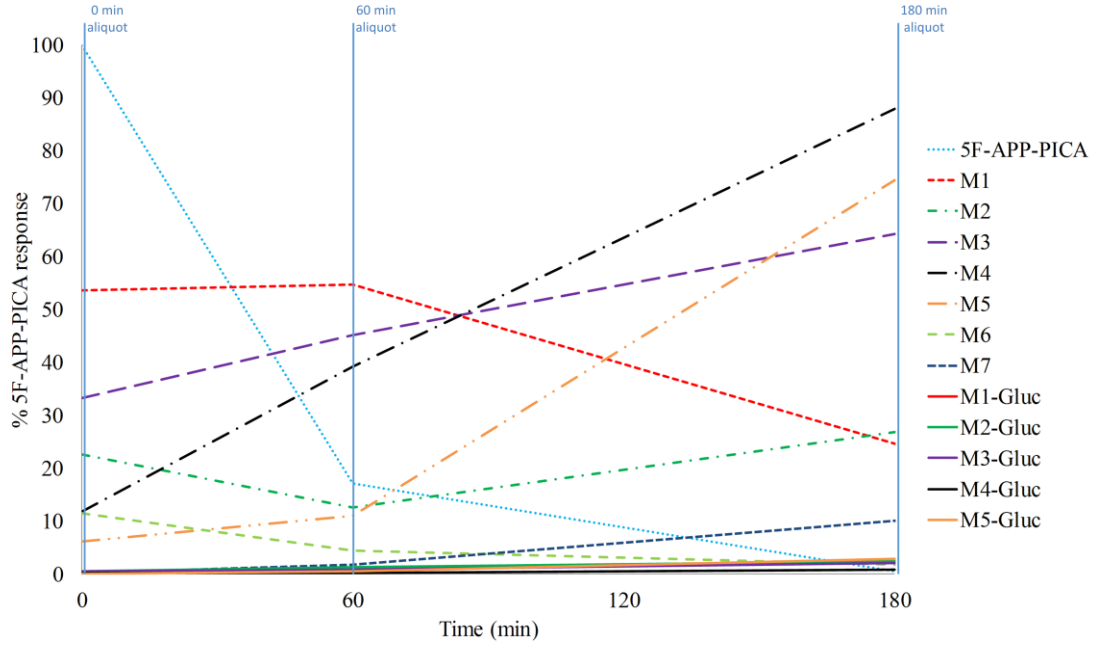

Fig. 3 Prevalence of 5F-APP-PICA and its metabolites in incubation over time. Signals are relative to those obtained for 5F-APP-PICA at 0 min

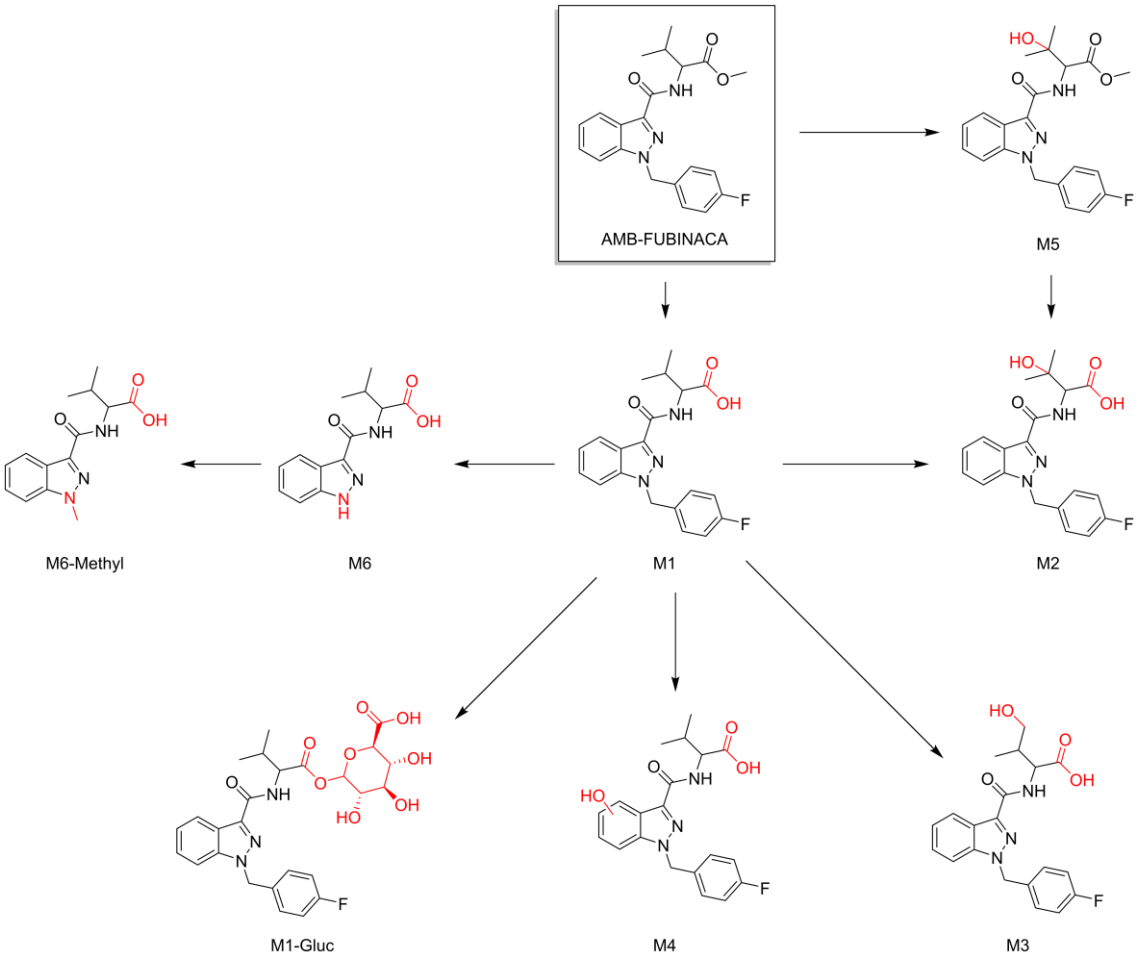

Fig. 4 Proposed metabolic pathway for AMB-FUBINACA, based on the metabolites elucidated by UHPLC-HRMS

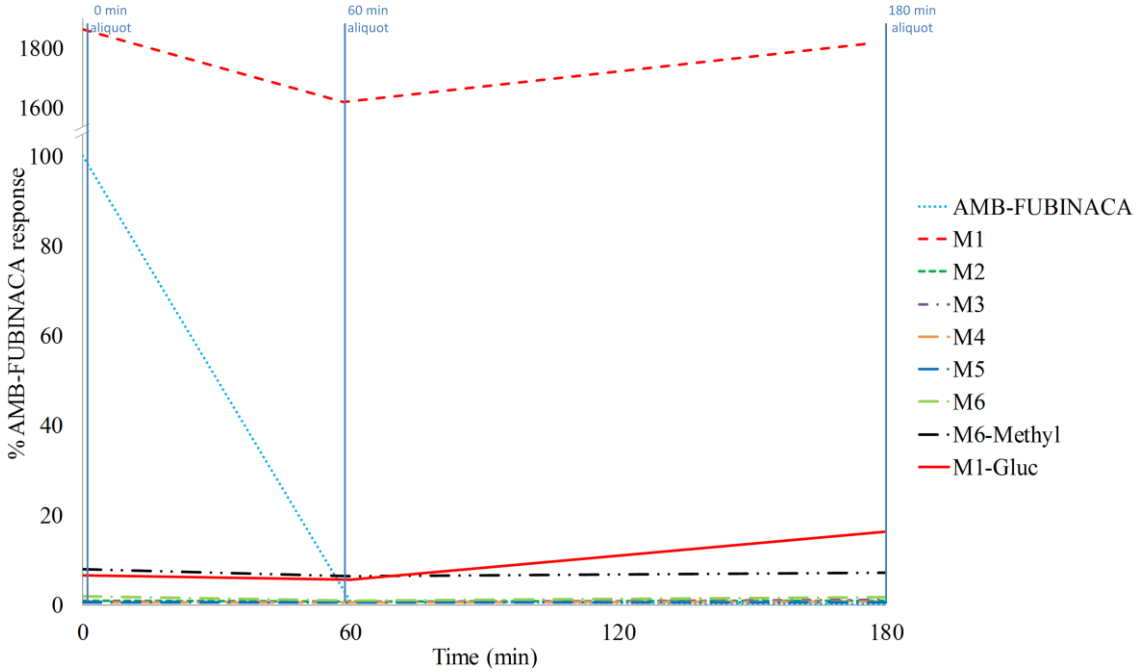

Fig. 5 Prevalence of AMB-FUBINACA and its metabolites in incubation over time. Signals are relative to those obtained for AMB-FUBINACA at 0 min

Table 1 Half maximal effective concentration (EC_{50}) and efficacy (E_{max}) of 5F-APP-PICA, AMB-FUBINACA and JWH-018 (control) at CB1 and CB2. The range of concentrations between brackets indicates the 95% confidence interval (CI).

Compound	EC_{50} (95% CI) (nM)		E_{max} (95% CI) (%)	
	CB1	CB2	CB1	CB2
5F-APP-PICA	-	83.2 (52.6–132)	-	96.6 (86.1–107)
AMB-FUBINACA	9.84 (0.56–17.3)	2.40 (1.30-4.42)	265 (237–292)	153 (139–167)
JWH-018 (control)	41.0 (33.4–50.3)	12.3 (9.89–15.4)	99.3 (95.8–103)	104 (100–108)

Electronic Supplementary Information

3. Results and discussion

3.3. 5F-APP-PICA metabolites

Phase I metabolites

As it has been commented, 7 different phase I metabolites were identified for 5F-APP-PICA. The 5 major metabolites (M1-M5) were initially identified in ESI^+, and also detected in ESI^- but showing lower sensitivity. The acquisition in ESI^- allowed the identification of 2 additional minor metabolites (M6-M7), not observed in ESI^+.

M1-M5 presented the same fragment at *m/z* 144 (also present in 5F-APP-PICA, see **Table SI1**), corresponding to the indole ring bonded to the carbonyl moiety ($C_9H_6NO^+$). Moreover, these metabolites (except M4) presented a fragment at *m/z* 116 corresponding to the indole ring ($C_8H_6N^+$). These two fragments evidenced that the indole moiety was not changed during hepatocyte incubation, unlike other synthetic cannabinoids for which the hydroxylation of the indole moiety has been reported [31,44]. Regarding M6 and M7 the fragment ion at *m/z* 116 ($C_8H_6N^-$) was also observed, indicating that this moiety remained unaltered. Thus, the biotransformations should be placed in the alkylic chain, both amide moieties, and/or the aromatic ring bonded to the α carbon atom of amide moieties.

M1 showed a $[M+H]^+$ at *m/z* 394.2116 ($C_{23}H_{28}N_3O_3^+$, -2.31 ppm), which would correspond to an oxidative defluorination. This hypothesis was confirmed after fragmentation evaluation. Fragment 2 (*m/z* 230.1170, $C_{14}H_{16}NO_2^+$, -1.93 ppm) corresponded to the indole ring, with the carbonyl moiety and the *N*-alkylic chain. The corresponding fragment was also present in 5F-APP-PICA (*m/z* 232). Moreover, Fragment 5 (*m/z* 87.0809, $C_5H_{11}O^+$, 5.11 ppm) corresponded to the *N*-alkyl disconnection and release of the 5-hydroxypentanylium ion, confirming the position of the hydroxyl group in the alkylic chain. After the dehydration of Fragment 5, cyclopentylium ion (*m/z* 69.0705, $C_5H_9^+$, 8.96 ppm) was observed for both M1 and 5F-APP-PICA. Other observed fragments (see **Table SI1**) could be justified based on the proposed

structure of M1. MS/MS spectra at 10 and 50 eV for M1, and the proposed fragmentation pathway can be found in **Figure SI5** and **Figure SI6**, respectively.

M2 $[M+H]^+$ was found at *m/z* 408.1908 ($C_{23}H_{26}N_3O_4^+$, -2.42 ppm), and corresponded to the oxidation of the hydroxyl group present in the *N*-alkyl chain of M1. Similarly to M1, fragments at *m/z* 244.0963 ($C_{14}H_{14}NO_3^+$, -1.95 ppm) *m/z* 101.6000 ($C_5H_9O_2^+$, 2.66 ppm) established the position of the biotransformation to be in the alkylic chain. Fragment 6 (*m/z* 83.0496, $C_5H_7O^+$, 5.78 ppm) was produced after Fragment 5 dehydration (similarly to M1), while Fragment 7 (*m/z* 55.0550, $C_4H_7^+$, 14.33 ppm) was produced after a CO loss from Fragment 6. These fragmentations can only be justified if there is a carboxylic acid moiety in the *N*-alkyl chain. Additional fragments (see **Table SISI1**) were justified based on the proposed structure. In **Figure SI7**, MS/MS spectra at 10 and 50 eV can be observed, and **Figure SI8** shows the proposed fragmentation pathway for M2.

M3 $[M+H]^+$ was observed at *m/z* 397.1916 ($C_{23}H_{26}FN_2O_3^+$, -2.42 ppm), corresponding to an oxidative deamination from 5F-APP-PICA. The four observed fragments were the same observed for 5F-APP-PICA (see **Table SI1**): *m/z* 232, 144, 116, and 69. Nevertheless, 5F-APP-PICA, and also M1 and M2, presented the loss of an ammonia molecule which was not observed for M3, indicating that the oxidative deamination occurred in the terminal amide moiety. Finally, the fragmentation pathway was proposed (**Figure SI10**) based on the MS/MS fragmentation at 10 and 50 eV (**Figure SI9**).

M4 presented a $[M+H]^+$ at *m/z* 395.1958 ($C_{23}H_{27}N_2O_4^+$, -1.85 ppm), corresponding to an oxidative defluorination plus an oxidative deamination. This metabolite shared some fragments with M1 (see **Table SI1**), concretely at *m/z* 230, 144, 87, and 69. Only the fragment ion corresponding to the indole ring (*m/z* 116) and the corresponding to the ammonia loss were not present in M4. This behaviour indicates that M4 correspond to the oxidative defluorination of the *N*-alkylic chain, followed by oxidative deamination of the terminal amide moiety (or vice

versa). In other words, M4 comes from M1 after an oxidative deamination, or from M3 after an oxidative defluorination. Once all the fragments were justified based on the structure of the metabolite, a plausible fragmentation pathway was proposed (**Figure SI12**). Additionally, MS/MS spectra at 10 and 50 eV can be checked in **Figure SI11**.

M5 $[M+H]^+$ was observed at *m/z* 409.1751 ($C_{23}H_{25}N_2O_5^+$, -1.61 ppm), sharing 6 fragment ions with M2 (see **Table SI1** and **Figure SI13**): *m/z* 244, 144, 116, 101, 83, and 55. Ammonia loss was not observed for this metabolite. Based on this information, this metabolite could be produced after the oxidation of the hydroxyl group present in the *N*-alkylic chain of M4, or after the oxidative deamination of M2. Thus, M5 presented two carboxylic acid moieties in both sides of the molecule. Finally, the fragmentation pathway of M5 was proposed, based on compound structure and observed fragmentation (**Figure SI14**).

M6 and M7 were only observed in ESI^-, presenting low sensitivity. M6 $[M–H]^-$ was detected at *m/z* 306.1250 ($C_{18}H_{16}N_3O_2^-$, 4.14 ppm). As explained previously, the detection of the fragment at *m/z* 116 (indole ring) revealed that this moiety was not affected during hepatocyte incubation. Based on the elemental composition, the biotransformation should correspond to the *N*-dealkylation of 5F-APP-PICA. Only two fragment ions were observed (see **Table SI1**), being Fragment 1 (*m/z* 189.0663, $C_{10}H_9N_2O_2^-$, 2.36 ppm) the loss of the indole ring as a neutral loss, and Fragment 2 the indole ring itself (*m/z* 116.0494, $C_8H_6N^-$, -0.91 ppm). **Figure SI15** shows MS/MS spectra at 10 and 50 eV. The fragmentation pathway proposed can be seen in **Figure SI16**.

M7 was the last phase I metabolite identified, which $[M–H]^-$ was found at *m/z* 307.1089 ($C_{18}H_{16}N_2O_3^-$, 3.90 ppm). The fragment at *m/z* 190.0504 ($C_{10}H_8NO_3^-$, 3.90 ppm) (see **Table SI1**) would be equivalent to *m/z* 189 in M6, whereas the fragment at *m/z* 116 was common to M6. Following the same metabolic pathway than M3, M4 and M5, and based on the elemental composition calculated, M7 was obtained after an oxidative deamination from M6 (the terminal

amide moiety changed to a carboxylic acid). The other three observed fragments (Fragments 2, 3 and 5, **Table SI1**) confirmed the hypothesis of the oxidative deamination from M6. Finally, a fragmentation pathway was proposed (**Figure SI18**), justifying all the fragments observed in MS/MS spectra at 10 and 50 eV (**Figure SI17**).

Phase II metabolites

Once identified the phase I metabolites, the phase II metabolites were searched for by considering different conjugations to phase I metabolites. Glucuronide, sulphate, phosphate and glutathione conjugates were investigated in both ionisation modes. Up to 5 glucuronides conjugates were detected in the DDA acquisition and thus, acquired in MS/MS in order to confirm the structure of the phase II metabolites (**Table SI1**).

M1-Gluc and M2-Gluc were only detected in ESI^-. For M1-Gluc, only the $[M–H]^-$ was observed, without any fragment ion, probably due to its low sensitivity or abundance. M2-Gluc showed 2 fragment ions: Fragment 1 at *m/z* 406, corresponding to the loss of the glucuronide (and thus, releasing the $[M–H]^-$ of M2), and Fragment 2 at *m/z* 116, corresponding to the indole ring. MS/MS spectra at 10 eV for M1-Gluc, and at 10 and 50 eV for M2-Gluc for both phase II metabolites are shown in **Figure SI19** and **Figure SI20**, respectively.

M3-Gluc, M4-Gluc and M5-Gluc were detected in both ionisation modes, but presenting a higher sensitivity in ESI^+. All the fragments ions were shared with their corresponding phase I metabolites (see **Table SI1**), being highly specific and locating the unequivocal position of the glucuronidation for metabolites M4 and M5 which possess two possible conjugation sites. So, M3, M4 and M5 presented conjugation on the carboxylic acid moiety linked to the amide moiety. MS/MS spectra at 10 and 50 eV corresponding to these three metabolites can be found in **Figure SI21** (M3-Gluc), **Figure SI22** (M4-Gluc) and **Figure SI23** (M5-Gluc).

3.4. AMB-FUBINACA metabolites

Phase I metabolites

M1-M5 presented a common fragment at *m/z* 109 ($C_7H_6F^+$), also present in AMB-FUBINACA, which corresponds to the fluorotropylium fragment ion. The presence of this unaltered fragment indicated that no biotransformations were expected on the fluorobenzyl side-chain. The absence of biotransformations on this moiety has also been described for other synthetic cannabinoids with an *N*-fluorobenzyl, such as AB-FUBINACA and ADB-FUBINACA [25,42].

M1 $[M+H]^+$ was observed at *m/z* 370.1560 ($C_{20}H_{21}FN_3O_3^+$, -0.30 ppm), corresponding to a demethylation. The presence of a water molecule loss (*m/z* 352.1455, $C_{20}H_{19}FN_3O_2^+$, -0.30 ppm) followed by a CO loss (*m/z* 324.1506, $C_{19}H_{19}FN_3O^+$, -0.29 ppm) indicated an *O*-demethylation in the terminal methyl ester moiety. This pathway is similar to AMB-FUBINACA, which presented a methanol loss (fragment at *m/z* 352) followed by a CO loss (fragment at *m/z* 324). Other fragments at *m/z* 271, 253 and 109 were shared with AMB-FUBINACA (see **Table SI2**). The high response of M1 allowed the detection of an additional fragment at *m/z* 72.0815 ($C_4H_{10}N^+$, 10.43 ppm), corresponding to the nitrogen atom bonded to the isopropyl moiety. After that, a plausible fragmentation pathway was proposed (**Figure SI25**) based on the MS/MS fragmentation at 10 and 30 eV (**Figure SI24**).

M2, M3 and M4 were observed at *m/z* 386, all 3 corresponding to hydroxylations of M1 (for the information of their complete fragmentation, see **Table SI2**). The position of the hydroxylation point was successfully determined after an accurate fragmentation study. The easiest one was M4 (*m/z* 386.1507, $C_{20}H_{21}FN_3O_4^+$, -0.95 ppm), rapidly identified after the evaluation of their fragments at *m/z* 269.0719 ($C_{15}H_{10}FN_2O_2^+$, -0.57 ppm) and *m/z* 109. The presence of the unaltered fluorotropylium ion (Fragment 3) indicated that the hydroxylation was on the indazole ring. The Fragment 2 (*m/z* 269) would correspond to the fragment ion 4 of AMB-FUBINACA (*m/z* 253). All fragments observed in MS/MS spectra (**Figure SI26**) were

successfully justified based on the proposed structure, and the fragmentation pathway was also proposed (**Figure SI27**).

M2 (*m/z* 386.1508, $C_{20}H_{21}FN_3O_4^+$, -0.63 ppm) and M3 (*m/z* 386.1513, $C_{20}H_{21}FN_3O_4^+$, 0.71 ppm) structures were not so directly identified as M4. The presence of a fragment ion at *m/z* 253 (shared with AMB-FUBINACA) revealed that the indazole and fluorophenyl moieties were not changed. Both compounds presented an initial loss of a water molecule (fragment at *m/z* 368); for M3, a second loss of water was observed (*m/z* 350) whereas for M2 the loss of water plus CO was found (fragment at *m/z* 322) (see **Table SI2**). As AMB-FUBINACA presented also the loss of a water molecule followed by a CO loss, it was expected that M2 and M3 were hydroxylated on the isopropyl moiety, explaining the second water loss observed for these metabolites. Nevertheless, M3 presented a characteristic fragment ion, which revealed the position of the hydroxyl group in this metabolite. The Fragment 3 of M3 (*m/z* 310.1349, $C_{18}H_{17}FN_3O^+$, -0.52 ppm) corresponded to a CH_2O + CO loss from Fragment 1. The CO loss was originated from the carbonyl moiety after the first water loss; the CH_2O loss could only be explained if the hydroxyl group was in one of the methyl groups of the isopropyl moiety. This CH_2O + CO loss was not observed for M2, and the fragmentation occurred through losses of water and CO molecules, indicating that the hydroxyl group should be on the tertiary carbon of the isopropyl group. All the fragment ions observed for M2 and M3 (see **Table SI2**) in the MS/MS spectra at 10 and 30 eV (**Figure SI28** and **Figure SI30**, respectively) were successfully justified based on the proposed structure, and their fragmentation pathways could be proposed (**Figure SI29** and **Figure SI31**, respectively).

M5 (*m/z* 400.1674, $C_{21}H_{23}FN_3O_4^+$, 1.69 ppm) was produced after the hydroxylation of AMB-FUBINACA. On the basis of the fragmentation observed for the parent compound and M2-M4, the position of the hydroxyl group could be directly stablished. As a fragment ion at *m/z* 253 was observed, the hydroxylation on the indazole ring was discarded. M5 fragmentation

was similar to M3, keeping in mind that M3 was *O*-demethylated respect M5. Fragment at *m/z* 350 (Fragment 2) was observed for M5 and M3, and the CH_2O loss observed for M2 was not present. Based on these premises, M5 should have a hydroxyl on the tertiary carbon of the isopropyl. The proposed fragmentation pathway (**Figure SI33**) could justify all the observed fragments in MS/MS spectra at 10 and 30 eV (**Figure SI32**).

M6 was observed at *m/z* 262.1185 ($C_{13}H_{16}N_3O_3^+$, -0.57 ppm), and its elemental composition revealed that this metabolite should be produced after an *N*-dealkylation from M1, as the mass difference respect to the parent, corresponded to a fluorobenzyl loss. Fragment 3 (*m/z* 145.0396, $C_8H_5N_2O^+$, -0.52 ppm) and 2 (Fragment 3+H_2O, *m/z* 163.0501, $C_8H_7N_2O_2^+$, -0.48 ppm) confirmed the *N*-dealkylation of this metabolite. Moreover, the consecutive losses of H_2O and CO observed in Fragment 1 (*m/z* 216.1131, $C_{12}H_{14}N_3O^+$, 0.02 ppm) confirmed the presence of a carboxylic acid moiety, as these losses were also observed for M1. Thus, all the MS/MS fragments (**Figure SI34**, **Table SI2**) were justified based on the proposed structure for M6, and the fragmentation pathway was stablished (**Figure SI35**).

M7 was the last phase I metabolite identified for AMB-FUBINACA, observed at *m/z* 276.1342 ($C_{14}H_{18}N_3O_3^+$, -0.23 ppm). Based on the elemental composition, it was expected that M7 was the *N*-dealkylation product of AMB-FUBINACA. Nevertheless, the fragmentation evaluation revealed that this preliminary evaluation was not the correct one. Similar to M6 and M1, the consecutive losses of H_2O and CO (Fragment 1, *m/z* 230.1288, $C_{13}H_{16}N_3O^+$, -0.15 ppm) indicated the presence of a carboxylic acid moiety on the molecule. Thus, M7 should also correspond to an *O*-demethylation. The correct position of this extra methyl moiety was determined by Fragment 3 (*m/z* 159.0552, $C_9H_7N_2O^+$, -0.52 ppm), locating it in the nitrogen of the indazole ring after an *N*-methylation of M6. On this way, a tentative fragmentation pathway (**Figure SI37**) was proposed for this structure, justifying all the MS/MS fragments (**Figure SI36**, **Table SI2**).

Phase II metabolites

Only one phase II metabolite was identified in the DDA analyses in ESI^+ and confirmed by MS/MS (**Table SI2**) to be the glucuronide corresponding to M1 (M1-Gluc).

M1-Gluc presented exactly the same fragmentation than M1, including the fragment ion corresponding to the loss of the glucuronide, this is, to M1 (Fragment 1, *m/z* 370). The complete fragmentation of M1-Gluc can be checked in **Table SI2**, and the MS/MS spectra in **Figure SI38**.

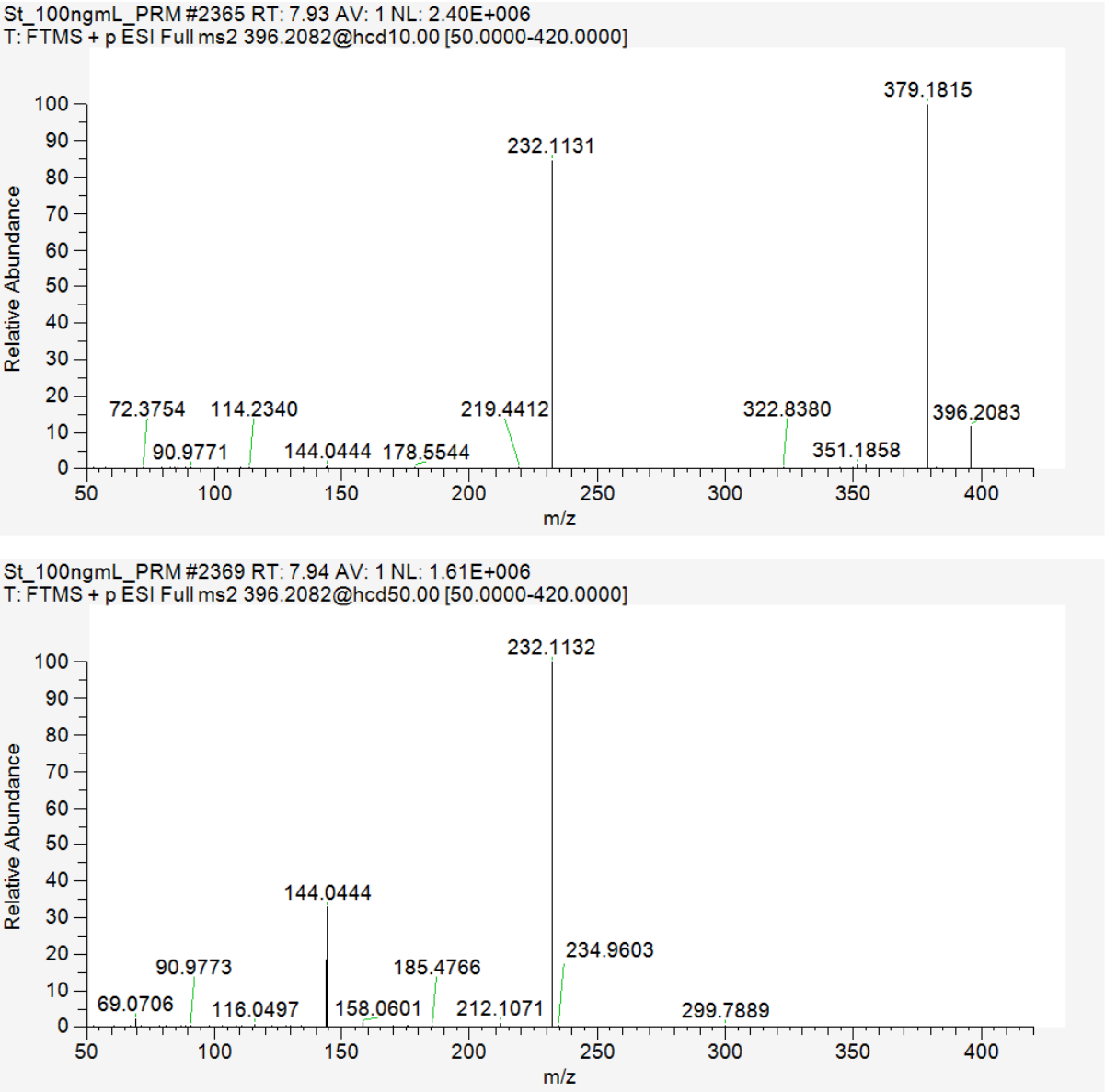

Figure SI1. MS/MS spectra of 5F-APP-PICA at 10 eV (top) and 50 eV (bottom) collision energy.

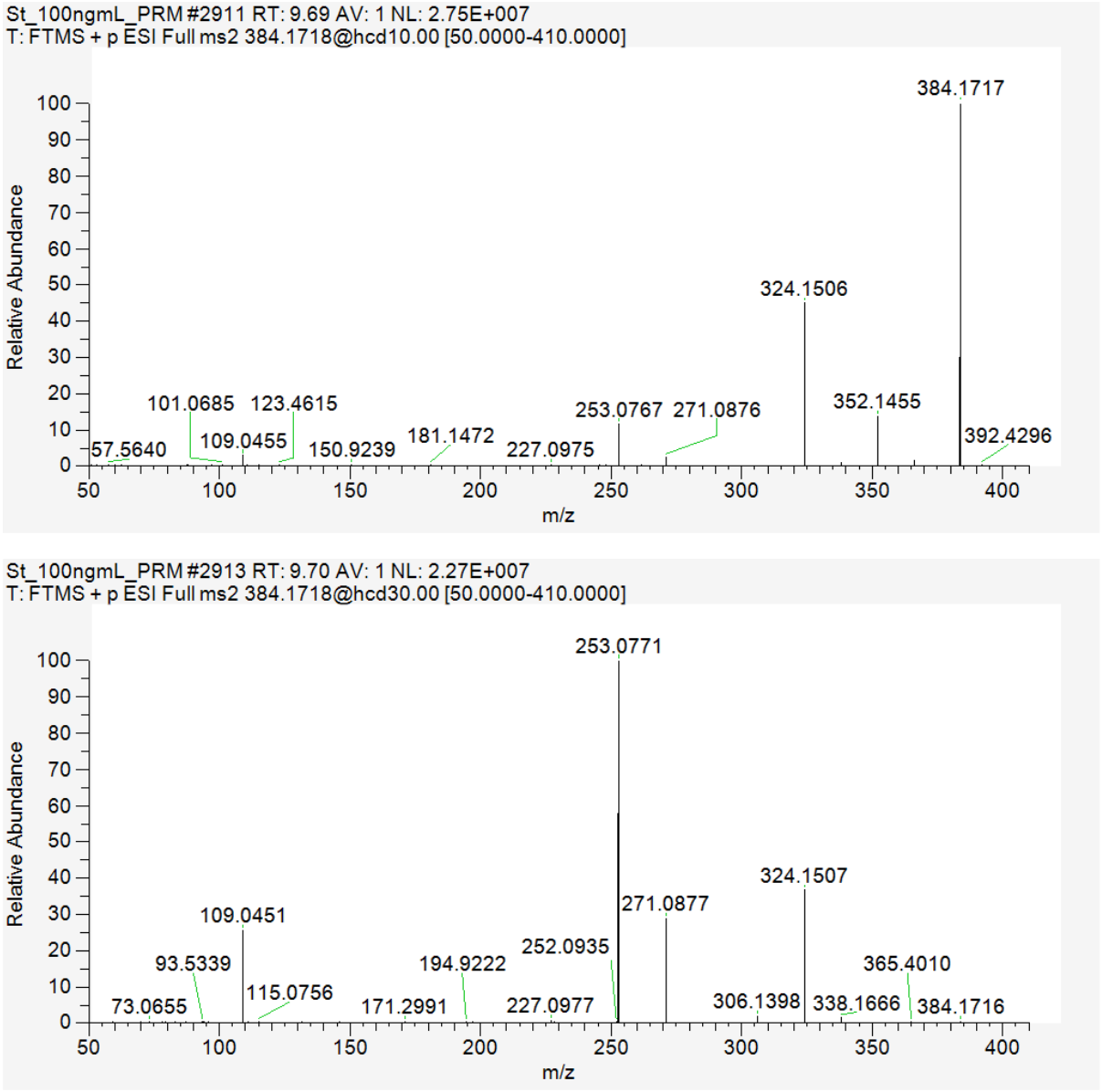

Figure SI2. MS/MS spectra of AMB-FUBINACA at 10 eV (top) and 30 eV (bottom) collision energy.

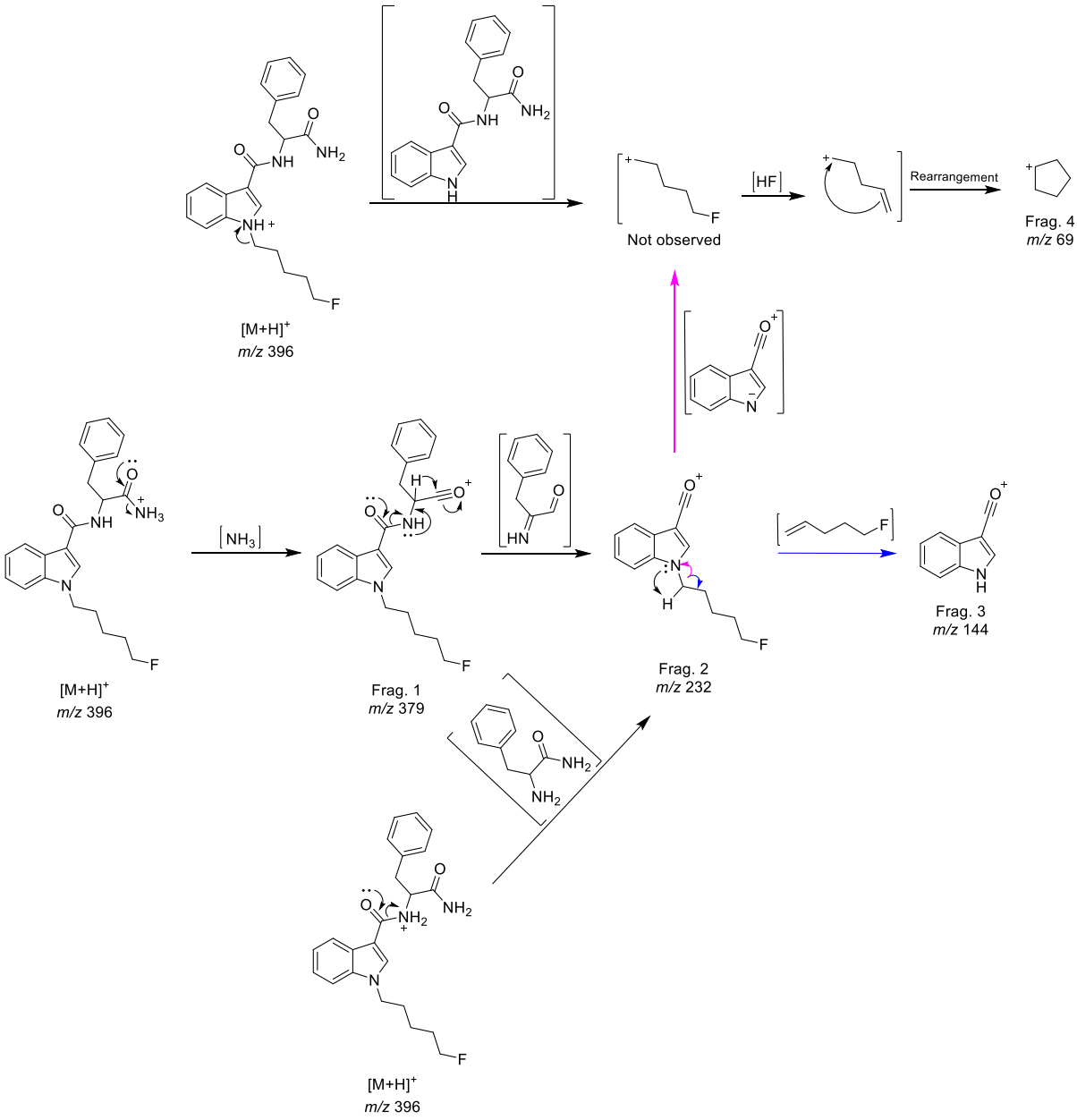

Figure SI3. Proposed fragmentation pathway for 5F-APP-PICA based on the observed MS/MS fragmentation.

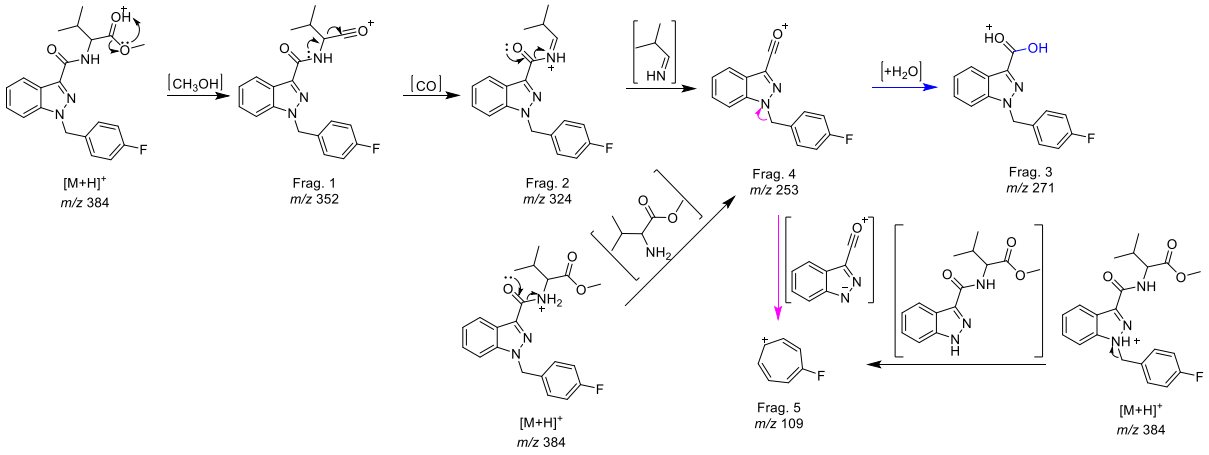

Figure SI2. Proposed fragmentation pathway for AMB-FUBINACA based on the observed MS/MS fragmentation.

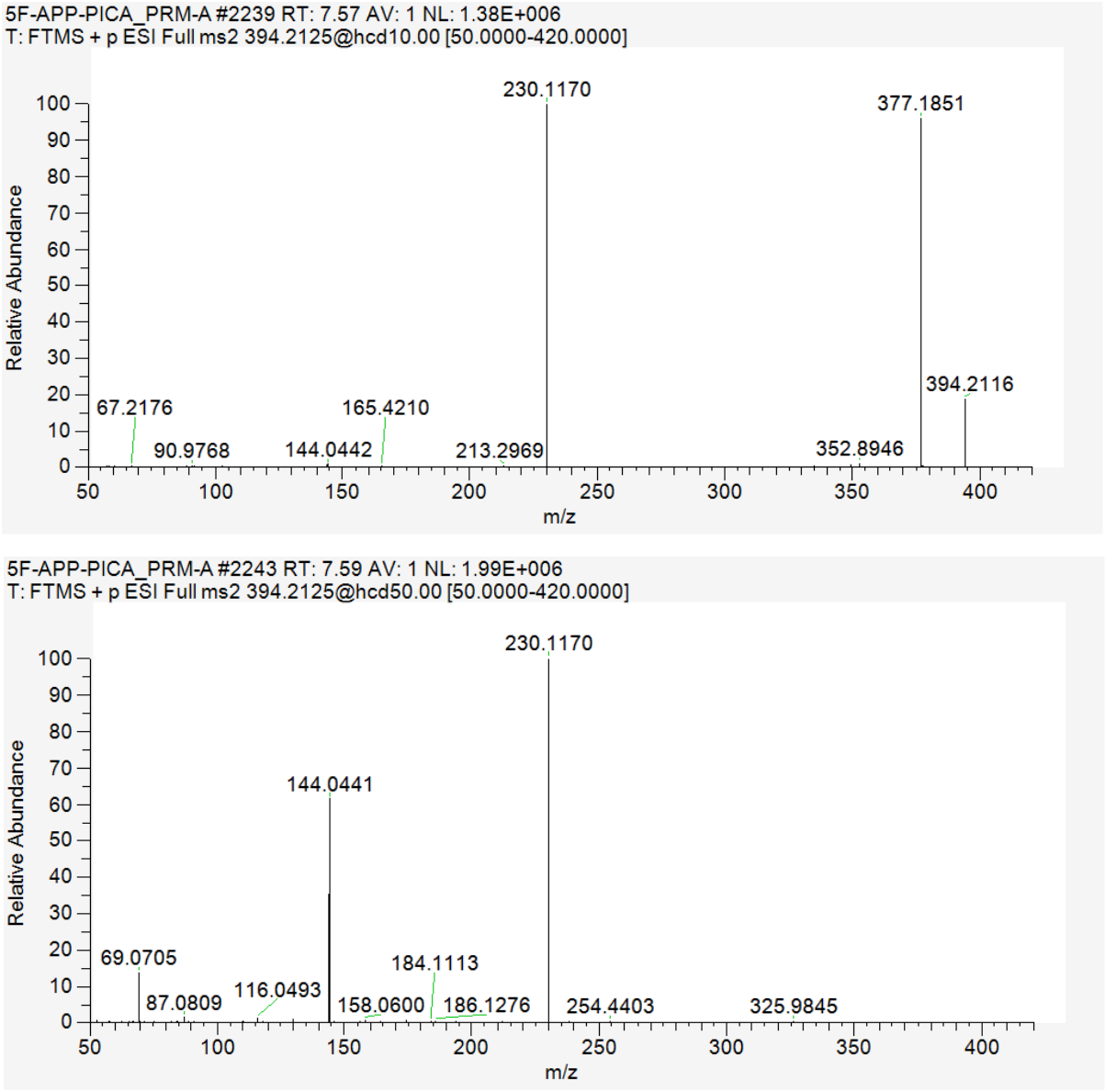

Figure SI3. MS/MS spectra of 5F-APP-PICA M1 at 10 eV (top) and 50 eV (bottom) collision energy.

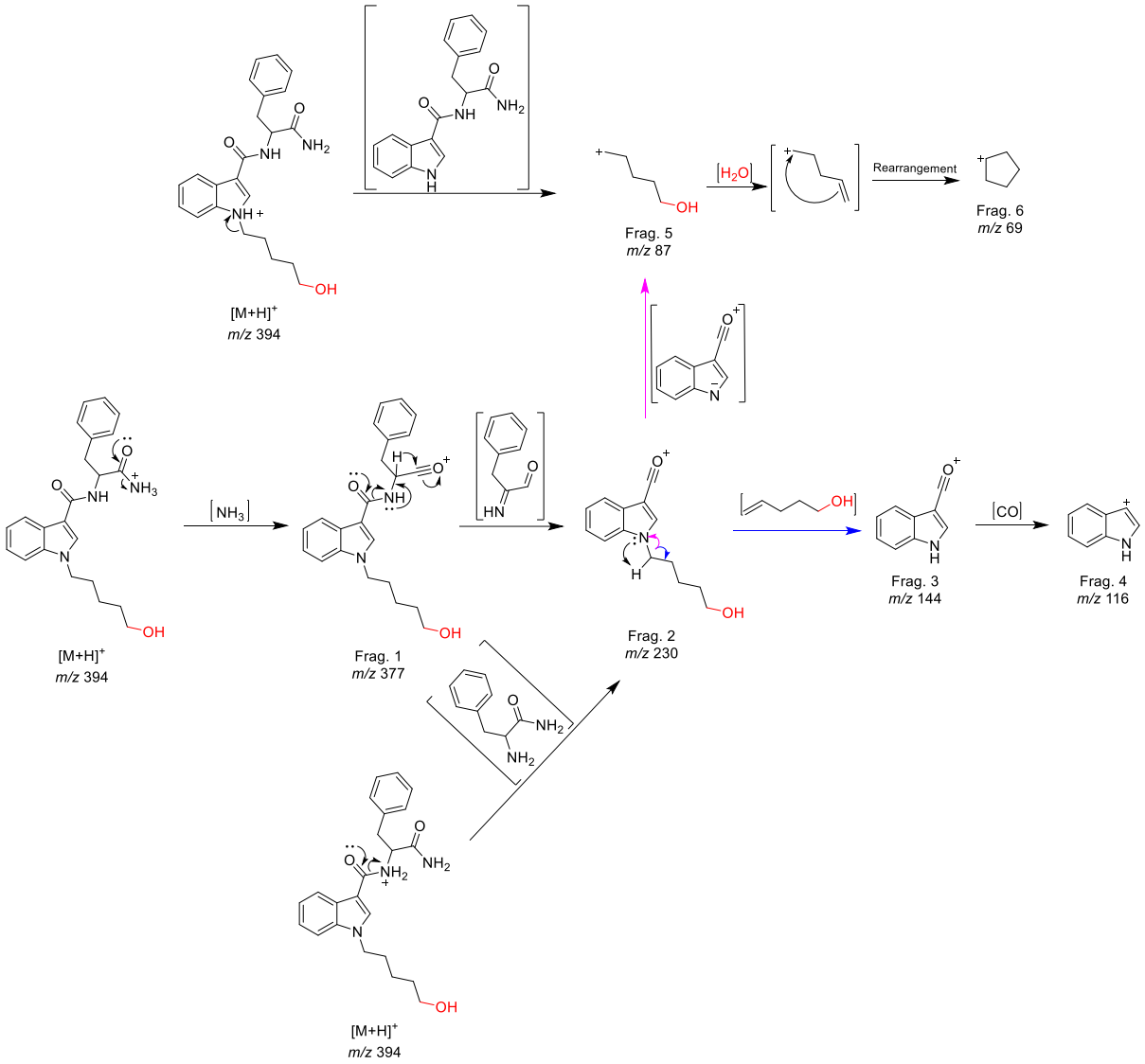

Figure SI4. Proposed fragmentation pathway for 5F-APP-PICA M1 based on the observed MS/MS fragmentation.

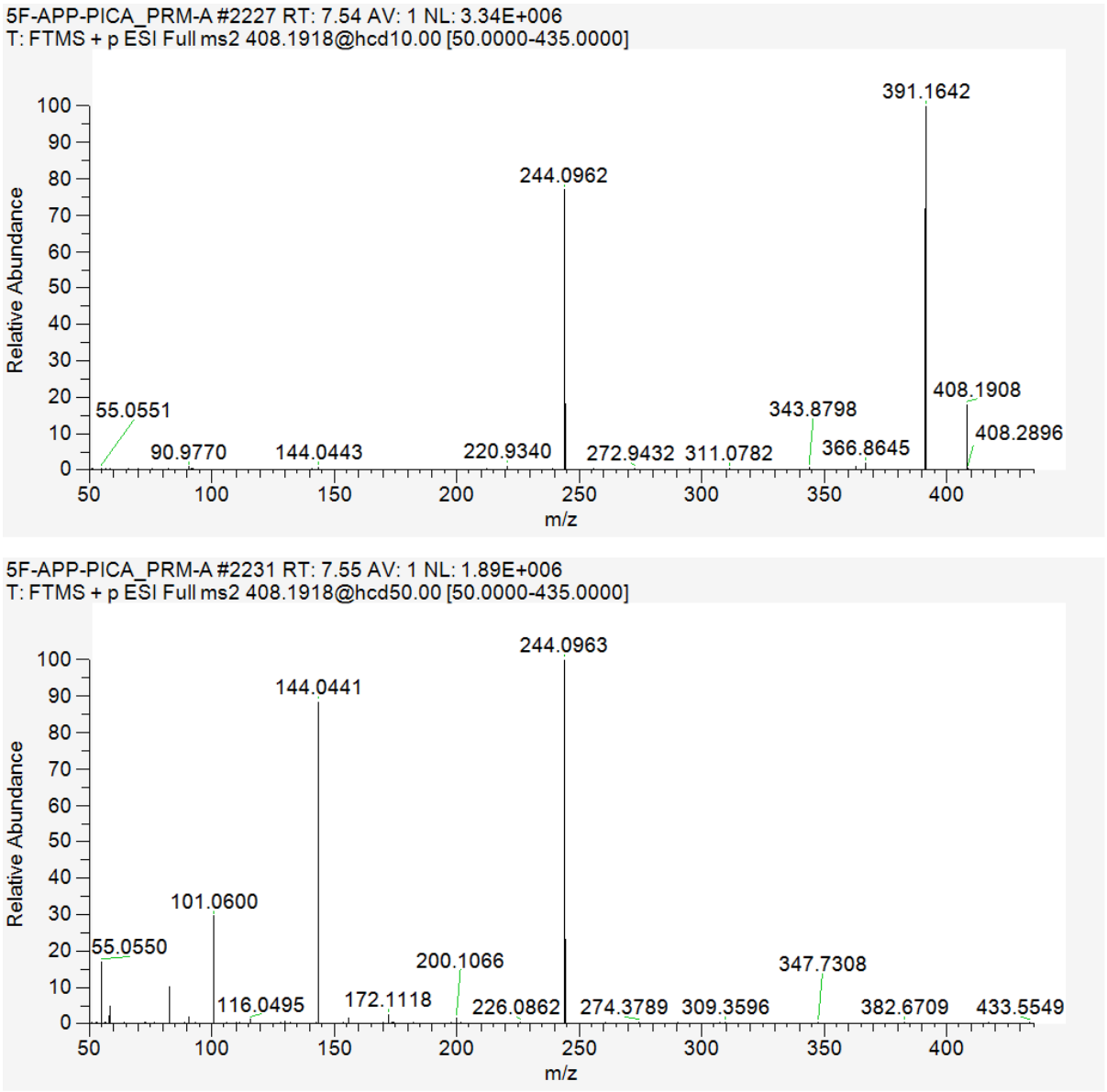

Figure SI5. MS/MS spectra of 5F-APP-PICA M2 at 10 eV (top) and 50 eV (bottom) collision energy.

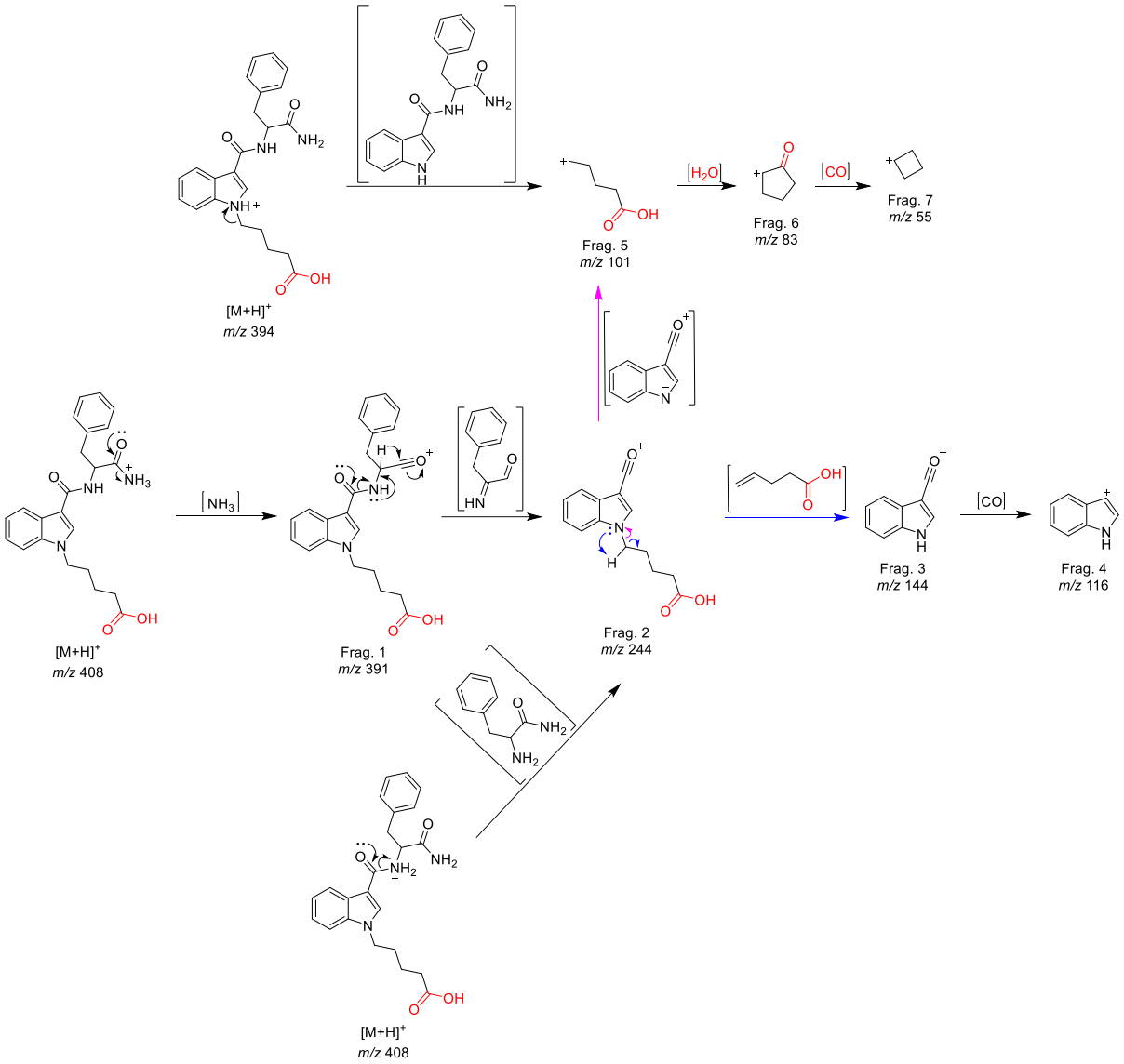

Figure SI6. Proposed fragmentation pathway for 5F-APP-PICA M2 based on the observed MS/MS fragmentation.

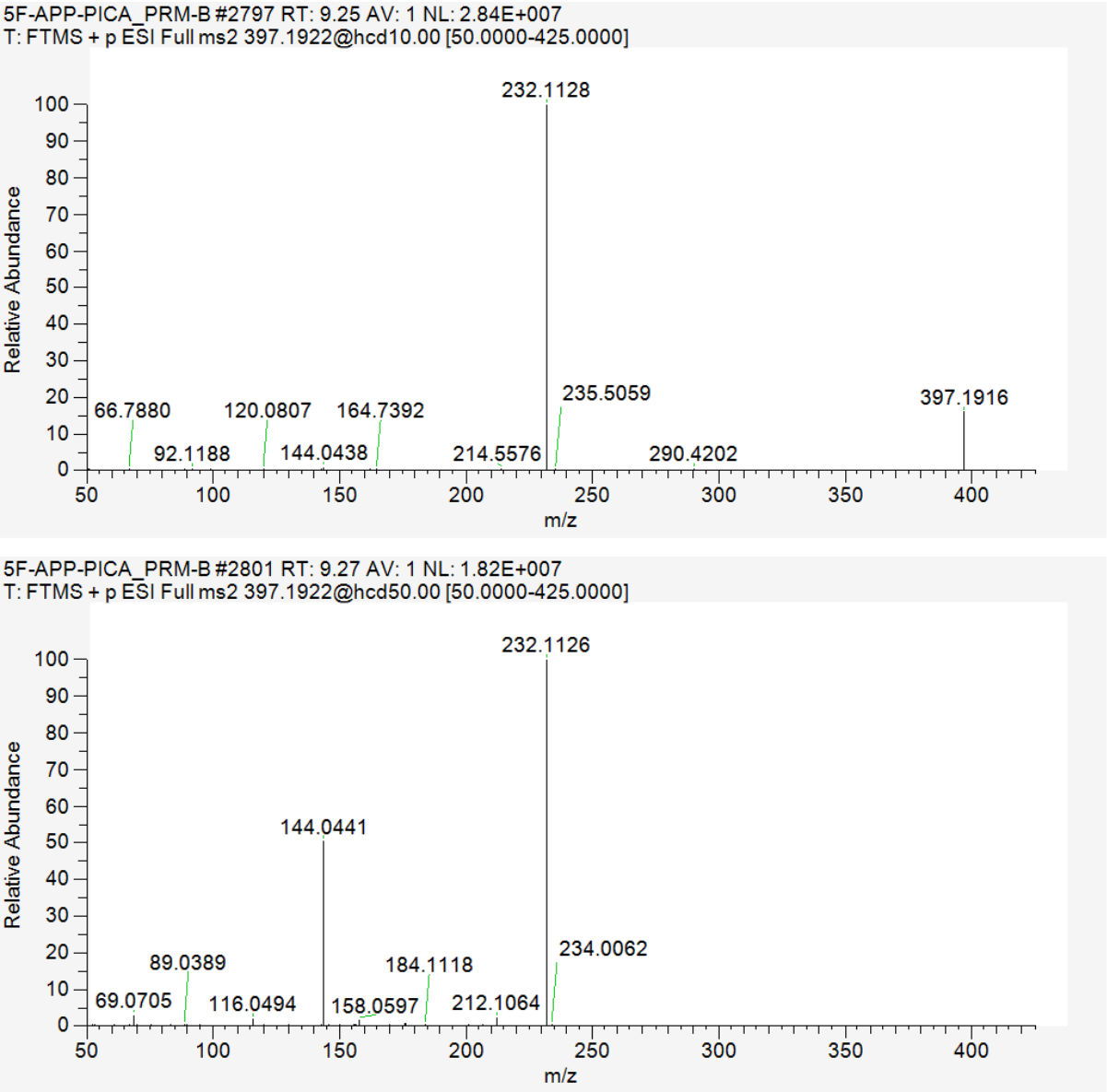

Figure SI7. MS/MS spectra of 5F-APP-PICA M3 at 10 eV (top) and 50 eV (bottom) collision energy.

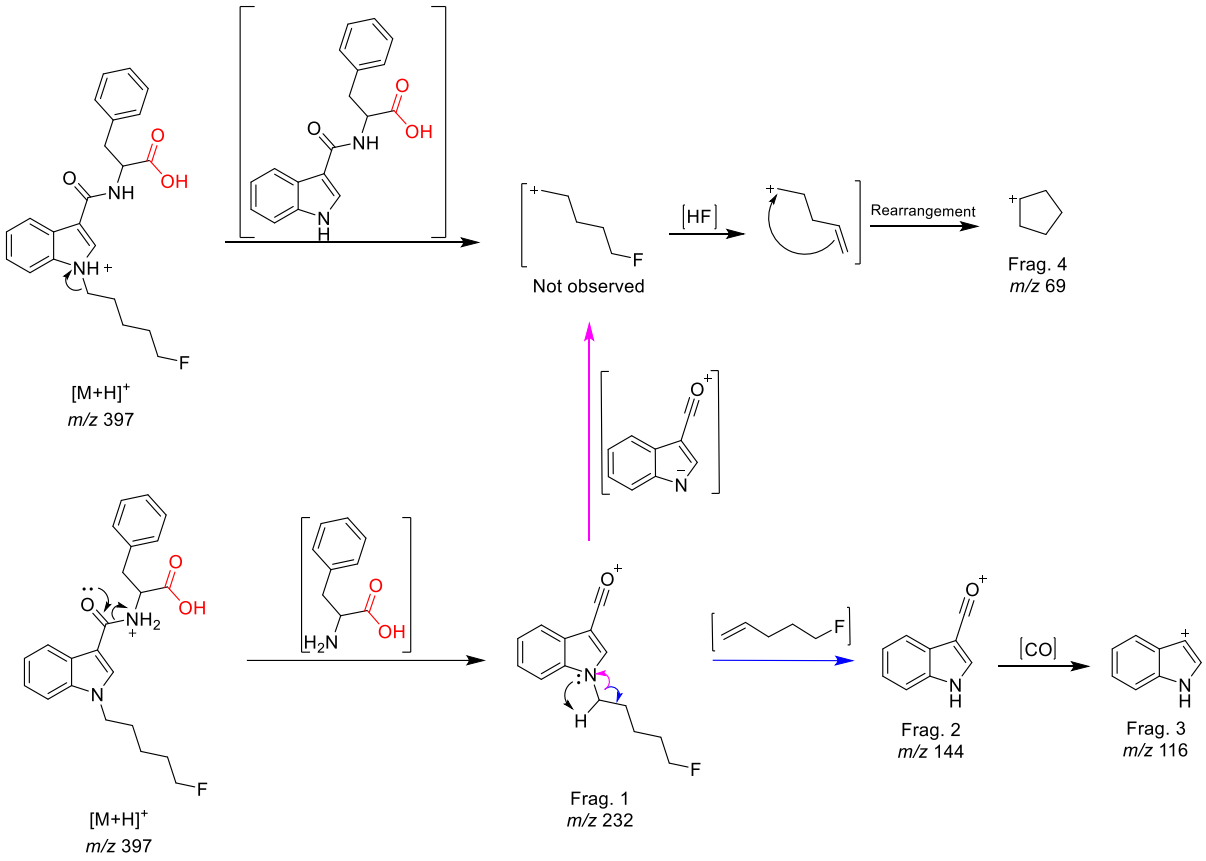

Figure SI8. Proposed fragmentation pathway for 5F-APP-PICA M3 based on the observed MS/MS fragmentation.

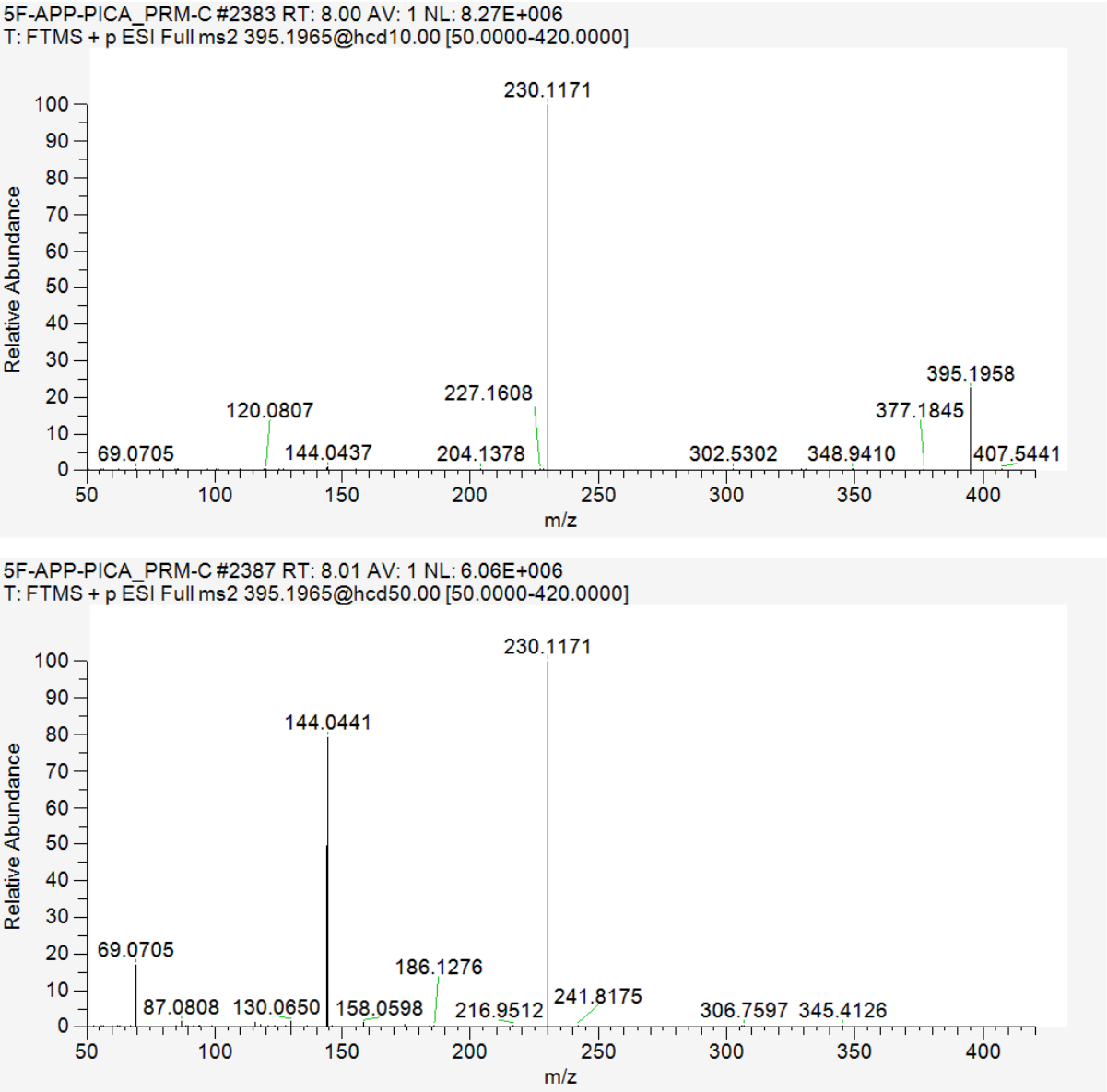

Figure SI9. MS/MS spectra of 5F-APP-PICA M4 at 10 eV (top) and 50 eV (bottom) collision energy.

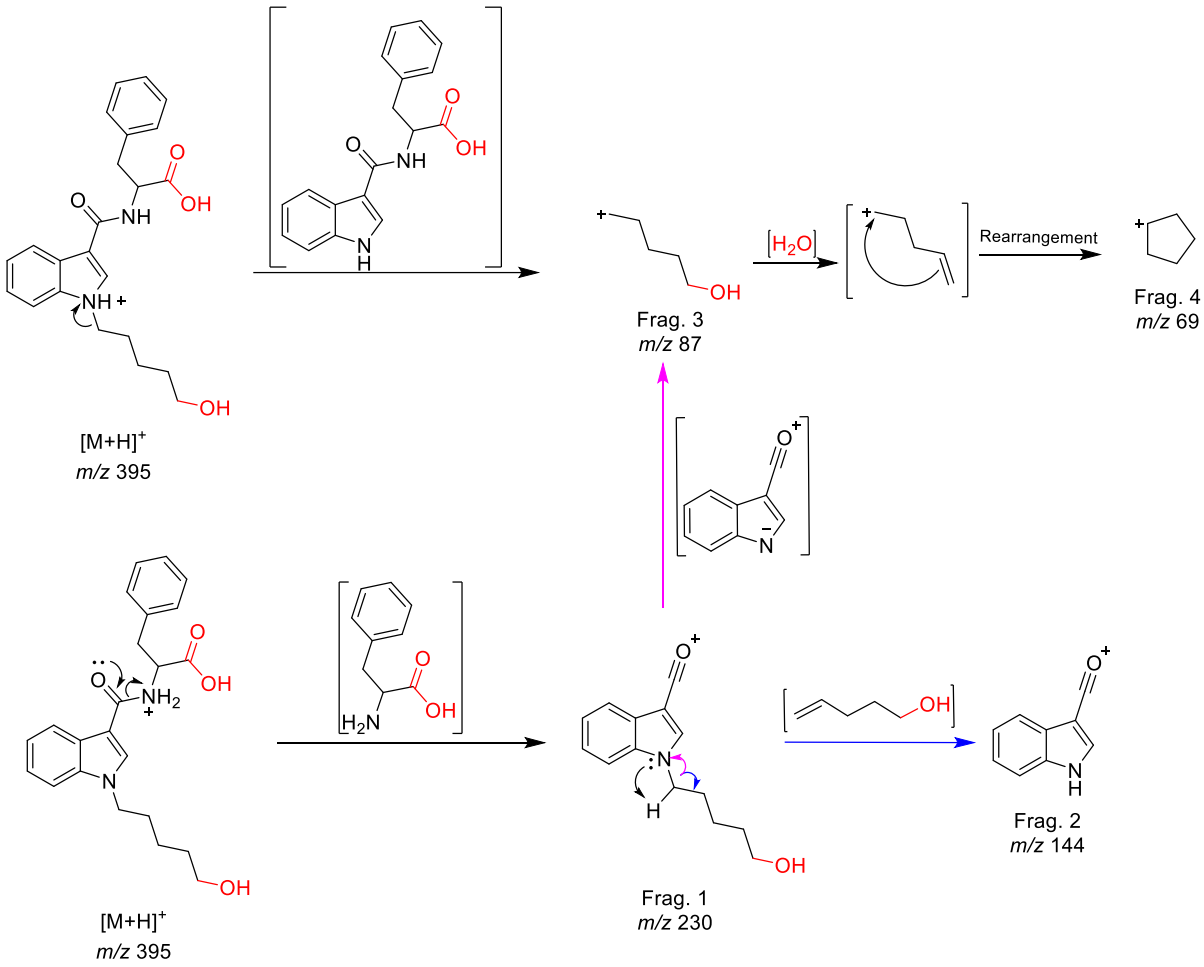

Figure SI10. Proposed fragmentation pathway for 5F-APP-PICA M4 based on the observed MS/MS fragmentation.

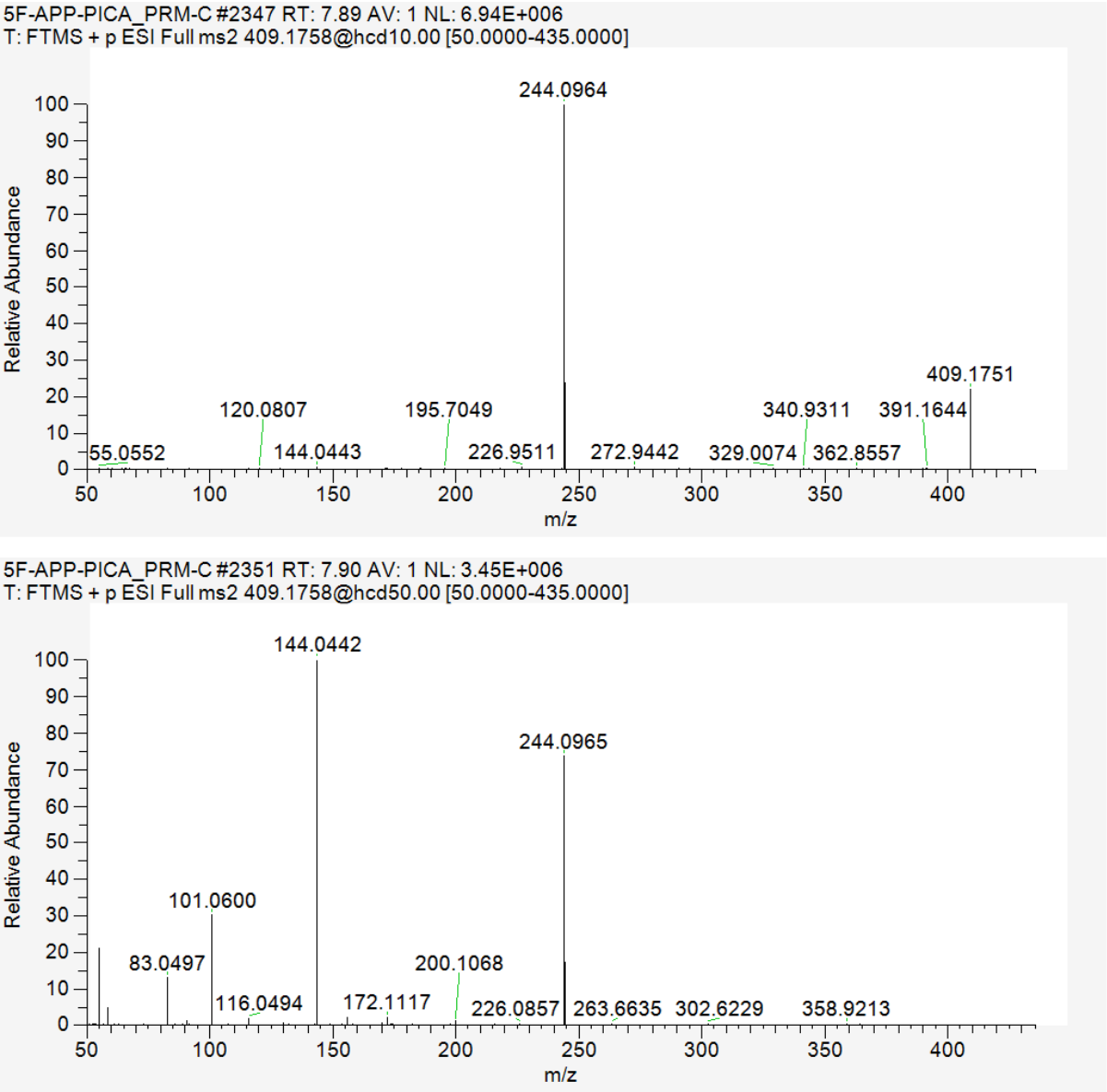

Figure SI11. MS/MS spectra of 5F-APP-PICA M5 at 10 eV (top) and 50 eV (bottom) collision energy.

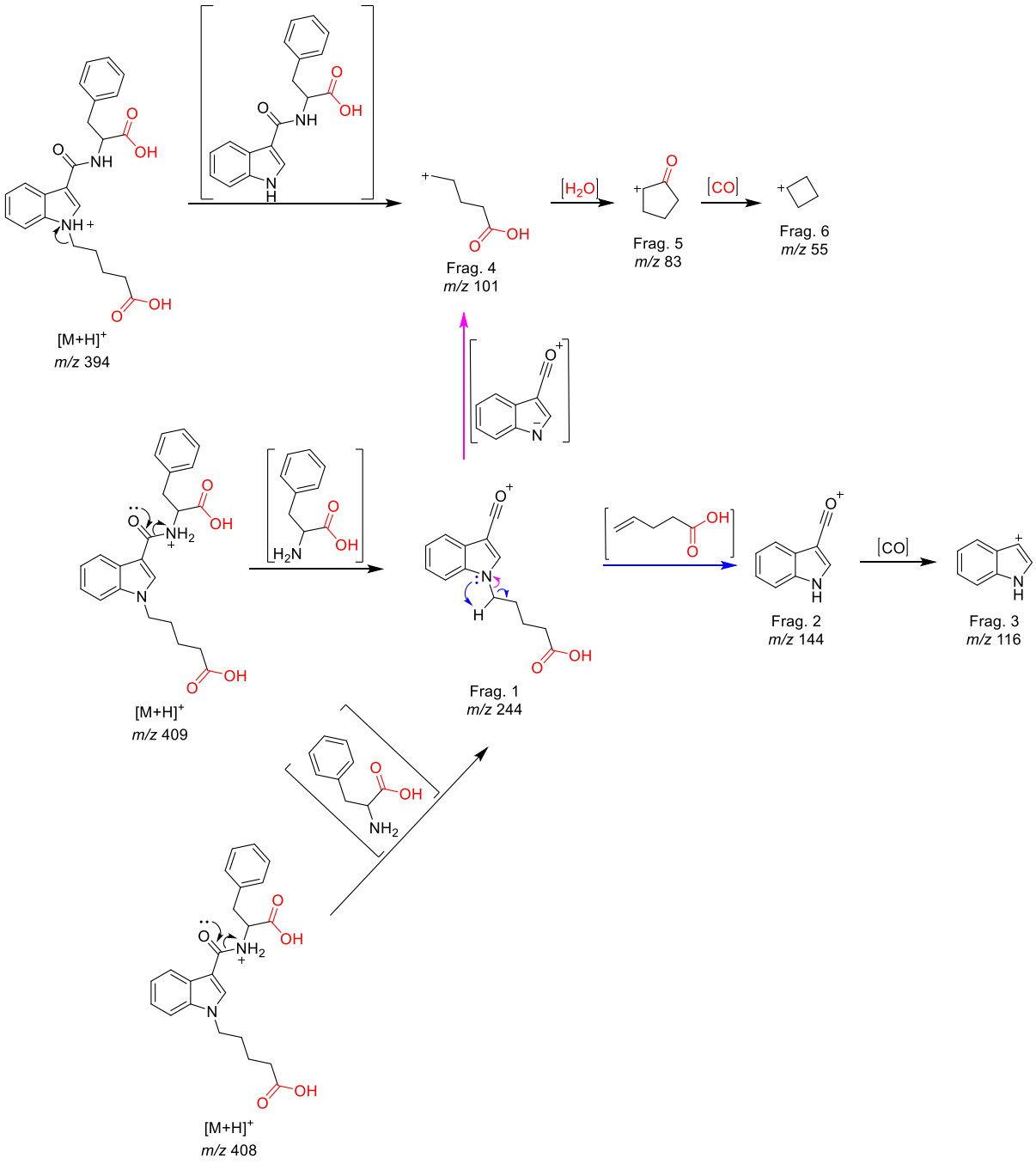

Figure SI12. Proposed fragmentation pathway for 5F-APP-PICA M5 based on the observed MS/MS fragmentation.

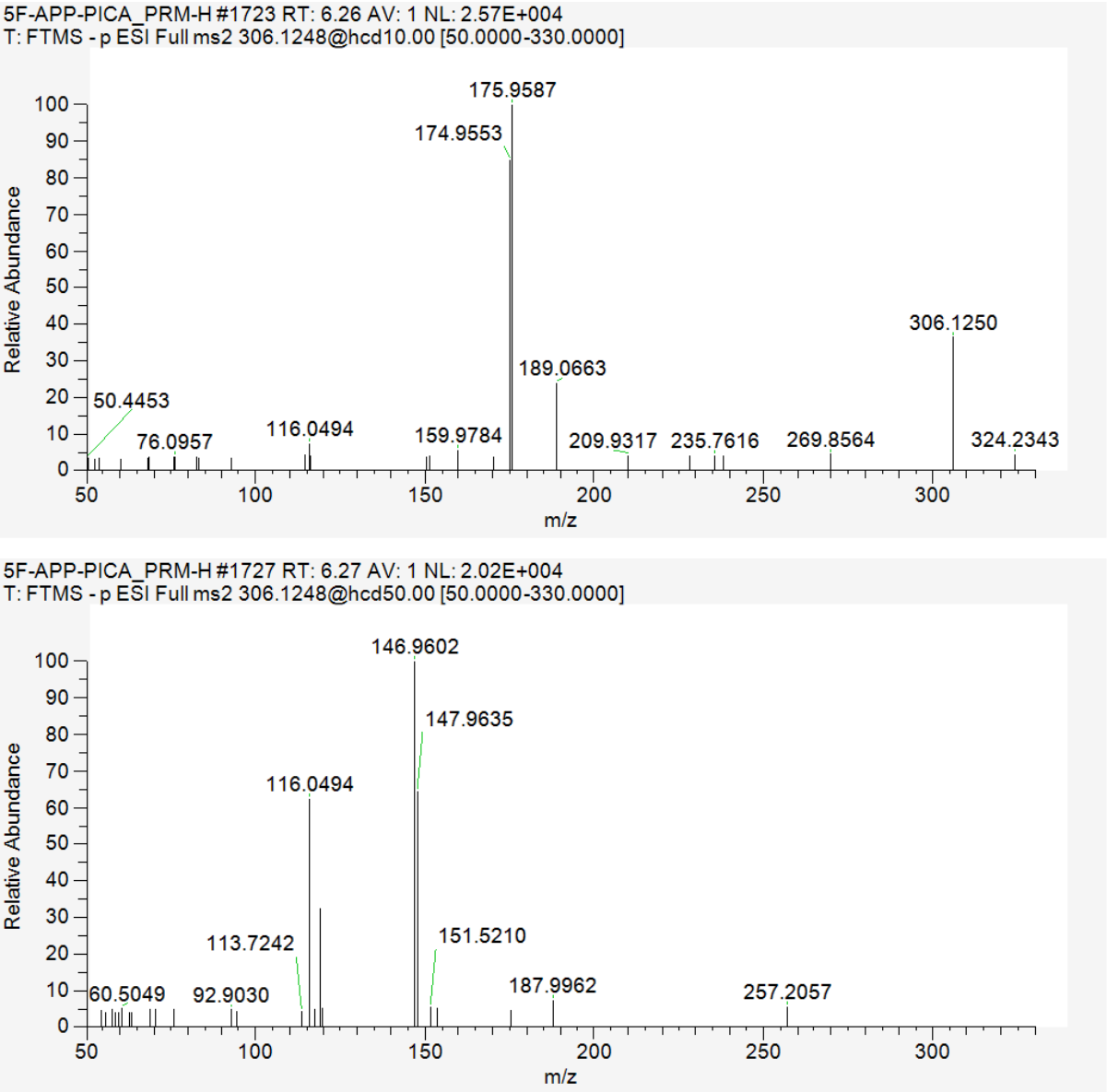

Figure SI13. MS/MS spectra of 5F-APP-PICA M6 at 10 eV (top) and 50 eV (bottom) collision energy.

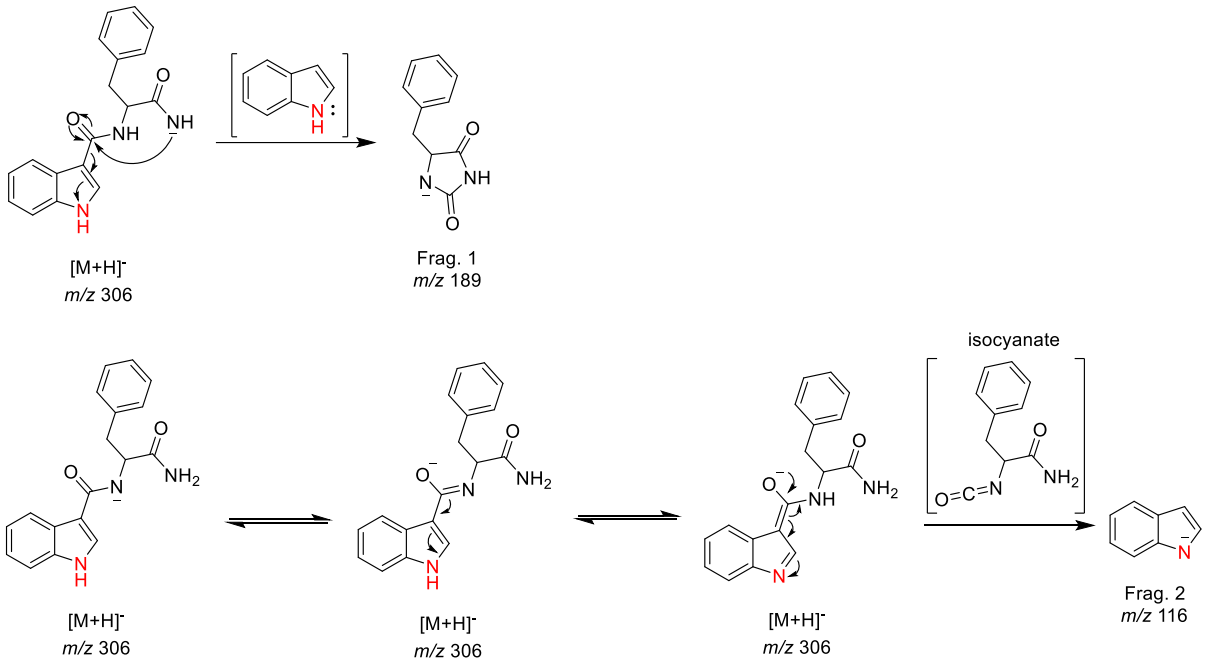

Figure SI14. Proposed fragmentation pathway for 5F-APP-PICA M6 based on the observed MS/MS fragmentation.

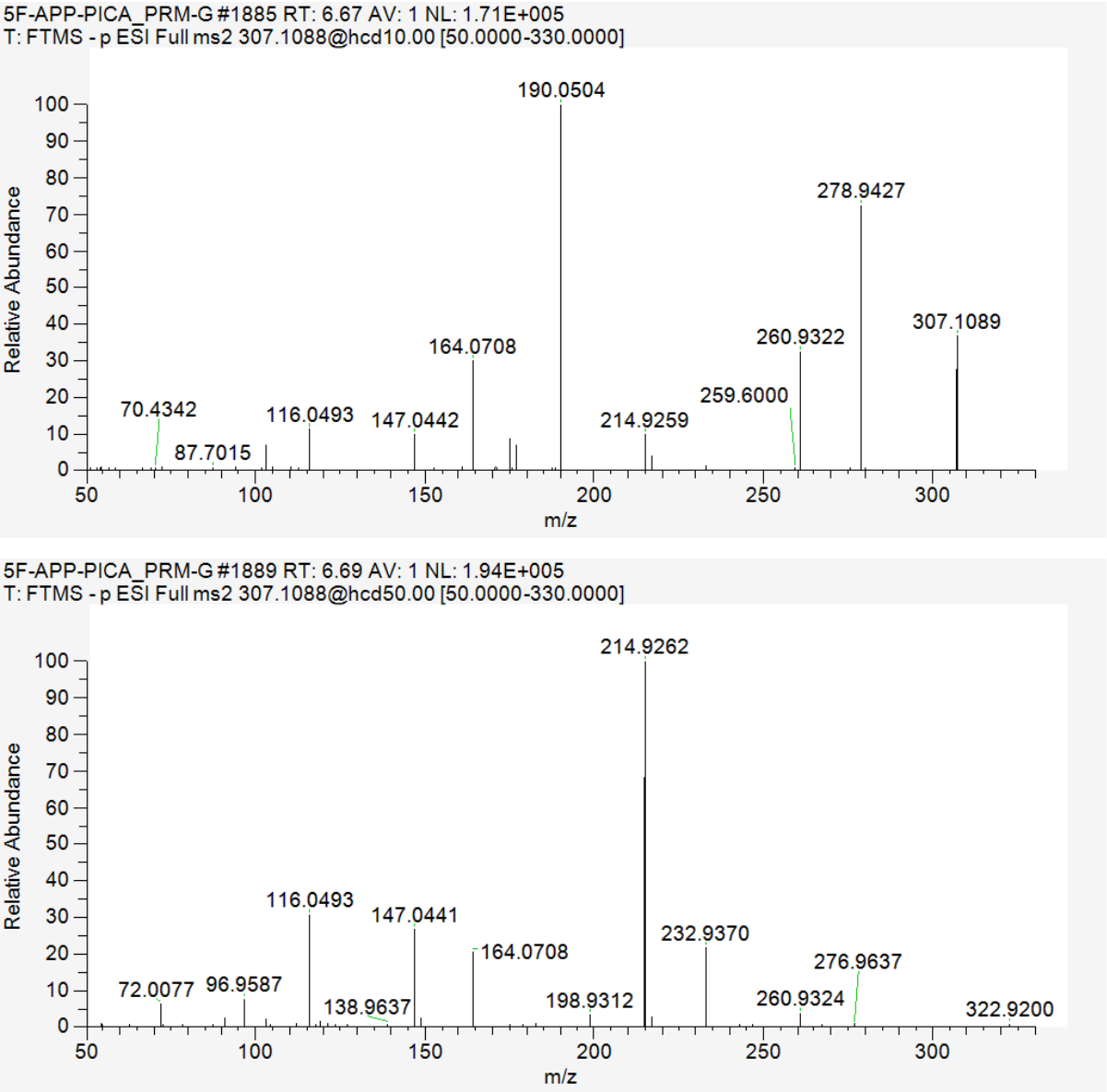

Figure SI15. MS/MS spectra of 5F-APP-PICA M7 at 10 eV (top) and 50 eV (bottom) collision energy.

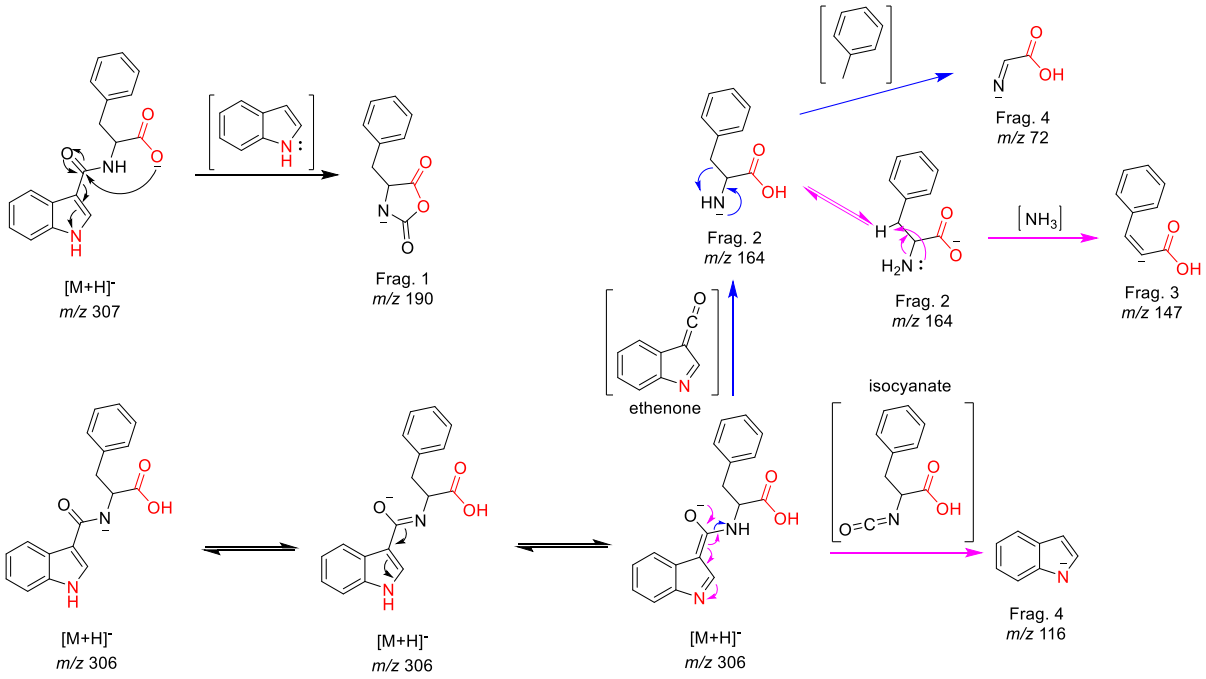

Figure SI16. Proposed fragmentation pathway for 5F-APP-PICA M6 based on the observed MS/MS fragmentation.

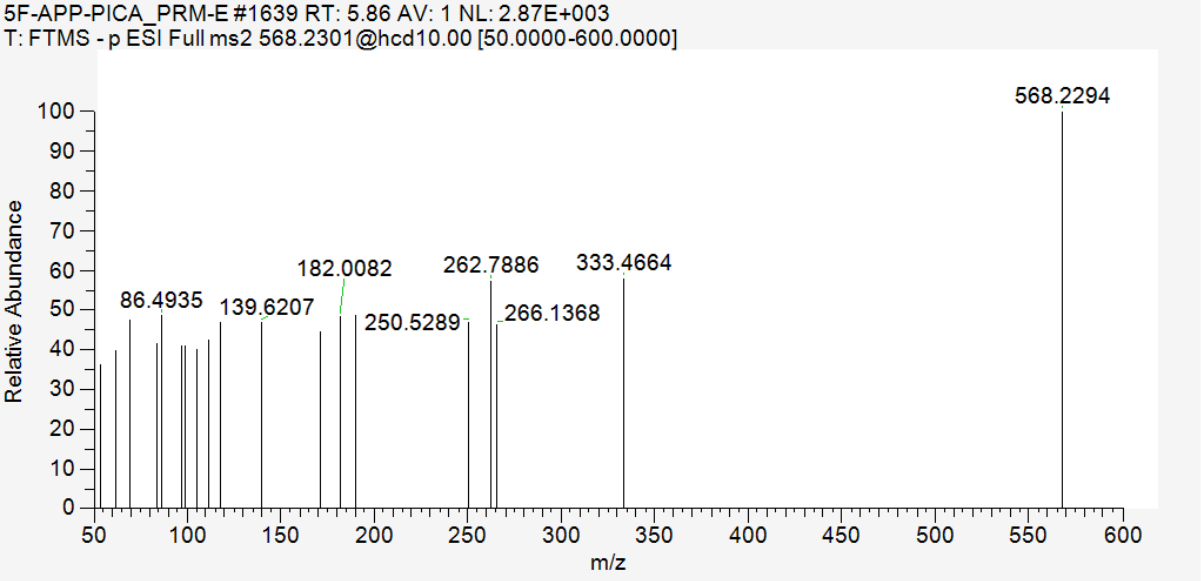

Figure SI17. MS/MS spectrum of 5F-APP-PICA M1-Gluc at 10 eV collision energy.

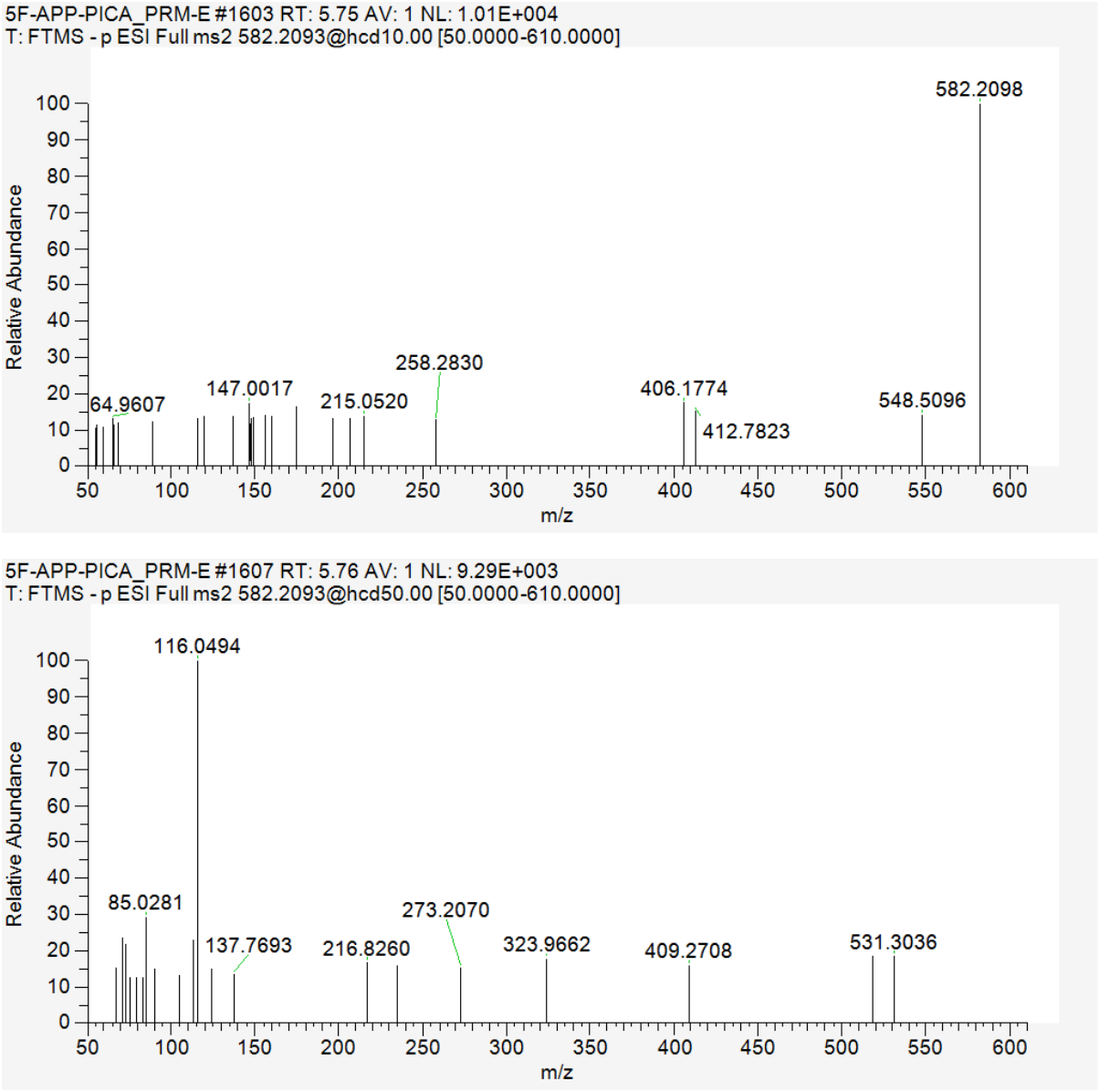

Figure SI18. MS/MS spectra of 5F-APP-PICA M2-Gluc at 10 eV (top) and 50 eV (bottom) collision energy.

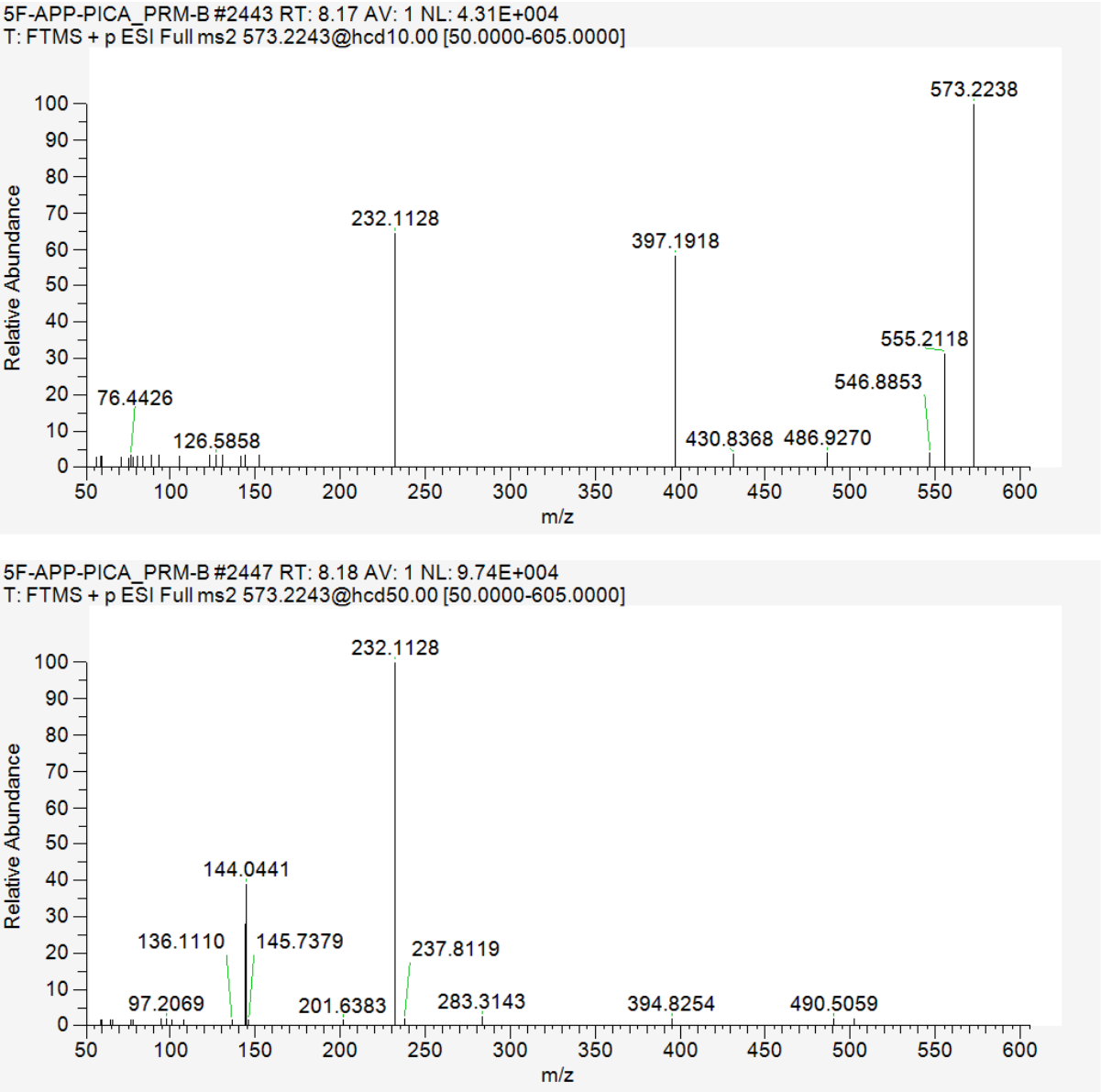

Figure SI19. MS/MS spectra of 5F-APP-PICA M3-Gluc at 10 eV (top) and 50 eV (bottom) collision energy.

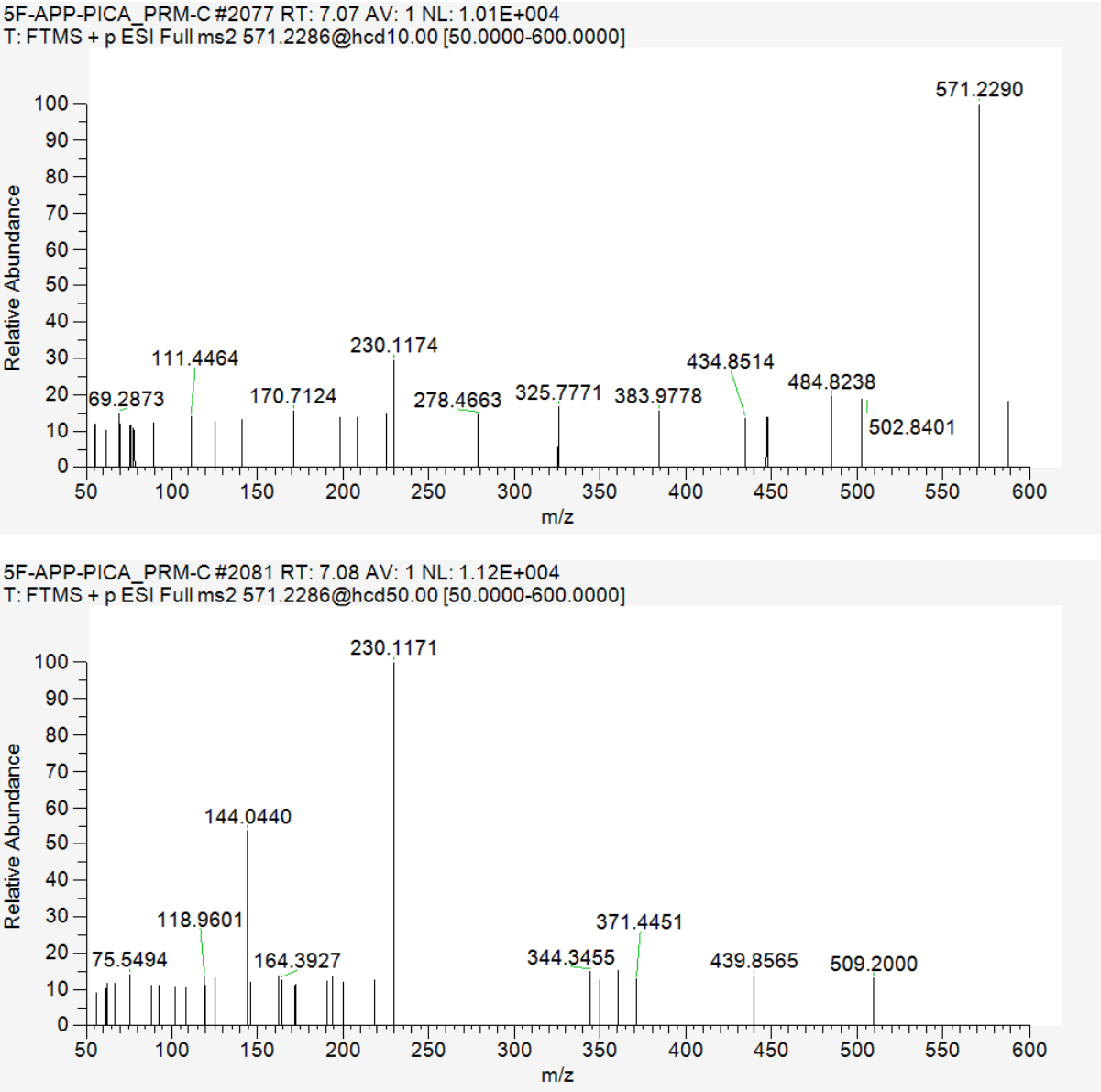

Figure SI20. MS/MS spectra of 5F-APP-PICA M4-Gluc at 10 eV (top) and 50 eV (bottom) collision energy.

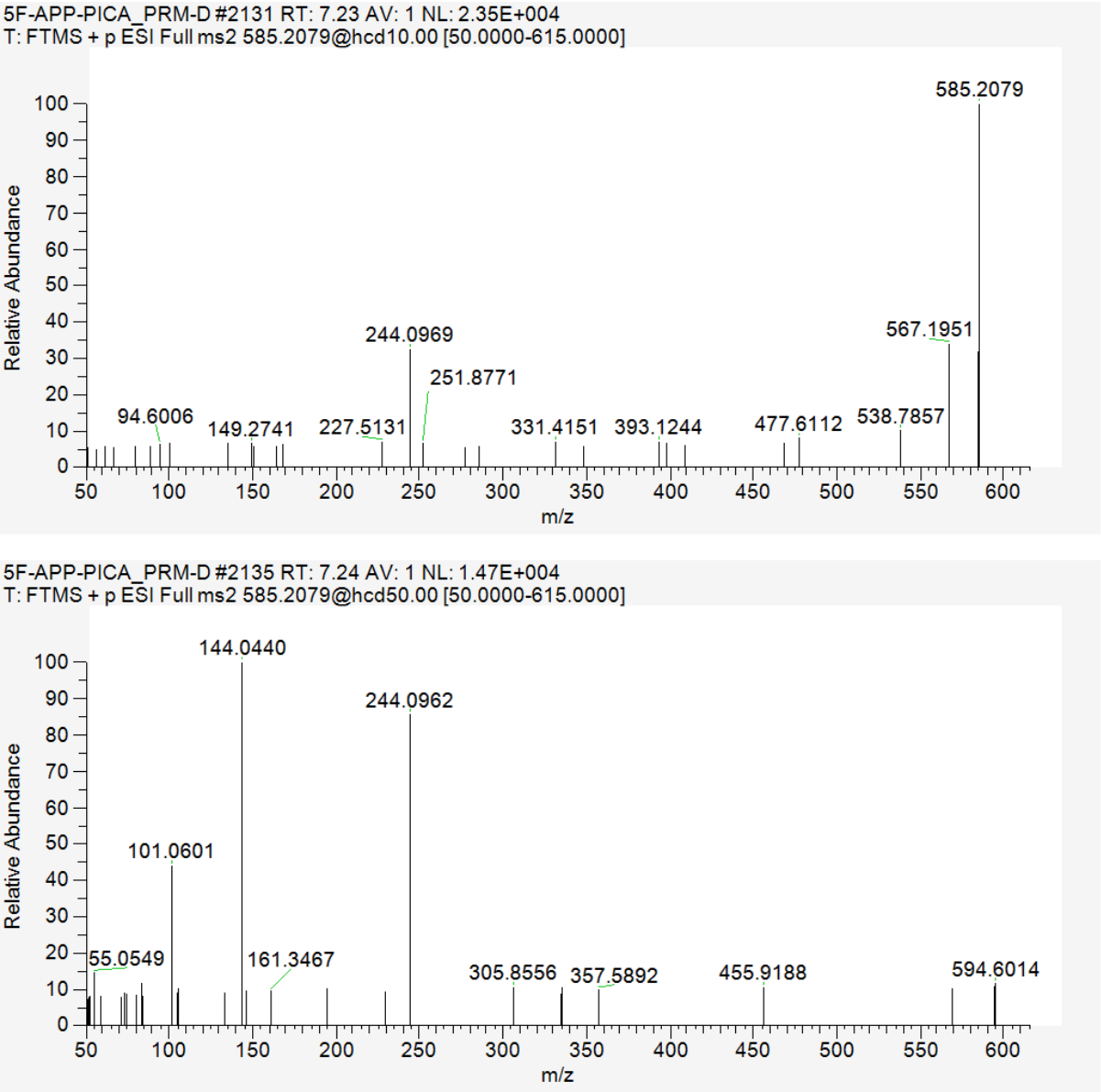

Figure SI21. MS/MS spectra of 5F-APP-PICA M5-Gluc at 10 eV (top) and 50 eV (bottom) collision energy.

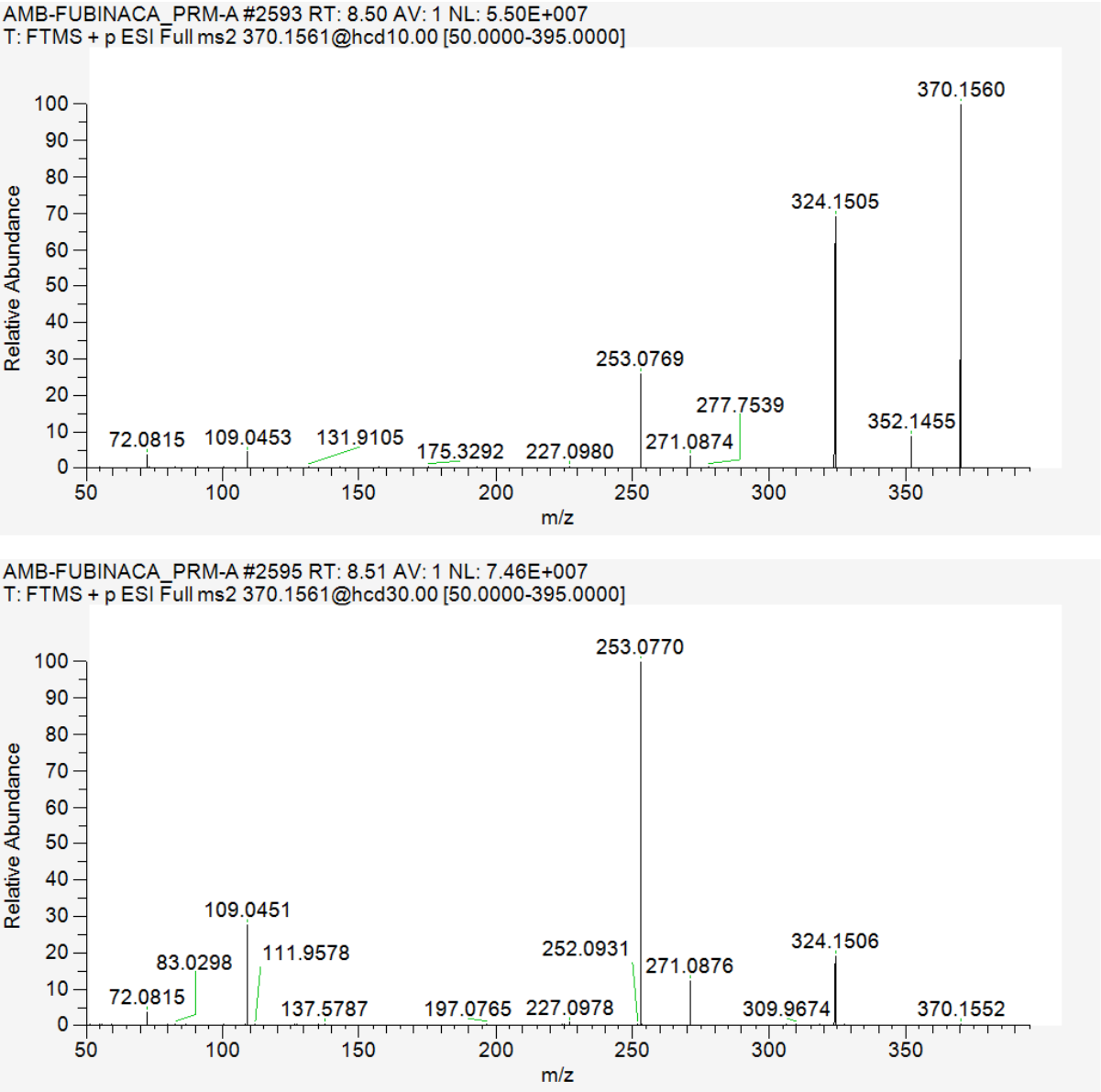

Figure SI22. MS/MS spectra of AMB-FUBINACA M1 at 10 eV (top) and 30 eV (bottom) collision energy.

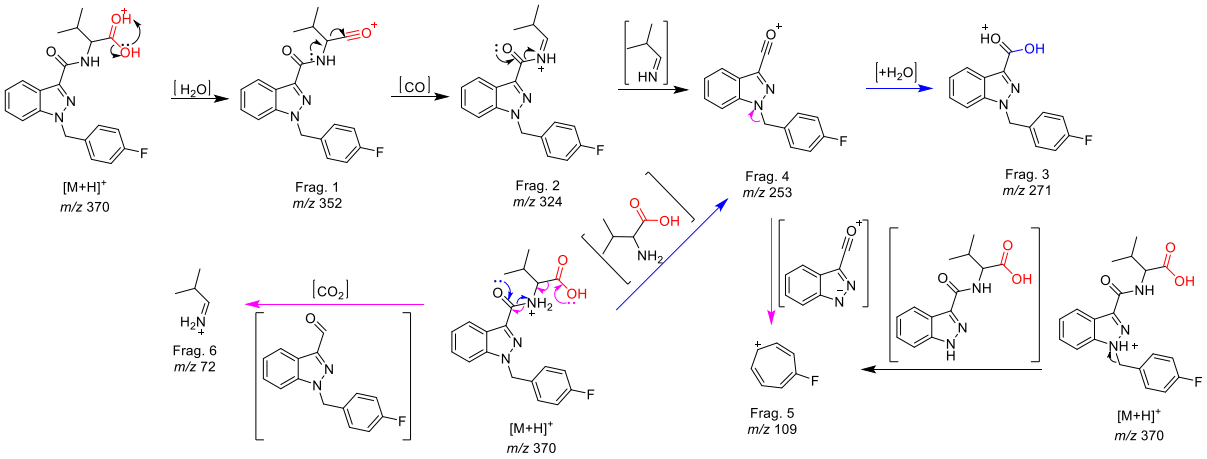

Figure SI23. Proposed fragmentation pathway for AMB-FUBINACA M1 based on the observed MS/MS fragmentation.

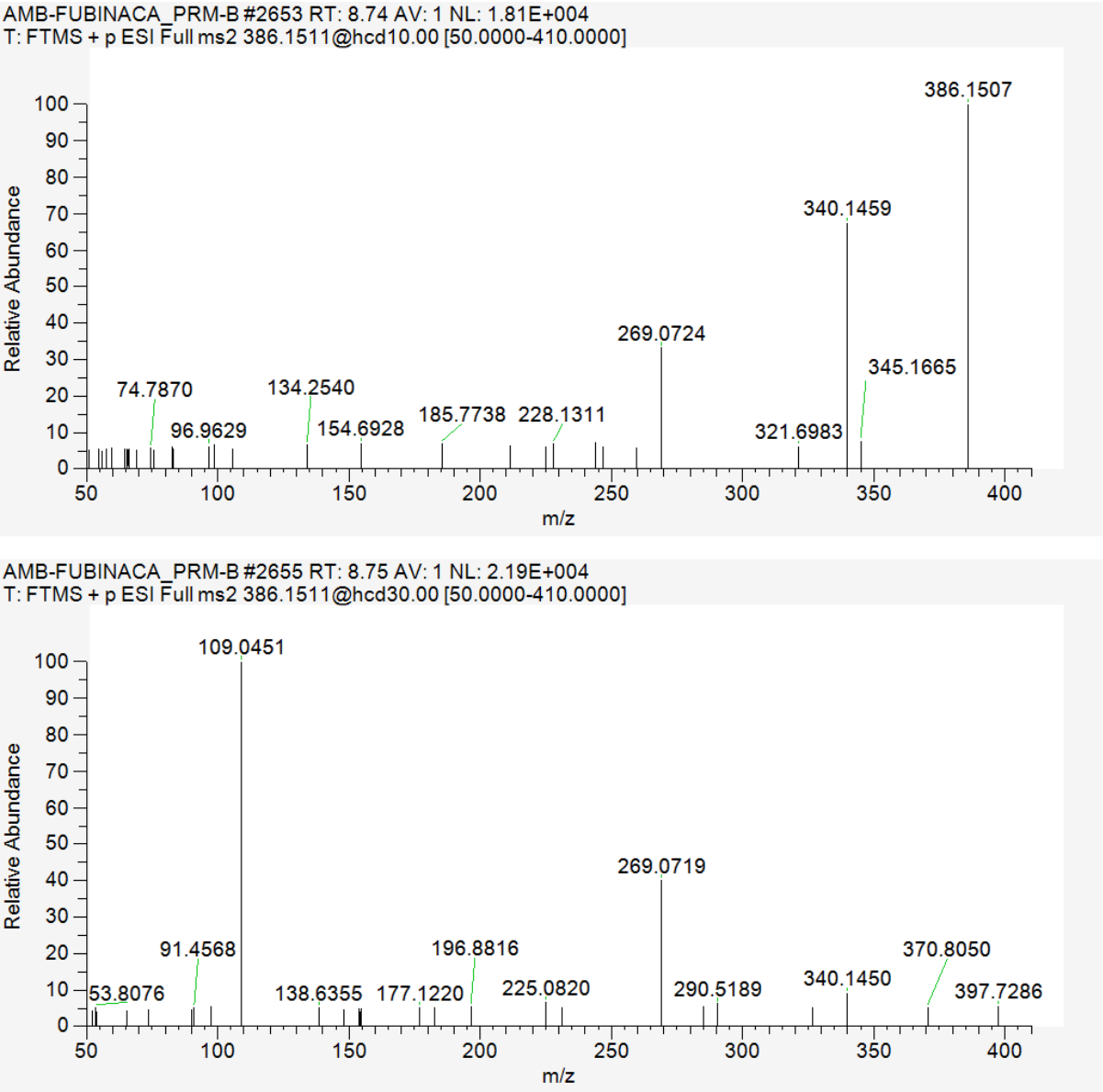

Figure SI24. MS/MS spectra of AMB-FUBINACA M4 at 10 eV (top) and 30 eV (bottom) collision energy.

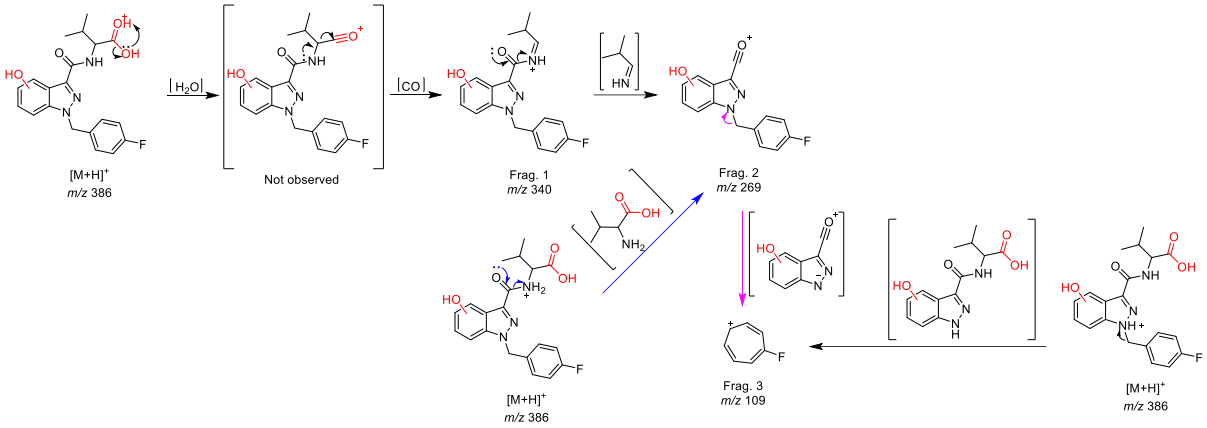

Figure SI25. Proposed fragmentation pathway for AMB-FUBINACA M4 based on the observed MS/MS fragmentation.

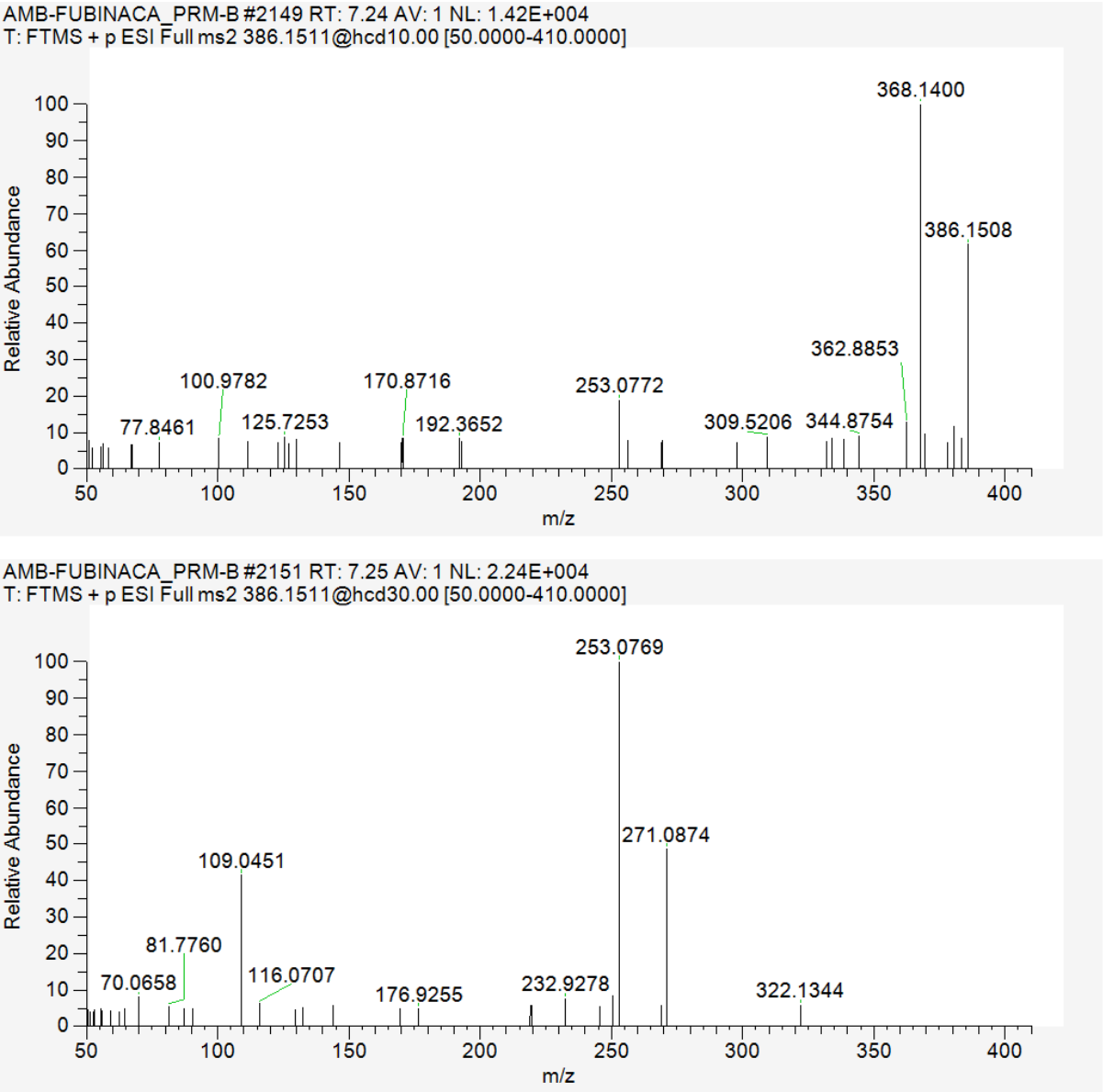

Figure SI26. MS/MS spectra of AMB-FUBINACA M2 at 10 eV (top) and 30 eV (bottom) collision energy.

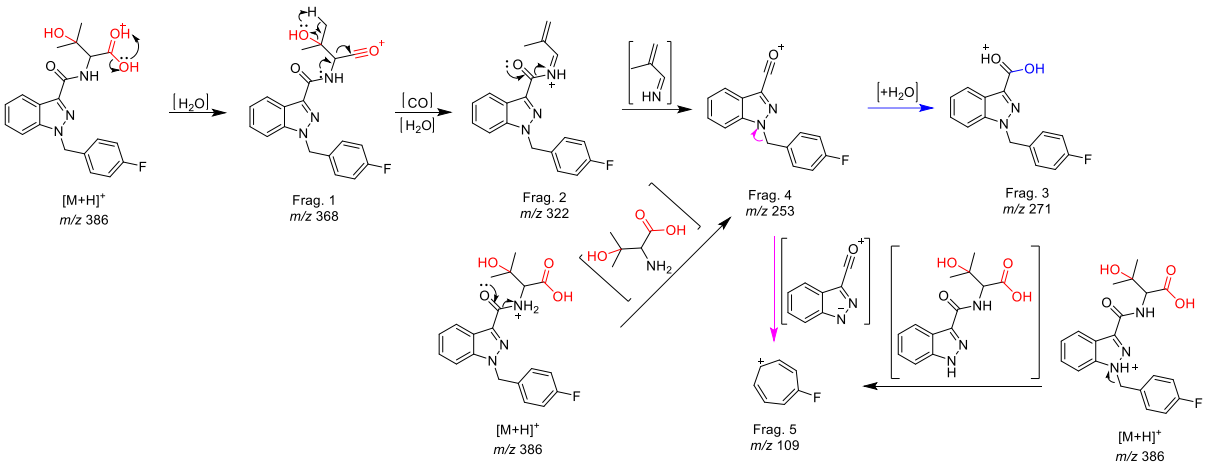

Figure SI27. Proposed fragmentation pathway for AMB-FUBINACA M2 based on the observed MS/MS fragmentation.

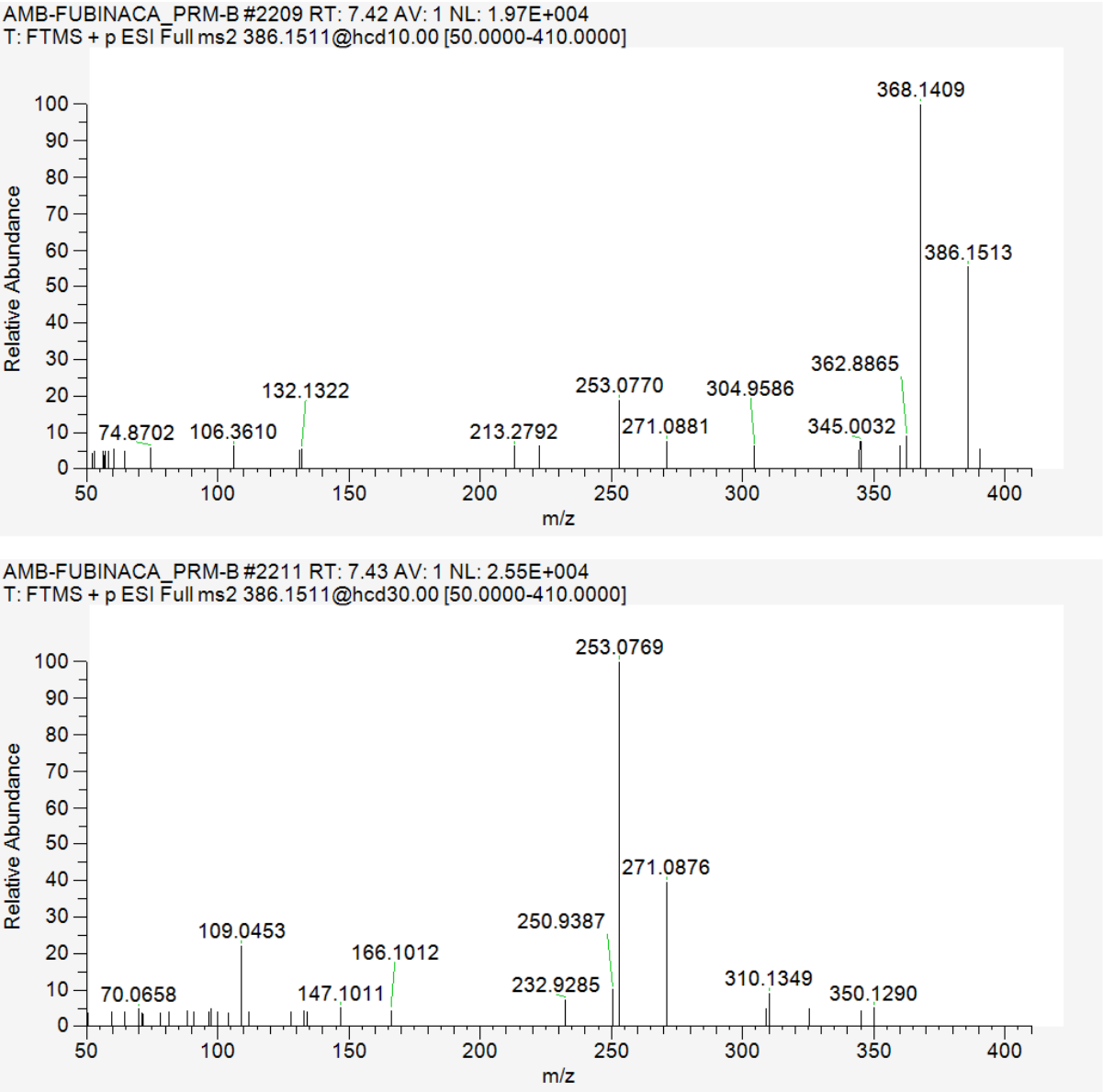

Figure SI28. MS/MS spectra of AMB-FUBINACA M3 at 10 eV (top) and 30 eV (bottom) collision energy.

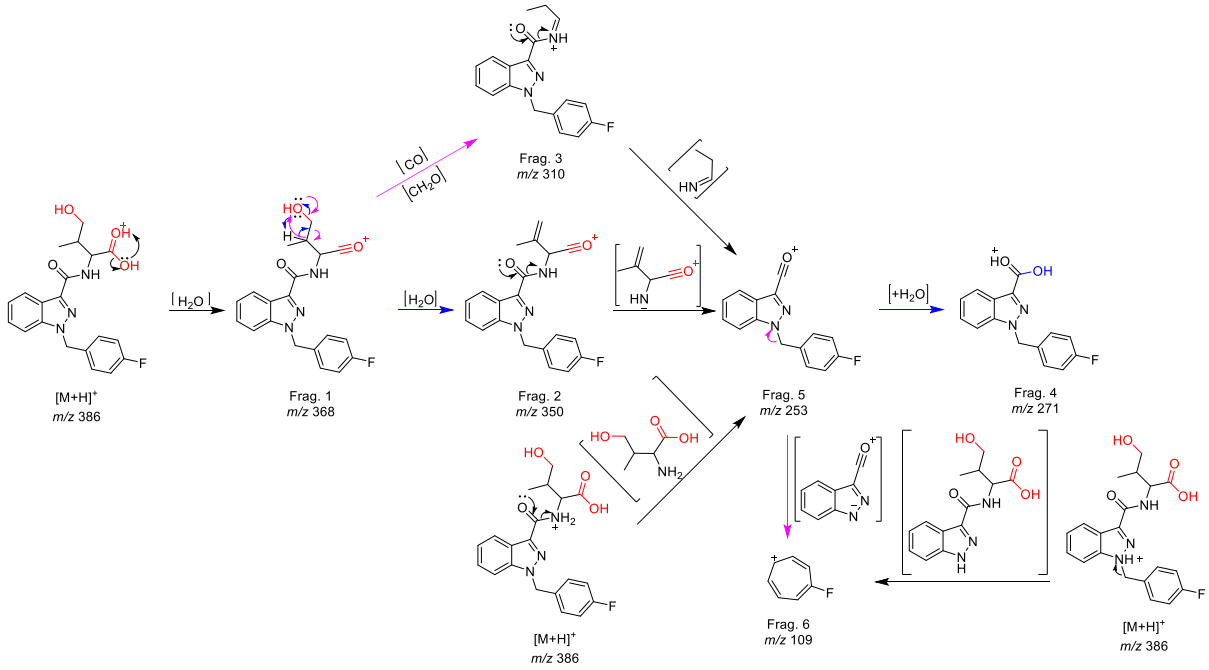

Figure SI29. Proposed fragmentation pathway for AMB-FUBINACA M3 based on the observed MS/MS fragmentation.

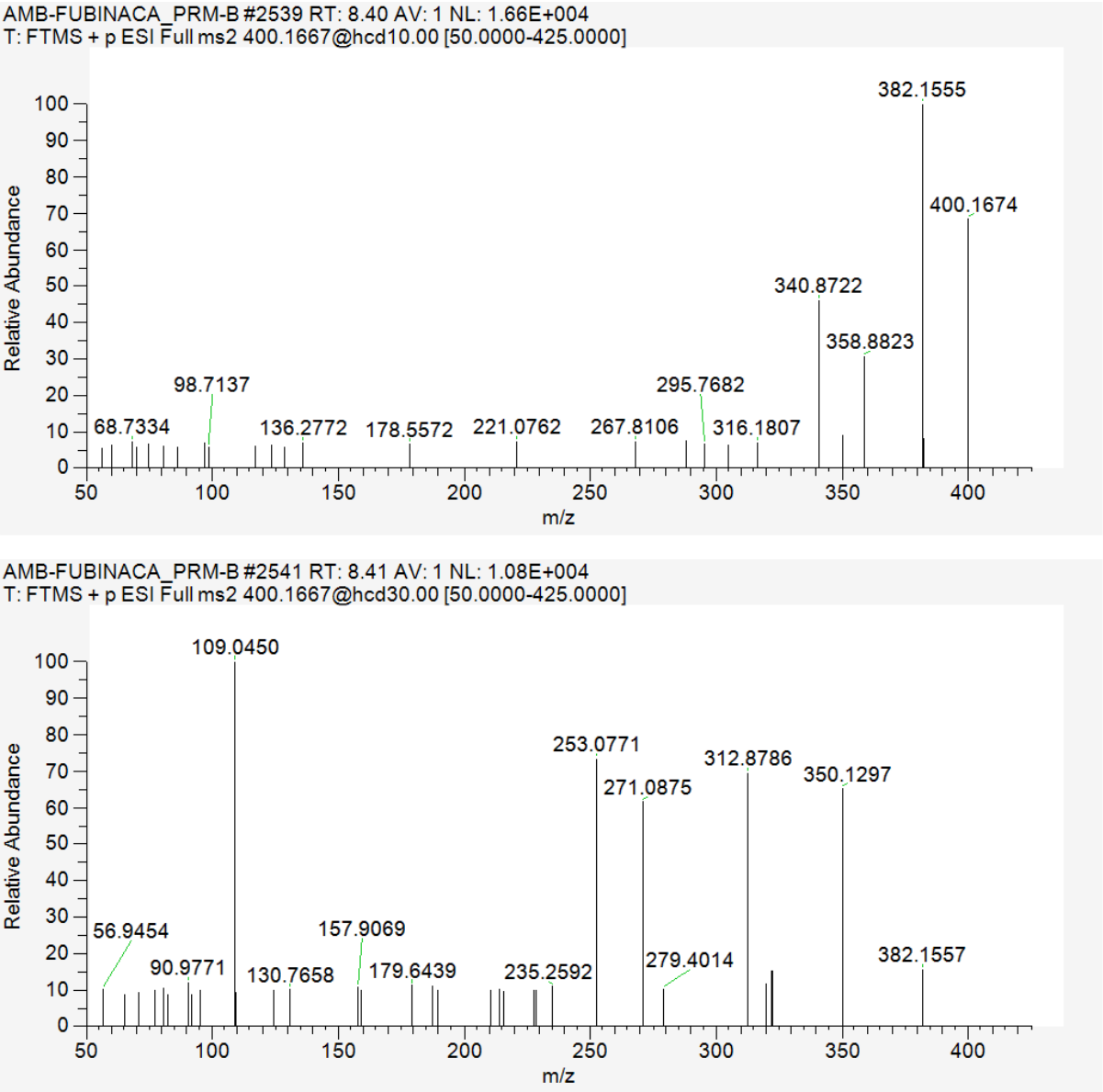

Figure SI30. MS/MS spectra of AMB-FUBINACA M5 at 10 eV (top) and 30 eV (bottom) collision energy.

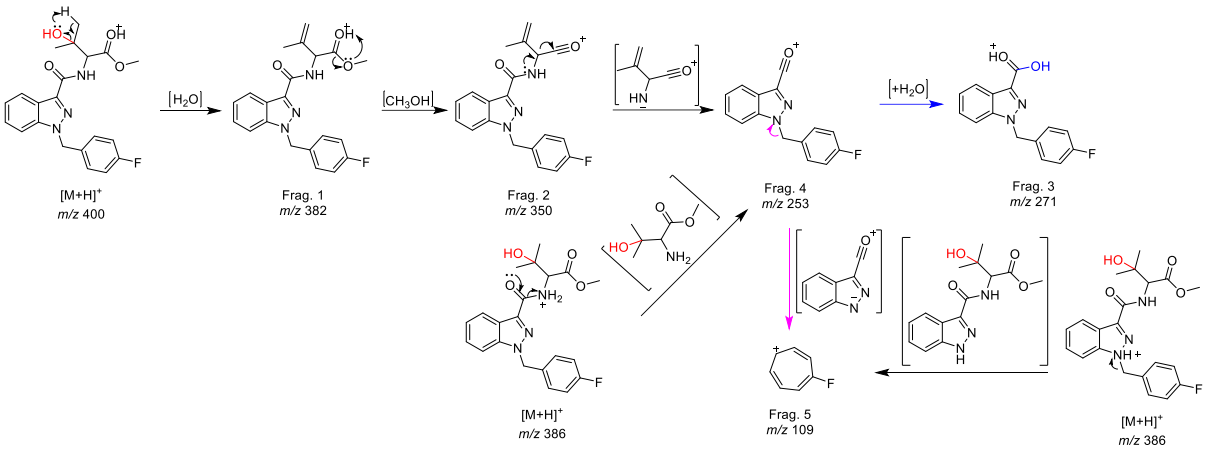

Figure SI31. Proposed fragmentation pathway for AMB-FUBINACA M5 based on the observed MS/MS fragmentation.

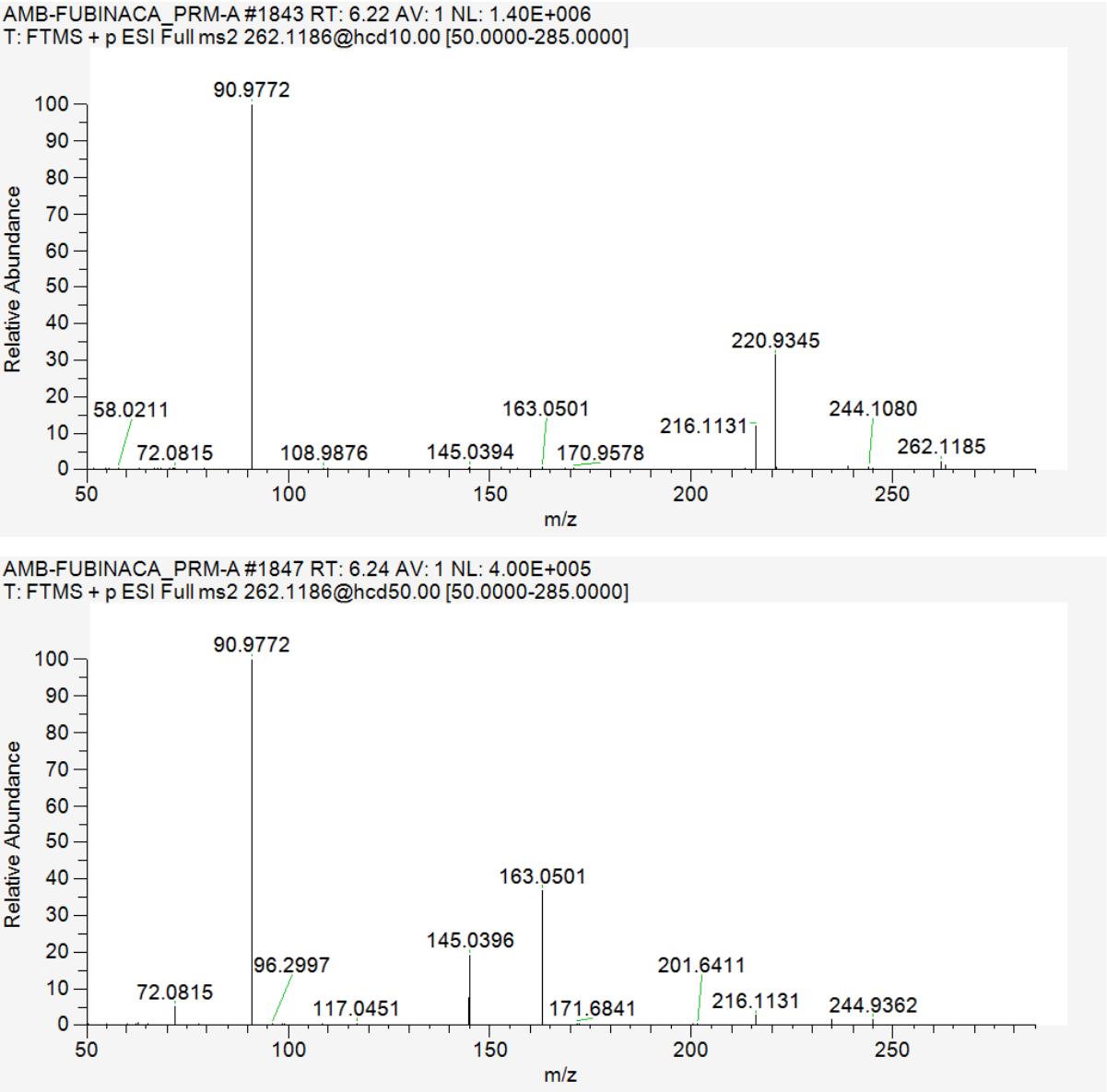

Figure SI32. MS/MS spectra of AMB-FUBINACA M6 at 10 eV (top) and 50 eV (bottom) collision energy.

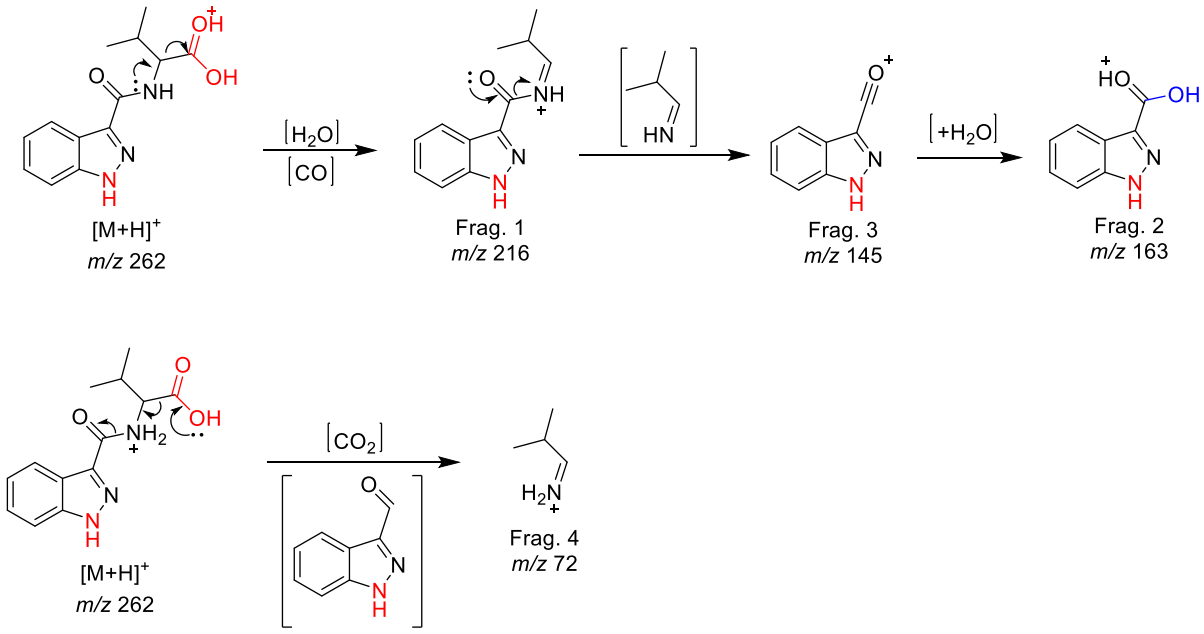

Figure SI33. Proposed fragmentation pathway for AMB-FUBINACA M6 based on the observed MS/MS fragmentation.

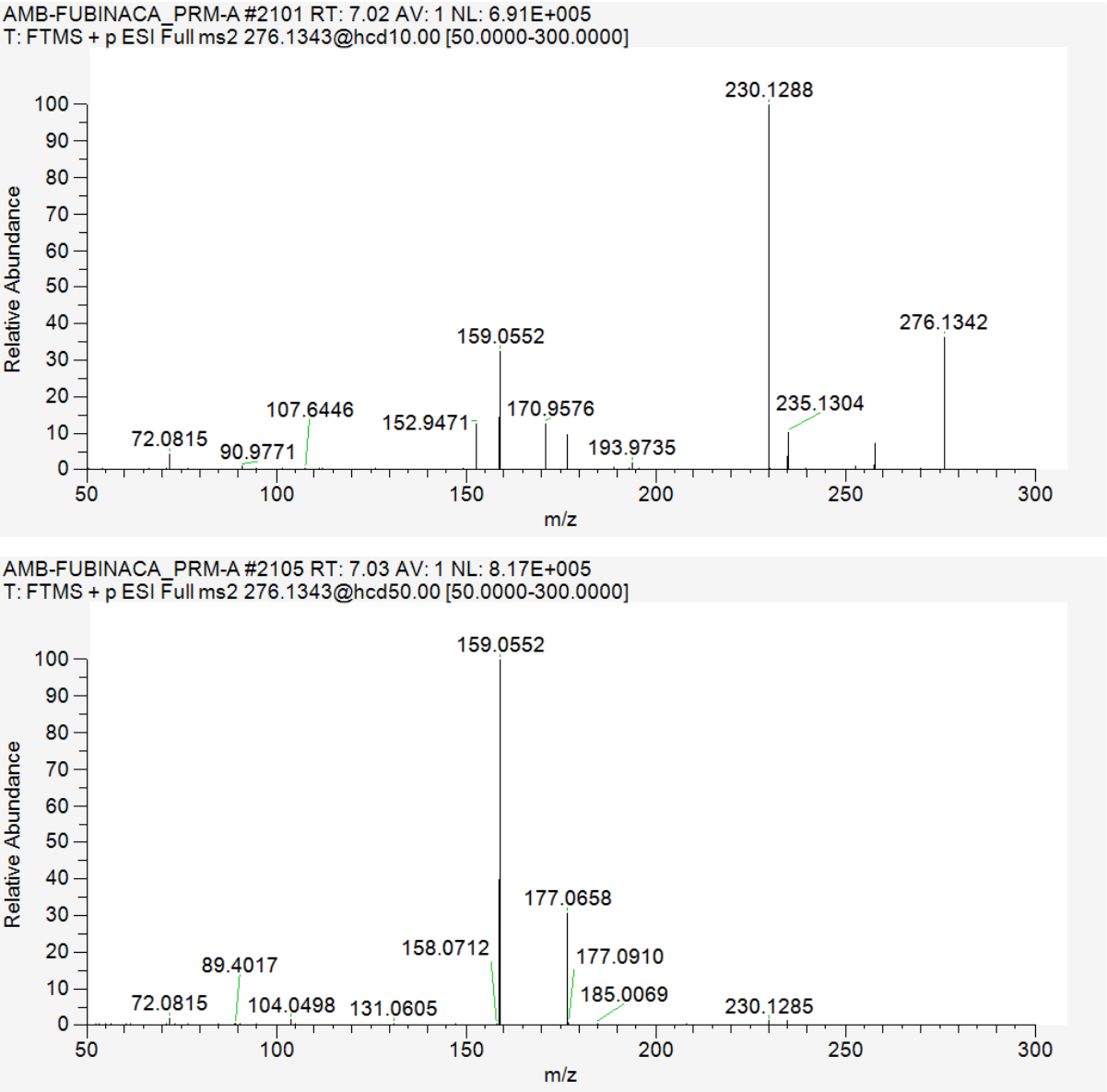

Figure SI34. MS/MS spectra of AMB-FUBINACA M7 at 10 eV (top) and 50 eV (bottom) collision energy.

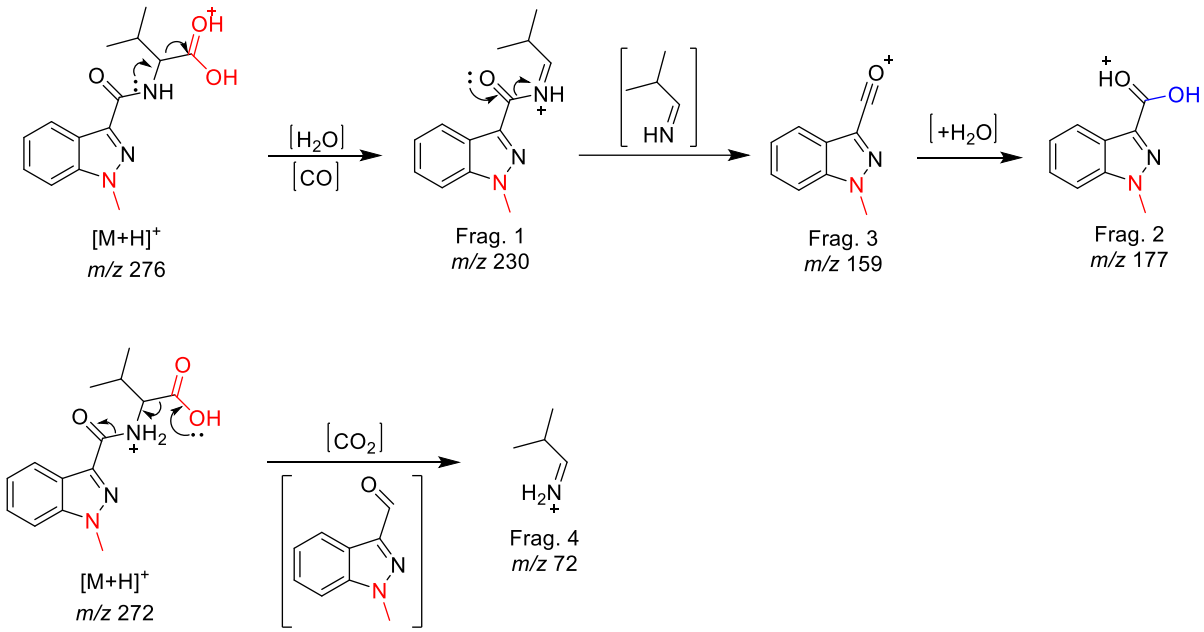

Figure SI35. Proposed fragmentation pathway for AMB-FUBINACA M7 based on the observed MS/MS fragmentation.

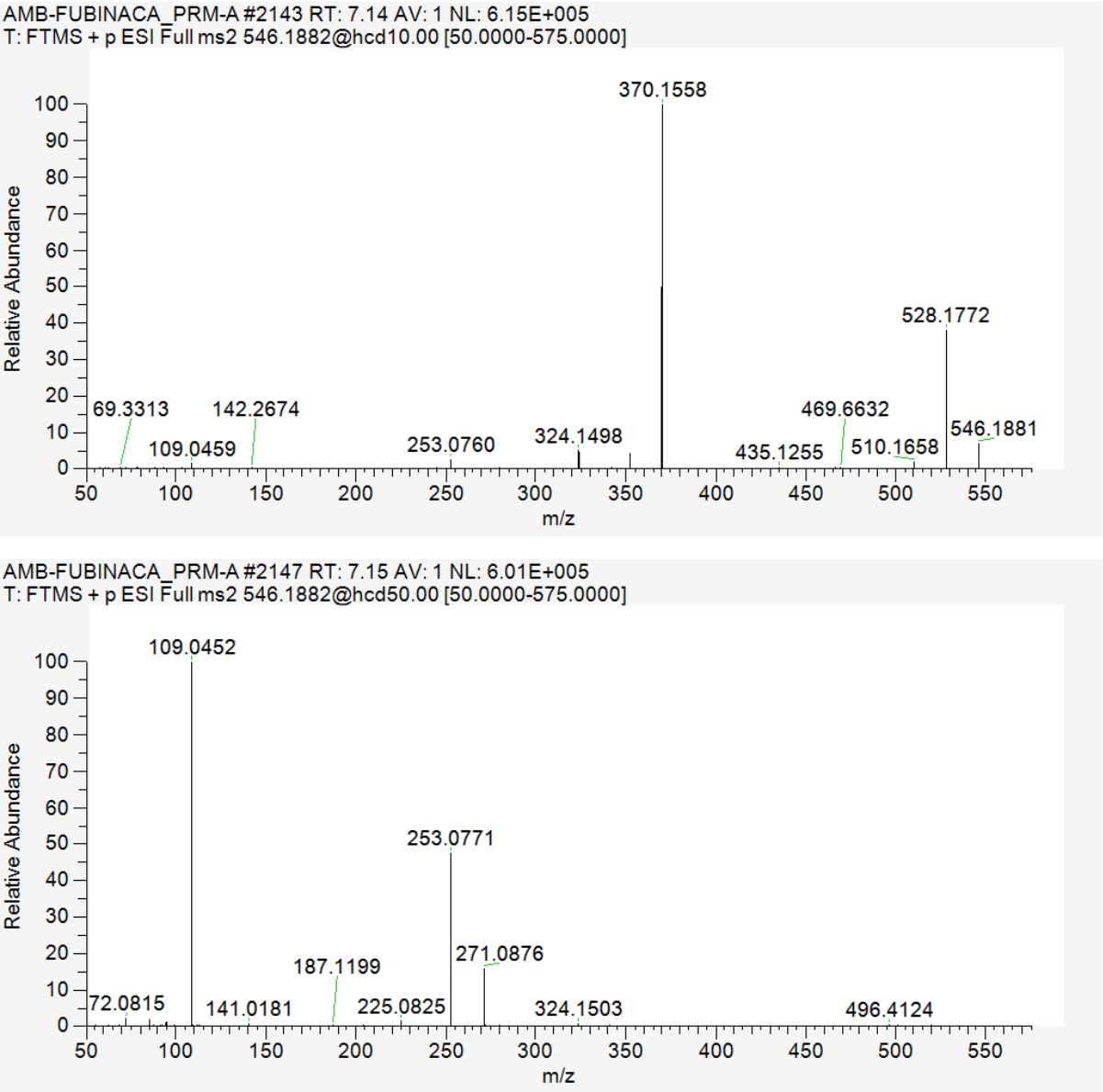

Figure SI36. MS/MS spectra of AMB-FUBINACA M1-Gluc at 10 eV (top) and 50 eV (bottom) collision energy.

Table SI1. MS/MS fragmentation of 5F-APP-PICA and its metabolites, including retention time, ionization mode, and elemental composition, accurate mass and mass error (in ppm) for (de)protonated molecule and fragment ions.

Metabolite	Retention time (min)	ESI	$[M+H]^{+/-}$ (*m/z*)	Elemental composition	Mass error (ppm)	Fragment ion (*m/z*)	Elemental co
5F-APP-PICA	7.94	+	396.2083	$C_{23}H_{27}FN_3O_2^+$	0.18	379.1815	$C_{23}H_{24}FN_2O_2$
						232.1132	$C_{14}H_{15}FNO^+$
						144.0444	$C_9H_6NO^+$
						69.0706	$C_5H_9^+$
M1	6.70	+	394.2116	$C_{23}H_{28}N_3O_3^+$	-2.31	377.1851	$C_{23}H_{25}N_2O_3^+$
						230.1170	$C_{14}H_{16}NO_2^+$
						144.0441	$C_9H_6NO^+$
						116.0493	$C_8H_6N^+$
						87.0809	$C_5H_{11}O^+$
						69.0705	$C_5H_9^+$
M2	6.63	+	408.1908	$C_{23}H_{26}N_3O_4^+$	-2.42	391.1642	$C_{23}H_{23}N_2O_4^+$
						244.0963	$C_{14}H_{14}NO_3^+$
						144.0441	$C_9H_6NO^+$
						116.0495	$C_8H_6N^+$
						101.6000	$C_5H_9O_2^+$
						83.0496	$C_5H_7O^+$
						55.0550	$C_4H_7^+$
M3	8.32	+	397.1916	$C_{23}H_{26}FN_2O_3^+$	-1.61	232.1128	$C_{14}H_{15}FNO^+$
						144.0441	$C_9H_6NO^+$
						116.0494	$C_8H_6N^+$
						69.0705	$C_5H_9^+$
M4	7.07	+	395.1958	$C_{23}H_{27}N_2O_4^+$	-1.85	230.1171	$C_{14}H_{16}NO_2^+$
						144.0441	$C_9H_6NO^+$
						87.0808	$C_5H_{11}O^+$
						69.0705	$C_5H_9^+$
M5	6.98	+	409.1751	$C_{23}H_{25}N_2O_5^+$	-1.61	244.0964	$C_{14}H_{14}NO_3^+$
						144.0442	$C_9H_6NO^+$
						116.0494	$C_8H_6N^+$
						101.0600	$C_5H_9O_2^+$
						83.0497	$C_5H_7O^+$
						55.0552	$C_4H_7^+$
M6	6.32	–	306.1250	$C_{18}H_{16}N_3O_2^-$	4.14	189.0663	$C_{10}H_9N_2O_2^-$
						116.0494	$C_8H_6N^-$
M7	6.74	–	307.1089	$C_{18}H_{15}N_2O_3^-$	3.90	190.0504	$C_{10}H_8NO_3^-$
						164.0708	$C_9H_{10}NO_2^-$
						147.0441	$C_9H_7O_2^-$
						116.0493	$C_8H_6N^-$
						72.0077	$C_2H_2NO_2^-$
M1-Gluc	5.89	–	568.2294	$C_{29}H_{34}N_3O_9^-$	0.73		
M2-Gluc	5.80	–	582.2098	$C_{29}H_{32}N_3O_{10}^-$	2.78	406.1774	$C_{23}H_{24}N_3O_4^-$
						116.0494	$C_8H_6N^-$
M3-Gluc	7.24	+	357.2238	$C_{29}H_{34}FN_2O_9^+$	-0.93	555.2118	$C_{29}H_{32}FN_2O_9^-$
						397.1918	$C_{23}H_{26}FN_2O_3^-$
						232.1128	$C_{14}H_{15}FNO^+$

						144.0441	$C_9H_6NO^+$
M4-Gluc	6.19	+	571.2290	$C_{29}H_{35}N_2O_{10}^+$	0.67	230.1172	$C_{14}H_{16}NO_2^+$
						144.0440	$C_9H_6NO^+$
M5-Gluc	6.14	+	585.2079	$C_{29}H_{33}N_2O_{11}^+$	0.00	224.0963	$C_{14}H_{14}NO_3^+$
						144.0440	$C_9H_6NO^+$
						101.0601	$C_5H_9O_2^+$

Table SI2. MS/MS fragmentation of AMB-FUBINACA and its metabolites, including ionization mode, and elemental composition, accurate mass and mass error (in ppm) for (de)protonated molecule and fragment ions.

Metabolite	Retention time (min)	ESI	$[M+H]^{+/-}$ (*m/z*)	Elemental composition	Mass error (ppm)	Fragment ion (*m/z*)	Elemental composition	Mass error (ppm)	Collision energy (eV)
AMB-FUBINACA	9.73	+	384.1717	$C_{21}H_{23}FN_3O_3^+$	-0.35	352.1455	$C_{20}H_{19}FN_3O_2^+$	-0.12	10
						324.1507	$C_{19}H_{19}FN_3O^+$	0.09	30
						271.0877	$C_{15}H_{12}FN_2O_2^+$	-0.09	30
						253.0771	$C_{15}H_{10}FN_2O^+$	-0.14	30
						109.0451	$C_7H_6F^+$	3.45	50
M1	8.55	+	370.1560	$C_{20}H_{21}FN_3O_3^+$	-0.30	352.1455	$C_{20}H_{19}FN_3O_2^+$	-0.30	10
						324.1506	$C_{19}H_{19}FN_3O^+$	-0.29	30
						271.0876	$C_{15}H_{12}FN_2O_2^+$	-0.43	30
						253.0770	$C_{15}H_{10}FN_2O^+$	-0.50	30
						109.0452	$C_7H_6F^+$	2.82	50
						72.0815	$C_4H_{10}N^+$	10.43	30
M2	7.33	+	386.1508	$C_{20}H_{21}FN_3O_4^+$	-0.63	368.1400	$C_{20}H_{19}FN_3O_3^+$	-1.31	10
						322.1344	$C_{19}H_{17}FN_3O^+$	-1.82	30
						271.0874	$C_{15}H_{12}FN_2O_2^+$	-1.33	30
						253.0769	$C_{15}H_{10}FN_2O^+$	-1.10	30
						109.0451	$C_7H_6F^+$	3.17	50
M3	7.50	+	386.1513	$C_{20}H_{21}FN_3O_4^+$	0.71	368.1409	$C_{20}H_{19}FN_3O_3^+$	1.01	10
						350.1290	$C_{20}H_{17}FN_3O_2^+$	-2.67	30
						310.1349	$C_{18}H_{17}FN_3O^+$	-0.52	30
						271.0876	$C_{15}H_{12}FN_2O_2^+$	-0.54	30
						253.0769	$C_{15}H_{10}FN_2O^+$	-1.10	30
						109.0453	$C_7H_6F^+$	2.82	50
M4	8.75	+	386.1507	$C_{20}H_{21}FN_3O_4^+$	-0.95	340.1459	$C_{19}H_{19}FN_3O_2^+$	1.01	10
						269.0719	$C_{15}H_{10}FN_2O_2^+$	-0.57	30
						109.0451	$C_7H_6F^+$	2.89	50
M5	8.45	+	400.1674	$C_{21}H_{23}FN_3O_4^+$	1.69	382.1555	$C_{21}H_{21}FN_3O_3^+$	-1.57	10
						350.1297	$C_{20}H_{17}FN_3O_2^+$	-0.20	30
						271.0875	$C_{15}H_{12}FN_2O_2^+$	-0.99	30
						253.0771	$C_{15}H_{10}FN_2O^+$	-0.20	30
						109.0450	$C_7H_6F^+$	2.89	50
M6	6.31	+	262.1185	$C_{13}H_{16}N_3O_3^+$	-0.57	216.1131	$C_{12}H_{14}N_3O^+$	0.02	10
						163.0501	$C_8H_7N_2O_2^+$	-0.48	50
						145.0396	$C_8H_5N_2O^+$	-0.52	50
						72.0815	$C_4H_{10}N^+$	10.22	50
M7	7.06	+	276.1342	$C_{14}H_{18}N_3O_3^+$	-0.19	230.1288	$C_{13}H_{16}N_3O^+$	-0.15	10
						177.0658	$C_9H_9N_2O_2^+$	-0.50	50
						159.0552	$C_9H_7N_2O^+$	-0.52	50
						72.0815	$C_4H_{10}N^+$	10.22	50
M1-Gluc	7.17	+	546.1881	$C_{26}H_{29}FN_3O_9^+$	-0.23	528.1772	$C_{26}H_{27}FN_3O_8^+$	-0.80	10
						370.1558	$C_{20}H_{21}FN_3O_3^+$	-0.87	10

324.1503	$C_{19}H_{19}FN_3O^+$	-0.10	30
271.0876	$C_{15}H_{12}FN_2O_2^+$	-0.43	50
253.0771	$C_{15}H_{10}FN_2O^+$	-0.26	50
109.0452	$C_7H_6F^+$	3.31	50
72.0815	$C_4H_{10}N^+$	10.75	30